MAGNETOTRANSPORT OF HOT ELECTRONS AND HOLES IN THE SPIN-VALVE TRANSISTOR

Promotiecommissie

Voorzitter, secretaris:	Prof. dr. ir. A. J. Mouthaan	Univ. Twente, EWI
Promotor:	Prof. dr. J.C. Lodder	Univ. Twente, EWI
Assistent promotor:	Dr. R. Jansen	Univ. Twente, EWI
Leden:	Prof. dr. J. Schmitz	Univ. Twente, EWI
	Prof. dr. ir. H.J.W. Zandvliet	Univ. Twente, TNW
	Prof. dr. D. Weiss	Univ. Regensburg, Germany
	Prof. dr. ir. J. de Boeck	IMEC, The Netherlands
	Prof. dr. B. Koopmans	Univ. Eindhoven, TN

The work is part of the research program of the "Stichting voor Fundamenteel Onderzoek der Materie (FOM)", which is financially supported by the "Nederlandse Organisatie voor Wetenschappelijk Onderzoek (NWO)".
The work was performed in the Systems and Materials for Information Storage Group (SMI) of the MESA+ Institute for Nanotechnology, University of Twente.

Printed by Wöhrmann Print Service

ISBN 90-365-2396-6

MAGNETOTRANSPORT OF HOT ELECTRONS AND HOLES IN THE SPIN-VALVE TRANSISTOR

PROEFSCHRIFT

ter verkrijging van
de graad van doctor aan de Universiteit Twente,
op gezag van de rector magnificus,
prof. dr. W.H.M. Zijm,
volgens het besluit van het College voor Promoties
in het openbaar te verdedigen
op donderdag 13 juli 2006 om 15.00 uur

door

Hüseyin Gökcan

geboren op 15 December 1976

te Balikesir, Turkije

Dit proefschrift is goedgekeurd door

de promotor:	Prof. dr. J.C. Lodder
de assistent promotor:	Dr. R. Jansen

I dedicate this book to my beloved wife Elif and our daughter Asude.

Contents

Chapter 1

Introduction

The conventional electronics is based on the charge property of the electrons and holes. The approach to develop new or more efficient technologies is to miniaturize which faces difficulties and challenges due to the physical limits. One of the alternative is to utilize the spin property of the carriers in addition to the charge. This new route is called spintronics (or magnetoelectronics) [1]. The structures that are studied could be metallic, semiconductor or a combination of both where the latter are referred to as hybrid structures. It is important that the new devices are compatible with the current technology for the integration since it is desirable to use the conventional electronics and spintronics to take advantages of both technologies. The spin-valve transistor (SVT) [2] is one of the early spintronics devices which is used for studying the spin-dependent transport of hot-electrons in the ferromagnetic metals. In this chapter, we give a very brief historical background on spintronics and particularly introduce the spin-valve transistor and its characteristics. The understanding of hot-electron spin-dependent transport in ferromagnet/semiconductor hybrid structures is presented as is the recent development of spin transport using non-equilibrium holes instead of electrons. Finally, the motivation for studying the hot-carrier magnetotransport is given along with the thesis outline.

1.1 Spintronics

The resistance of a multilayer composed of ferromagnetic layers separated by a thin spacer of nonmagnetic metal is found to depend greatly on the relative orientation of the magnetization of neighboring magnetic films which is called giant magnetoresistance effect (GMR). With the discovery of Giant Magnetoresistance effect in 1988 [3], the spin property of the electrons became one of the interesting topics in the research under the name of spintronics. Early applications using GMR was highly sensitive magnetic field sensors [1, 4, 5] and the

commercial products in the magnetic read-heads of magnetic hard disc recording systems was already available by 1997. Another scientific breakthrough has been made in spintronics in 1995 with the discovery of tunnel magnetoresistance [6] (TMR) where large spin-dependent tunnelling is observed at room temperatures across 1-2 nm Al_2O_3 or MgO tunnel barriers. Based on these effects, a Magnetic Random Access Memory (MRAM) [7, 8, 9] is produced which has low power consumption, fast switching speed and is non-volatile.

While semiconductors are the building blocks of the conventional electronics, GMR and TMR is observed in structures with metals and insulators. The semiconductors allows designers to tune the properties of the devices by manipulating the electrical conductivity via electric fields through gates. It would be interesting to investigate spintronics devices with semiconductors where the spin lifetimes are reported to be long [10, 11]. More importantly, spintronics devices with semiconductors would be easier to integrate to the conventional electronics circuitry. Two approaches could be pursued. One is to have ferromagnetic semiconductors [12] where the spin property could be used as a degree of freedom and the the advantages of the semiconductor could be used. The second way is to combine the ferromagnetic metals such as Co, NiFe and the semiconductors like Si and GaAs to have hybrid structures. This thesis deals with such a hybrid structure; the spin-valve transistor (SVT).

1.2 The spin-valve transistor

Ferromagnets and semiconductor have been integrated in the spin-valve transistor (SVT) which is first presented in 1995 by Monsma et al [2]. The schematic structure of the SVT is shown in fig 1.1 on the top. It is a sandwich of a spin-valve metal base that contains two ferromagnets separated by a nonmagnetic metal between semiconductor emitter and collector. This is a three terminal device that operates with hot-electron transmission through the metal base. The collected hot-electron current depends on the relative orientation of the magnetic moments of the ferromagnets in the base. The state of the art SVT works at room temperature and shows large magnetic response in low magnetic field [13].

A typical SVT has a Si/Au/NiFe/Au/Co/Cu/Si structure which can be fabricated as explained in chapter 2. The metal contacts with the Si forms a Schottky diode that has a certain energy barrier which provides the transport to be made at higher energies than Fermi level. An applied bias across the emitter diode provides non-equilibrium hot electrons that are injected into the metal base as can be seen in the energy band diagram of the SVT in fig 1.1 in the middle. The energy of the electrons is determined by the Schottky barrier height which is typically between 0.5 and 1.0 eV. On the collector side, there is an another

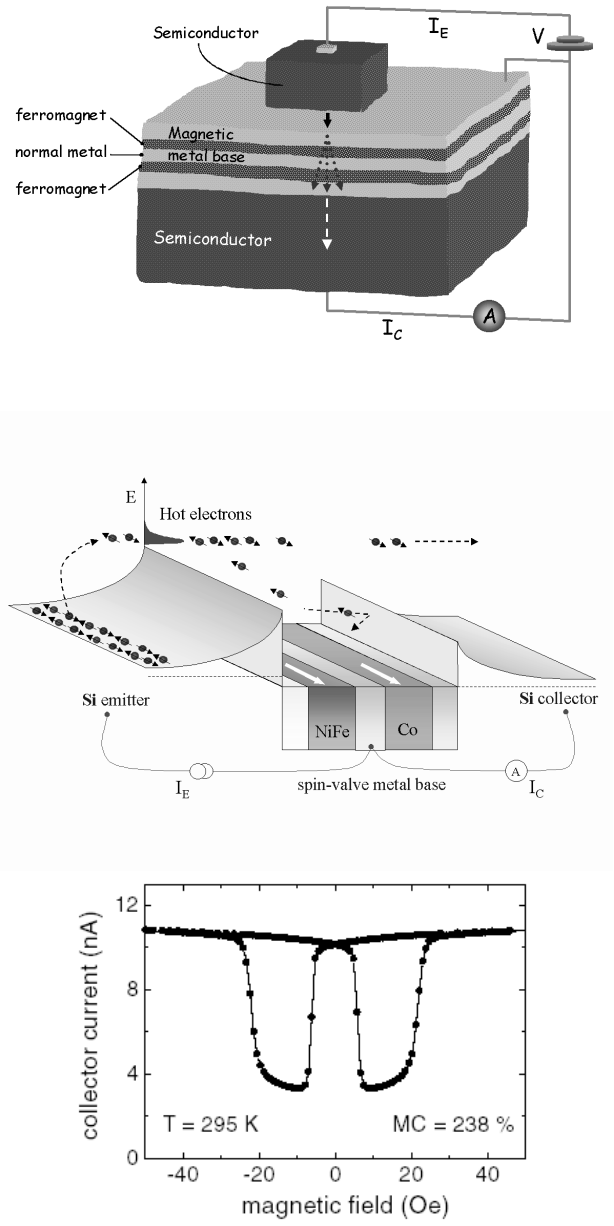

Figure 1.1: *(Top panel) Basic layout of the SVT. It has three terminals for electrical connection with semiconductor emitter on top, semiconductor collector in the bottom and a metallic base in between, consisting of two ferromagnetic thin films separated by a normal metal. (Middle panel) Schematic energy band diagram of the SVT. The stream of hot electrons that are injected from emitter is also depicted. (Bottom panel) The collector current as a function of magnetic field for a SVT with a Si(100) emitter, a Si(111) collector and Pt(2.0 nm)/NiFe(3.0 nm)/Au(3.5 nm)/Co(3.0 nm)/Au(2.0 + 2.0 nm) base. Emitter current (I_E) = 2 mA. Applied bias across the Schottky diode (V_{BC}) = 0. T = 295 K. (taken from [13])*

Schottky diode that has also an energy barrier. Therefore, those hot-electrons that have higher energy than the collector barrier height and right momentum can be collected. The collected hot-electron current strongly depends on the scattering events in the metal base. For a parallel alignment of the magnetic moments of the ferromagnets, the collector current is larger than the collector current for an antiparallel alignment. The collector current I_C as a function of applied magnetic field is plotted in fig 1.1 in the bottom [13] for a SVT with a Si(100)/Pt(2.0 nm) emitter, a NiFe(3.0 nm)/Au(3.5 nm)/Co(3.0 nm) spin-valve base and a Au(2.0+2.0 nm)/Si(111) collector at room temperature with a 2 mA of emitter current. At large magnetic fields, the magnetic moments of the Co and NiFe are parallel and a high collector current (I_C^P=11.2 nA) is observed. When the magnetic field is reversed, NiFe switches first since it has a lower coercivity than Co and the magnetic moments of Co and NiFe become aligned antiparallel and a low collector current (I_C^{AP}=3.3 nA) is measured. Magnetic response of the device could be defined as magnetocurrent MC=$\frac{I_C^P - I_C^{AP}}{I_C^{AP}}$. The MC in fig 1.1 is 240%. The high magnetic response shows a great potential of the device. However, the transfer ratio which is defined as the ratio of the collector current (I_C^P) to the emitter current (I_E^P) is at best 10^{-4} [13]. The reasons that determines the transfer ratio and the magnetocurrent will be discussed in more detail in the following section.

1.3 Physics of hot-electron magnetotransport

The scattering rates of the hot-electrons in ferromagnets are known for quite some time to be spin-dependent. A wide range of energies from 1.5 eV to 5 eV has been probed and all experimental work has shown that the inelastic mean free path of hot-electrons is spin dependent in ferromagnets [14, 15, 16, 17] and it is shorter for the minority spin electrons. It is interpreted that the difference originates from the number of unoccupied states for the hot-electrons to scatter into assuming that electron-hole pair excitations are the dominant scattering mechanism.

The spin-dependent scattering of hot-electrons which leads to spin-filtering and the hot-electron spin-valve effect are employed in spin-polarized electron spectroscopies in order to study the magnetic materials. It is also exploited in the magnetic version of the ballistic electron emission microscopy (BEHM) [18, 19] is exploited to have magnetic imaging with nanometer resolution [20, 21]. With the introduction of the spin-valve transistor [2], it was possible to study the spin-dependent scattering processes of hot-electrons at lower energy range between 0.5 eV and 1.5 eV. It was also easy to change experimental parameters for SVT such as the temperature, the magnetic field, etc which gave new insight into the origin of the spin-dependent scattering processes [13].

The difference in the hot-electron collector current for parallel alignment I_C^P and antiparallel alignment I_C^{AP} in the SVT originates from the asymmetry in the hot-electron attenuation lengths and the transmission of current for each spin depends exponentially on the film thickness. This leads to a filtering of the minority spin electrons and a dominant transmission of the majority spin electrons in each magnetic layer in the base. The attenuation lengths in ferromagnets depend on some physical parameters. One of them is the elastic and inelastic scattering processes which are uniquely defined for a given material and energy. The energy and momentum selection of the semiconductor would also effect the attenuation lengths. Therefore, the geometry of the device, too, plays a role for the attenuation lengths along with the scattering processes. We will address the origin of the large magnetocurrent in the SVT in the following sections, which describe the scattering centers from interface or volume, elastic and inelastic scattering and spin waves.

Interface vs volume scattering

From spin-dependent scattering point of view, one might expect volume scattering as the dominant mechanism over interface scattering since hot-electron current attenuates exponentially with respect to the film thickness and the interfaces contribution remains to be the same. This has been demonstrated by an earlier work with SVT [22, 23] in which a series of identical SVTs are prepared except for one of the ferromagnetic film thickness. The SVTs had a Pt(3.0 nm)/$Ni_{80}Fe_{20}$(x)/ Au(4.4 nm)/Co(3.0 nm)/Au(4.4 nm) metal base where the thickness x $Ni_{80}Fe_{20}$ is changed from 0 nm to 10 nm. In fig 1.2, the hot-electron collector current (top panel) for parallel I_C^P and antiparallel I_C^{AP} alignment and the magnetocurrent MC (bottom panel) are plotted as as a function of NiFe thickness. The Co layer thickness is kept fixed at 3 nm. When the magnetic moments of Co and NiFe are parallel, only the majority spin electrons will contribute to the collector current I_C^P since the minority spin electrons are attenuated strongly in both ferromagnets. The attenuation length for the majority spin in NiFe can be extracted from the slope of I_C^P and it is found to be 4.3 nm, while the minority spin attenuation length was determined to be 1.0 nm [22].

The interface contribution for the majority spin was also obtained [22] by comparing the collector current I_C^P (169 nA) of a device with zero NiFe thickness and the extrapolated collector current of 78 nA of the data to zero NiFe thickness. The device with zero NiFe thickness has a 2.2 higher collector current than the extrapolated value. The extrapolated collector current at zero NiFe thickness is for the devices that has Pt/NiFe and NiFe/Au interfaces. The device with no NiFe in the metal base has only Pt/Au interface. Thus, the difference is due to one additional interface in one of the devices. Since the minority spins are filtered by the Co layer, the attenuation at the interface is for the majority spin. The reason for the attenuation is because of the mismatch of the electronic states

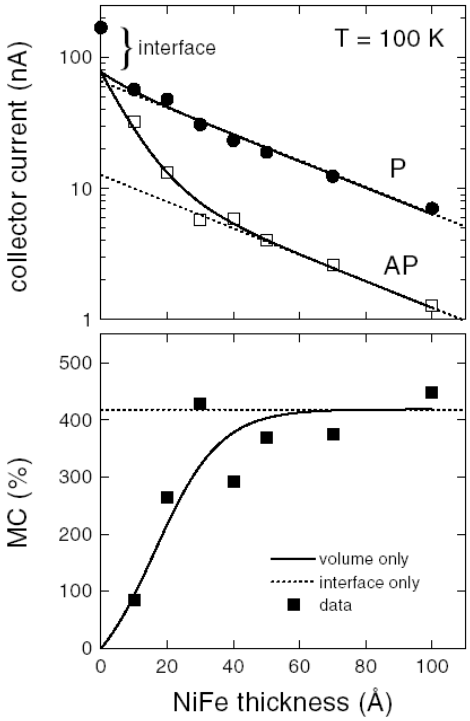

Figure 1.2: *The collector current for parallel I_C^P (circles) and antiparallel I_C^{AP} (squares) configuration of the magnetic moments of Co and NiFe (top) and magnetocurrent (bottom) as a function of NiFe thickness in SVTs. SVTs have Si/Pt(30 Å) emitter diode, NiFe(x Å)/Au(44 Å)/Co(30 Å) spin-valve base and a Si/Au(44 Å) collector diode. Solid and dashed lines, respectively, represent the calculated extreme cases with only spin-dependent volume scattering or only spin-dependent interface scattering. The difference between the data point for a SVT with zero NiFe thickness and the cross of extrapolated curve for parallel alignment is due to the Pt/NiFe and Au/NiFe interfaces. T = 100 K. Taken from [22]*

at both sides of the interface and elastic scattering due to the interface disorder, defects, etc.

It was also found [22] that there is an spin-dependent interface transmission. The ratio of the interface transmission factor for minority to majority spin electrons was found to be 0.8 ± 0.2. Even though the interface contributes to the spin-dependent transmission, the asymmetry in the attenuation lengths in the volume of the ferromagnets are the dominant mechanism. As an example, for a 3.0 nm of NiFe film, the attenuation for minority spin in NiFe is 10 times higher than the majority spin which concludes the volume scattering is the dominant

mechanism for the spin-dependent scattering.

Elastic vs inelastic

The inelastic scattering in the metal base causes attenuation in the hot-electron current. However, as argued in [13]elastic scattering contribution cannot be excluded. First of all, as it is discussed in the previous section that a single interface can reduce the hot-electron current by a factor 2.2. The interface scattering is an elastic scattering process due to disorder, defects, etc. The calculated transmission using the attenuation lengths in bulk of the ferromagnets without the interface scattering would give a transfer ratio of 10^{-2} which is a two orders of magnitude higher than the measured transfer ratios. Secondly, as the energy of the hot-electrons are increased in SVT [24], BEEM [21] and MTT [25], the overall transmission increases. This should be the opposite if the scattering mechanism was solely inelastic since according to Fermi's golden rule the lifetime is reduced when at higher energy more final states become available to scatter into.

Spin waves

In ferromagnets, it has been shown so far that the inelastic mean free paths of hot-electrons is shorter for minority spin electrons. This is attributed to the difference in the number of unoccupied states for the hot-electron to scatter into, assuming excitation of electron-hole pairs to be the dominant scattering mechanism. However, spin-wave excitations may also contribute as suggested by recent experimental [26, 27] and theoretical work [28, 29, 30]. Due to the conservation of angular momentum, the spin asymmetry is created by spontaneous spin-wave emission which is allowed only for minority spin. Spontaneous spin-wave emission is temperature independent even asserting itself at T=0 K and calculated to be dominant at electron energies below 1 eV [28, 29, 30]. The energy loss by this process is very small [26] typically of the order of meVs. There is also scattering of hot electrons by thermal spin waves which involves both emission and absorption of spin waves. Using temperature dependent measurements with SVT [27], the thermal spin wave attenuation lengths are found to reduce the attenuation lengths from 4.3 nm (T = 100 K) to 3.2 nm (at room temperature) for majority spin. From the same set of experiments, an attenuation length for spontaneous spin-wave emission (which is allowed only for minority spin) is estimated to be 1.0 nm which is close to the minority spin attenuation length as argued in [27]. It strongly suggests that the minority spin attenuation length is dominated by spontaneous spin wave emission as theory predicts. Since spontaneous spin wave emission is not possible for majority spin, the asymmetry in attenuation lengths could be due the spontaneous spin wave emission rather than spin-dependent rate of electron hole pair generation due the band structure of the ferromagnet.

1.4 Physics of hot-hole magnetotransport

There are two interpretations for the spin asymmetry in hot-electron attenuation lengths in ferrmagnets. One is the band structure where there are more states available to scatter into for minority spin electrons than majority spin. The second argument is that the spontaneous spin-wave emission could lead to a spin asymmetry in the attenuation length since spontaneous spin-wave emission is allowed only for the minority spin. One of the recent new developments [18, 19] that may give more insight is the study of spin-dependent transport of hot-holes with energy below the Fermi level. For the hot-holes in Co, no significant asymmetry is observed in the band structure below the Fermi level. However, in fig 1.3, a spin-dependent transmission of hot-holes (right) at 2 eV below the Fermi level is observed by a ballistic hole magnetic microscopy (BHMM) [18, 19]which injects hot-holes by a STM tip through tunnelling in vacuum into a Au(3 nm)/Co(1.8 nm)/Au(7 nm)/NiFe(1.8 nm)/Au (7 nm) metal base and the transmitted hot-holes are collected by a collector Si provided the hot-holes have enough energy and momentum. The magnetocurrent is quite high which is 130% as will be discussed in more detail in chapter6. The band structure of the ferromagnets is not enough to explain the spin-dependent transmission in this structure. It is suggested that the spontaneous spin wave emission might be the reason for the spin asymmetry in the attenuation lengths. The attenuation lengths in Co and NiFe are found to be as short as ≤ 1 nm which is consistent with the band structure since there are a lot of unoccupied states for both the minority and majority spin holes.

1.5 Motivation and thesis outline

In this thesis, spin-dependent transport of non-equilibrium electrons as well as holes is studied in ferromagnets and at ferromagnet/nonmagnetic metal interfaces by employing the spin-valve transistor (SVT). It is possible to change the materials or material properties in SVT so that different aspects of the spin-dependent transport of hot-carriers could be studied. There has been already an extensive investigation of the hot-electron transport in SVT and device characteristics. However, some of the topics are not fully covered. One of the motivation of this work is to extend our knowledge on the role of interfaces in the device characteristic and the hot-electron transport. It is known that the interfaces are source of elastic scattering which in turn causes 2 orders of magnitude loss in the hot-electron collector current of the device [13]. If better quality interfaces are achieved, the performance of the device can be improved. Another direction to explore the device performance may be to increase the emitter current. The collector current is expected to be linearly increasing with increasing

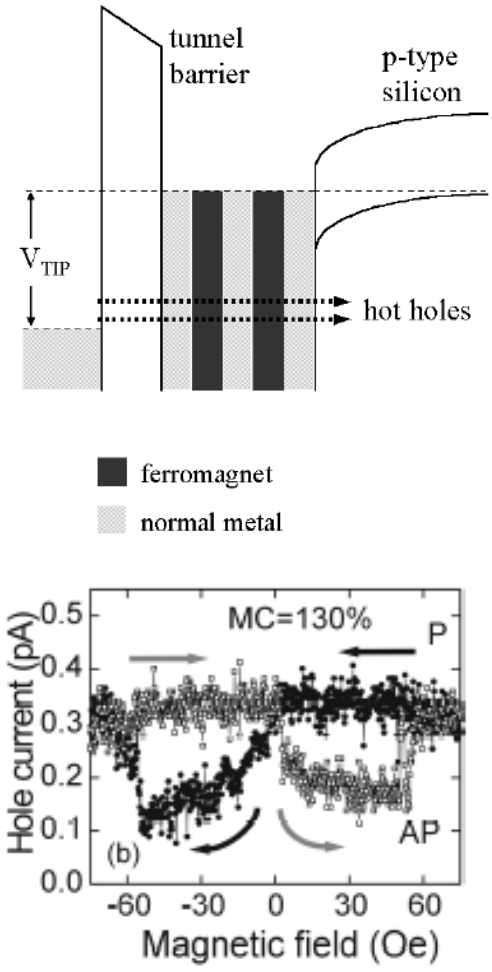

Figure 1.3: *(Top panel) Schematic energy diagram of ballistic hole magnetic microscopy of a magnetic trilayer on a p-type Si substrate. Holes are injected into the trilayer by tunnelling, spin-filtered during the transmission of the magnetic layers, and collected in the semiconductor. (bottom panel) Hole current vs magnetic field for p-Si/Au(7.0 nm)/NiFe(1.8 nm)/Au(7.0 nm)/Co(1.8 nm)/Au(3.0 nm) at +2 V and 10 nA hole injection current.(taken from [19])*

.

emitter current therefore higher collector signal could be achieved. This is one aspect that is investigated in this thesis.

One of the important parameters in spintronics is the spin-relaxation length. It is the length that describes how far a spin can travel before it loses its previous spin information. The materials that are used before like Au and Cu have long spin-relaxation lengths compared to the thicknesses that are used in the SVT. However, nonmagnetic transition metals such as Ta could differ in that respect since they have short inelastic lifetimes for both spin channels due to high number unoccupied states at hot-electron energies. The spin-relaxation length in a metal is proportional to the elastic scattering length which could be short due the number of unoccupied states to scatter into. We have therefore investigated this using SVTs' with Ta as nonmagnetic layer.

As will be shown in this thesis, the spin-valve transistor could also be used to inject and collect hot-holes therefore the hot-hole transport could be studied. One of the motivation to study the hot-holes is that many physical systems that use non-equilibrium carriers has both electrons and holes. The complete understanding of the transport requires the study of the hot-holes, too. In addition to that, a large asymmetry for majority and minority spin in the band structure of the ferromagnets for hot-holes is not observed which is considered to be the origin of the asymmetry in the attenuation lengths of the hot-electrons for majority and minority spin. Yet, a recent ballistic hole magnetic microscopy BHMM measurement shows spin-filtering of hot-holes in ferromagnets. Even for a NiFe(1.8 nm)/Au/Co(1.8 nm) spin-valve base, 130% magnetocurrent is observed in BHMM samples. With SVT, thicker ferromagnetic films can be studied which is not possible for BHMM to have more insight into the understanding of the spin-dependent hot-hole transport. Another motivation to study the hot-hole transport is that the conventional electronics work with both electrons and holes. This enables us to design circuitry with low power consumption and improved characteristics. Therefore, it is desirable for the spintronics applications to search for devices that can work with both electrons and holes.

The scattering processes are studied in SVT by measuring the transmitted carriers. The loss due to the scattering is reflected on the transmission allowing us to study the scattering mechanisms. As will be shown in this thesis, the SVT can be modified to study the scattering process by observing the scattered carriers. A similar approach was recently taken in BHMM [18, 19], where it is observed by reverse ballistic hole magnetic microscopy that the excitation of hot-holes are spin-dependent. With the modified SVT, the origin of the hot-electron spin asymmetry in attenuation lengths can be studied since the hot-electrons will create hot-holes via the the inelastic scattering processes.

The thesis starts with a description of the fabrication process of the spin-valve transistor which has already been used in earlier studies. The characterization of the device is presented where the basic transport measurements are

described under applied magnetic field.

In chapter 3, we will investigate the hot-electron transport in the SVT by focusing on the interfaces and the variation of the emitter current. First, the Schottky diodes which are used to inject and collect hot-electrons in the device will be discussed. Then, SVTs with Au and Cu spacers will be introduced in which the interfaces with ferromagnets are changed. For further analysis, we fabricate devices that has Cu/ferromagnet interfaces everywhere in the metal base which is expected to give better interface quality. Finally, the emitter current has been increased to study the effect on the magnetic sensitivity and the transfer ratio of the SVT.

The materials studied so far by the SVT had long spin relaxation lengths compared to the film thicknesses which is a measure of how far a spin can travel without losing its previous knowledge on its spin. The hot-electron transport in Ta and at Ta/ferromagnet interfaces are studied in chapter 4. The Ta in this respect differs from the metals used before. The Ta is a nonmagnetic transition metal which strongly effects the magnetic sensitivity and the transmission of the hot-electrons.

After studying the hot-electron transport in the SVT, we explore the spin-dependent hot-hole transport in the SVT. Even though no significant spin asymmetry is observed in the band structure of the ferromagnets like Co, spin- dependent transmission has been observed in spin-valve structures with ballistic hole magnetic microscopy [18, 19]. The SVT offers a different geometry for the study of hot-holes which is the main topic of the chapter 5. The silicon substrates are chosen to be p-type in order to inject and collect hot-holes. Spin-dependent hot-hole transmission in the NiFe/Au/Co spin-valve base is explored to determine the interface and volume contribution. Hot-hole scattering parameters in Co are investigated particularly. A model is introduced to analyze the spin-dependent hot-hole transmission.

After the discussion of the spin-dependent hot-electron and -hole transport in chapter 3, 4 and 5, the hot-holes that are created by inelastic scattering of injected hot-electrons will be discussed in chapter 6. For this purpose, an n-type Si is used for hot-electron injection and a p-type Si for the hot-hole collection. The spin-dependent behavior of the excited hot-holes will be investigated by varying the thickness of the NiFe layer in the spin-valve base of the device. Finally, a model is introduced to understand spin-filtering of the excited hot-holes in ferromagnetic films and compare it with the experimental results. The thesis ends with a summary of the conclusions in chapter 7.

Chapter 2

Experimental Procedures

In this chapter, we summarize the experimental procedures to fabricate and electrically characterize a spin-valve transistor which has been already described before in literature [31, 32]. First, the device fabrication will be presented focusing on the critical steps to realize an SVT. The samples are grown by a molecular beam epitaxy (MBE). The device is defined by a series of lithography, dry and wet etching steps. Finally, the electrical characterization of the device is given.

2.1 The spin-valve transistor fabrication

In this section, we will describe the realization of the SVTs which has a typical structure of Si/Au/NiFe/Au/Co/Cu//Cu/Si where "//"denotes vacuum metal bonding which will be discussed below. The Si substrates has to be cleaned before the deposition in the pre-bond cleaning step. Then, the deposition of the metals are done followed by a vacuum metal bonding in the MBE system [33]. The lithographical steps are used to define the emitter and base. Finally, the ohmic contacts are deposited for the electrical connections to the device.

A SVT relies on good Schottky diodes to inject and collect hot-carriers. Therefore, instead of growing Si on top of a thin metal film which will grow amorphously, an alternative fabrication technology based on metal bonding was developed. A schematic of the metal bonding (bottom) is shown in fig 2.1 with the bond robot (top) that is used for realizing the bond. In ultrahigh vacuum, the metal layers are deposited on the emitter Si first while the collector Si is protected from deposition by a shutter. Then, the shutter on collector Si is opened. The final nonmagnetic metal film layer, usually Au or Cu, is deposited simultaneously on both pieces until the surfaces of the metal coated Si wafers are brought in contact. A metal-metal bond is formed that sticks the two wafers together. The deposition and bonding is done under ultrahigh vacuum conditions in an MBE system. More details on bonding have been previously de-

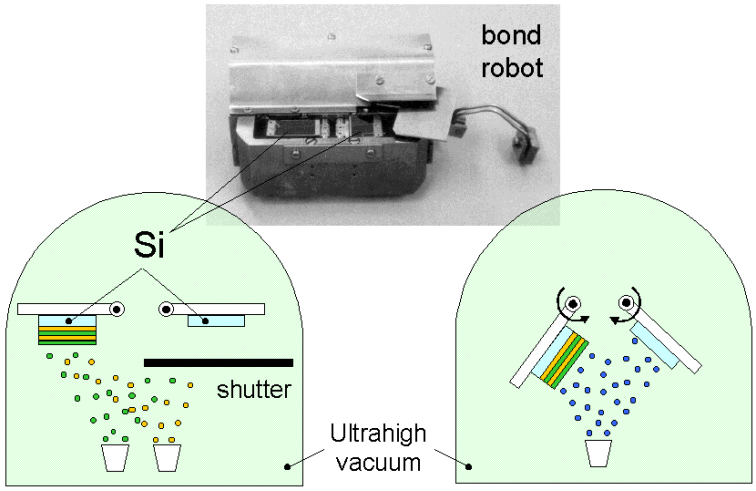

Figure 2.1: *The schematic of vacuum metal bonding in an ultra high vacuum chamber. The bond robot is also shown on top of the figure with two Si substrates on the plates. The illustration of vacuum metal bonding. See text for details.*

scribed [33].

Pre-bond cleaning

It is important to have clean and smooth surfaces to have a strong bonding. For this purpose, a thorough cleaning of the Si substrates are required. Silicon on insulator (SOI) wafers are used for emitter so that the built-in oxide layer provides an etch stop for emitter thinning stage. The device Si is 2.5 μm thick and has a low-doping ($N_d \simeq 10^{16}$ cm^{-3}) for good Schottky diode on the metal-base side of the SVT and a high-doping of $N_d \simeq 10^{21}$ cm^{-3} for an ohmic contact on the built-in oxide side. For the collector, double side polished (DSP) Si wafers with a low doping ($N_d \simeq 10^{16}$ cm^{-3}) are used. Both SOI and DSP Si wafers are 30 nm dry-oxidized and protected by 3.5 μm photoresist before they are sawn into 11.9 $\times$ 20.9 mm^2 emitter and 11.9 $\times$ 17.9 mm^2 collector pieces so that they can be fitted on the bond robot that is used for deposition. First, the organic contaminants and the photoresist are removed by 100% HNO_3. Second, the native oxide on the Si particles at the edge of the pieces, that are created by sawing, are removed by HF 1% so that these Si particles can be etched away with 5% TMAH (tetramethylammonium hydroxide). The Si particles on the edges would prevent the surfaces of the two substrates to come in contact during the bonding step. Finally, just before loading into the MBE system, the grown 30 nm silicon oxide

layer is removed by HF 50% (Si is H-terminated) and the samples are placed on the bonding robot as can be seen in fig 2.1. The bonding robot is immediately (within 5 minutes) transferred to the MBE system in order to avoid oxidation of Si since the H-termination will not protect the Si wafer long time.

Deposition and bonding

Molecular beam epitaxy is used to deposit metals on the Si substrates to realize spin-valve transistors (SVTs). MBE is chosen for growth since it gives better Schottky diodes than other techniques like sputtering. The energy of the atoms deposited in sputtering is higher than in MBE. Therefore, the interfacial mixing and the silicide formation [34] is higher in sputtering which results in a lower quality Schottky diodes.

We have used a DCA Metal 600 (MBE system) with a base pressure of 1×10^{-10} mbar. The electron guns (e-guns) are used to deposit all metals except copper. The deposition rate for metals evaporated by e-guns is around 1 $\mathring{A}$/sec. The copper is deposited by effusion cells with a rate between 0.1-0.2 $\mathring{A}$/sec which is due to the limitations of the effusion cell. It is found that films grown at high rates are smoother than lower rates. The growth chamber is cooled by liquid nitrogen to maintain ultrahigh vacuum and prevent the heating of the samples.

The Au/NiFe/Au(Cu,Ta)/Co metal multilayer is grown on emitter Si wafer while the shutter on the collector Si wafer is closed. The shutter is opened for the vacuum metal bonding [33] with Cu. In order to have a successful bonding, the sample holders should be parallel and the samples should come in contact with a certain force. The force for the pieces to come in contact can be controlled by the tension of the spring in the bond robot. It is important to have a good vacuum metal bonding because the bond interface is part of the metal base of the SVT and should not negatively effect the transport. In addition, a strong bond is required since the sample should survive the emitter thinning. During the emitter thinning, the mechanical stress on the emitter Si increases. If the bonding force is not stronger than this mechanical force, the bonded area will open and the Si substrates will be exposed to the Si etching chemical. Therefore, the full structure will be etched away leaving no structure to be processed.

Emitter definition

Cr/Au is deposited on the back side of the collector to protect it from being etched as can be seen in fig 2.2 on the left where the bonded structure is illustrated. The emitter definition starts by thinning down the Si on top of the built-in SiO2 with TMAH 10% at 85^0C which etches ≈0.75-1.0 μm/min and takes approximately 8-9 hours in total and the etching is stopped at SiO2 since TMAH 10% cannot etch SiO2. If the bonding is strong enough, the thinning down process does not effect the metal base area. We can continue to define emitter area for the structure in fig 2.2 (middle) by photolithographically. The

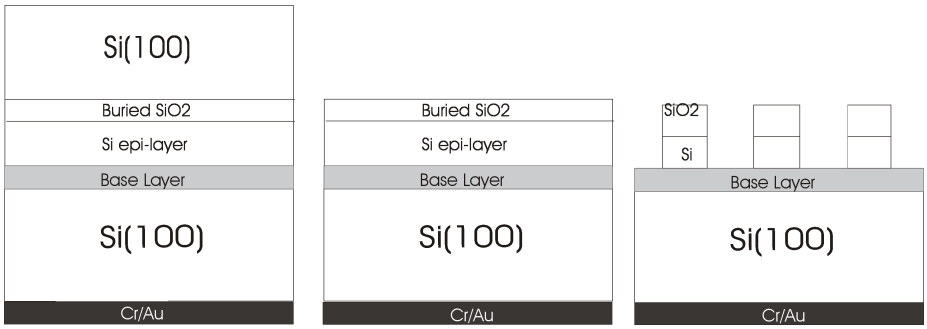

Figure 2.2: *The side view of the silicon on insulator (SOI) and double side polished silicon (DSP Si) bonded with a metal base on the left. In the middle, handle silicon of the SOI is removed. On the right, SiO2 and device Si is defined in blocks which is the emitter of the device.*

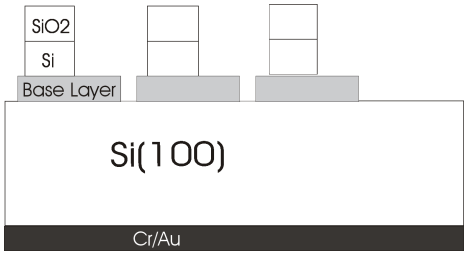

Figure 2.3: *The metal base of is defined with ion beam etching. See text for details.*

SiO2 that is not covered by photoresist is etched by BHF. After removing the photoresist by aceton, unprotected Si is etched by TMAH 10% at 85^0C that stops on the metallic multilayer as can be seen in fig 2.2 on the right. The blocks will be used as emitter.

Base definition

The base is defined by photoresist. The metallic area which is not covered by photoresist is removed by Ion Beam Etching (IBE) and the final result is seen in fig 2.3. It is important to note that the IBE damages the silicon in a way that Si becomes highly doped with metal impurities due to the high energy of the ions. The damage asserts itself as a leakage in the Schottky diodes. Therefore, we insert the structure in fig 2.3 in TMAH 10% at 85^0C for removing the damaged Si as much as possible (between 2-3 min). The sample could not be kept in TMAH too long since TMAH will attack the metal base for an extended time. The damage repair in TMAH will reduce the leakage current induced by IBE.

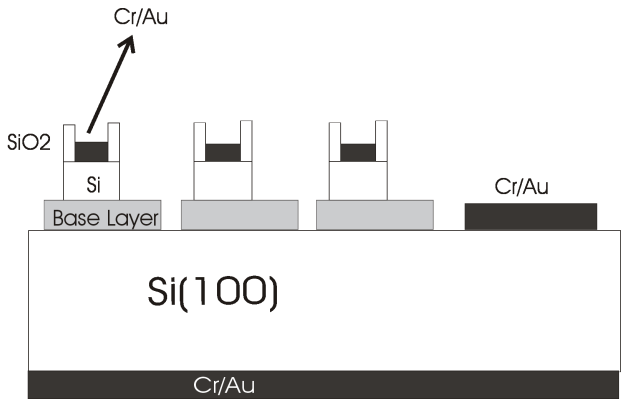

Figure 2.4: *The ohmic contact for emitter and collector is deposited. See text for details.*

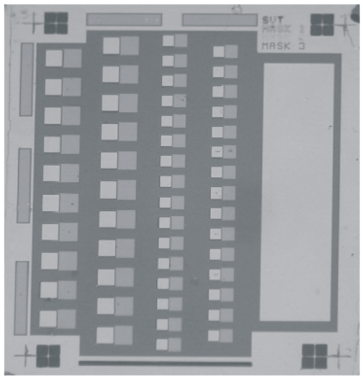

Figure 2.5: *An optical image of a chip with 52 spin-valve transistors (SVT). The big pad on the right is the common collector contact. The first two rows on the left are SVTs with 500×500 μm^2 emitters and 1000×500 μm^2 bases. The smaller devices on the right two rows have emitter and base size of 350×350 μm^2 and 750×350 μm^2, respectively.*

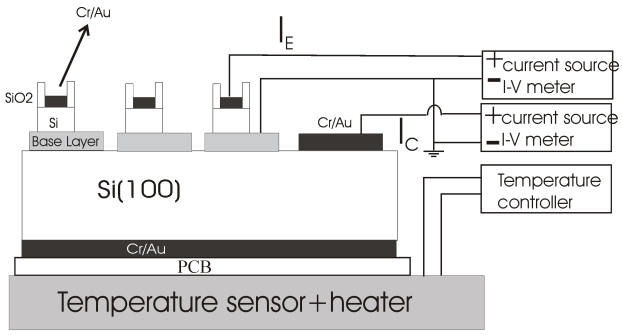

Figure 2.6: *The side view of the electrical connections to a spin-valve transistor on the chip. The base is grounded. The emitter and collector Si can be biased with any voltage depending on the type of the measurement. A temperature controller is attached to the back of the sample to measure and control the temperature.*

Ohmic contacts for emitter and collector

The final step is to put ohmic contacts on the emitter and collector Si to make electrical connections. We use one mask to define both emitter and collector contacts. For the emitter, photoresist on SiO2 has a hole smaller than the dimensions of the emitter and for the collector we have a big area left open in the photoresist where there are no emitter structures. The rest of the structure is covered by photoresist. Then, a Cr/Au (Au only for p-type Si) is sputtered which is followed by a lift-off process. The small area surrounded by SiO2 on emitter with Cr/Au (or Au) on it serves as the emitter contact and the big area with Cr/Au (or Au) on the bottom collector Si as the collector contact as can be seen in fig 2.4. In fig 2.5, a chip with 52 spin-valve transistors on it with one collector contact pad on the right edge of the sample is shown.

2.2 Electrical characterization of the device

In order to characterize the spin-valve transistor, we have used the measurement configuration as illustrated in fig 2.6. The metal base is grounded. The emitter and collector are connected to two separate I-V source/measure units which enables us to apply bias or inject current in the device and measure the resulting emitter current (I_E) and collector current (I_C). A temperature controller is connected which is in touch with a PCB that holds the device. The measurements can be done between 77 K and 300 K. The illustrated sample with the connections in fig 2.6 is inserted in between Helmholtz coils which can apply magnetic field in the plane of the metallic base.

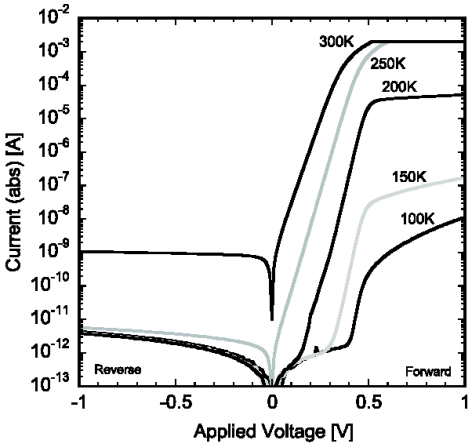

Figure 2.7: *Semi-log plot of the absolute value of the diode current for a n-Si/Au Schottky diode with an area of 700 × 350 μm^2 at different temperatures is shown.(T = 100, 150, 200, 250, and 300 K.)(taken from [32])*

.

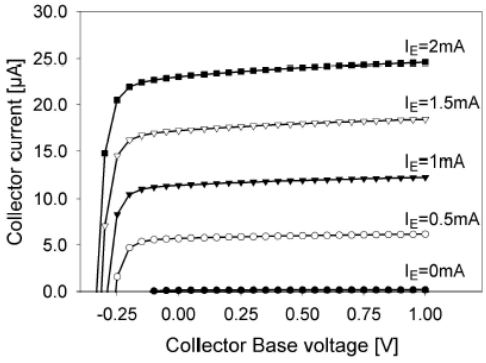

Figure 2.8: *The collector current as a function of applied bias across the collector diode for a SVT with n-Si/Au/n-Si structure.(taken from [31])*

.

Let us briefly describe the typical electrical measurements done on SVT's. The diodes can be characterized by I-V curves as shown in fig 2.7. We apply bias from -1.0 V to +1.0 V and measure the diode current. The diode is formed by a contact of n-type Si and nonmagnetic metal. The forward characteristics of the diode is exponentially dependence of the current to bias across the diode until it reaches a set compliance level 2 mA in this case at room temperature. The reverse of the diode, the current is as low as 1 nA. As the temperature drops, the current drops in all bias ranges since the contact resistance of the electrical connections increases. However, the general behavior does not change.

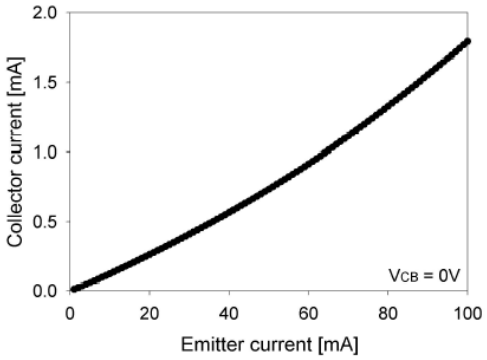

Figure 2.9: *The collector current of an SVT as a function of emitter current at zero applied bias across the collector diode.(taken from [31])*

.

The standard metal base characteristics for a SVT can also be measured. An example is shown in fig 2.8. The collector current I_C as a function of applied bias across the collector diode for a n-Si/Au/n-Si is shown for various emitter currents I_E. The collector current is independent of I_E for the positive applied bias. As the emitter current is increased, the collector current increases linearly. The linear relationship of the emitter current and the collector current can be observed in another measurement shown in fig 2.9. The collector current is measured as a function of emitter current at a constant applied bias across the collector diode (0 V in this case).

Finally, we present the characterization of a spin-valve transistor under an applied magnetic field where the spin-dependent transport of hot-carriers can be studied. The magnetic field is applied in the plane of the metal base of the SVT. We inject a constant emitter current typically a few mA. Usually no bias is applied to the collector current since the collector diode. The collector current is measured as a function of magnetic field which we sweep from -50 Oe to +50 Oe, and back to -50 Oe as in fig 6.5 for a SVT with the structure n-

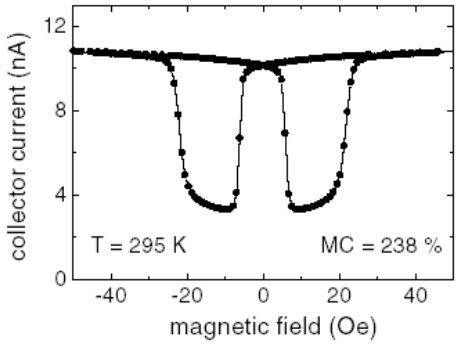

Figure 2.10: *The collector current as a function of applied magnetic field for a SVT with n-Si/Pt/NiFe/Au/Co/Au//Au/n-Si structure at 295 K and I_E = 2 mA. (taken from [13])*

.

Si/Pt/NiFe/Au/Co/Au//Au/n-Si. The emitter current is 2 mA and the temperature is 295 K.

Chapter 3

Hot-electron transport in the Spin-valve transistor: The role of interfaces

Hot-electron transport in the Spin-valve transistor (SVT) is studied by using different nonmagnetic spacers which results in different interfaces in the metal base of the SVT. The investigation starts with analyzing Schottky diodes which are used for carrier injection and collection. Then, the effect of Au and Cu nonmagnetic spacer (which changes the interfaces) on hot-electron transport will be presented. In the last part of the chapter, important parameters of the SVT such as the collector current, the transfer ratio and the magnetocurrent will be studied as a function of the emitter current.

3.1 Introduction

There are several factors that effects the performance of hybrid spintronic devices such as the ferromagnets in the spin-valve base, interfaces, the method of injecting and collecting carriers, etc. There are different methods of studying hot-electron transport in hybrid structures such as Ballistic Electron Emission Microscopy (BEEM) [21], Spin-valve Transistor (SVT) [2], and Magnetic Tunnel Transistor (MTT) [35]. BEEM, SVT and MTT has provided significant understanding of spin-dependent hot electron transport in thin film structures. However, the current transfer ratio has so far been limited to about 10^{-4} in SVT and BEEM, 10^{-3} in the MTT which has a single ferromagnetic base with on top a tunnel insulator and a ferromagnetic transition metal emitter electrode. The MC for this device is only 70-90% due to finite spin-polarized emitter current. The MTT with two ferromagnetic metal in the base has 400-600% MC which is comparable

to SVT. However, the transfer ratio is around 3x10^{-4}. The Spin-valve transistor differs from the other techniques in that it uses Schottky diode to inject carriers. BEEM and MTT use tunnelling to inject electrons. As the bias across the tunnel barrier increased for BEEM and MTT, the Fermi level with respect to the base increased. As the energy of the hot-electrons increased, the available number of density of states in the semiconductor collector increases. Therefore, the collector current and the transfer ratio increases rapidly. However, the increase is limited by the breakdown voltage of the tunnel barrier. In addition to this, as the energy of the carriers increased, the magnetic sensitivity decreases since minority carrier collection also increased. The Schottky diodes in a SVT have very high breakdown voltage [36] which enables us to have high current injection. As the emitter current increased in a SVT, the energy of the electrons stay constant. Hence, it should not suffer a lower magnetic sensitivity in high emitter current.

There have been extensive studies of hot-electron transport in the spin-valve transistor. Spin-dependent hot-electron transport in ferromagnets [22], spin wave contribution to spin asymmetry in ferromagnets [22], the role of Schottky barrier height on the transfer ratio [24] are a few examples of these investigations. The magnetic sensitivity in SVT is considered to be from the spin asymmetry of hot-electron attenuation lengths in ferromagnets such that the transmission of hot-electrons in ferromagnets such as NiFe, Co and CoFe is proportional to the thickness of the ferromagnets. Short hot-electron attenuation lengths are reported varying from 0.8 nm to 1.0 nm for minority spin and 2.1 nm to 4.3 nm for majority spin electrons [22]. Using these attenuation lengths, only spin scattering in a SVT using Co and $Ni_{80}Fe_{20}$ (will be denoted by NiFe in this thesis) with typical thickness of 2 and 5 nm would result in a transfer ratio of 10^{-2}. However, measured values are 10^{-4} or less. This difference is attributed to spin independent elastic interface scattering [13]. In fig 3.1, the collector current as a function of NiFe thickness for parallel and antiparallel alignment of base magnetic moments is shown [taken from [22]]. The solid lines represent a fit for only spin-dependent scattering in the ferromagnets. The dashed lines represent a fit for only spin-dependent interface scattering. The experimental data fits very well with spin-dependent scattering in ferromagnets. As the NiFe thickness goes to zero, parallel and antiparallel curves collapse on each other because only one ferromagnet is left. Note that at zero NiFe thickness, the extrapolated point for the solid line fit is 2.2 times lower than the SVT without NiFe in the metal base. This difference originates from the NiFe/nonmagnetic metal interfaces which does not exist at zero NiFe thickness. The elastic scattering at the interfaces changes the momentum distribution of the electrons which results in reduction of collected electrons [37]. Hence, if the transmission across the interfaces is improved, the transfer ratio might be improved significantly.

This has been demonstrated by a magnetic tunnel transistor [38] which uses a tunnel barrier as the emitter instead of a Schottky barrier. In fig 3.2, the

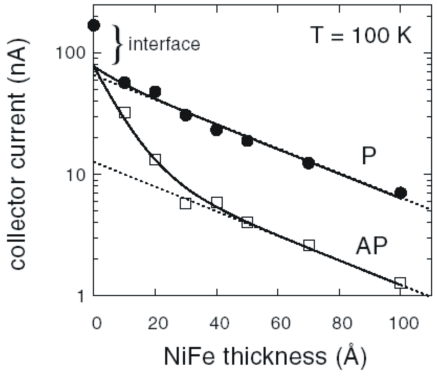

Figure 3.1: *The collector current for parallel I_C^P (circles) and antiparallel I_C^{AP} (squares) configuration of the magnetic moments of Co and NiFe as a function of NiFe thickness in SVTs. SVTs have Si/Pt(30 Å) emitter diode, NiFe(x Å)/Au(44 Å)/Co(30 Å) spin-valve base and a Si/Au(44 Å) collector diode. Solid and dashed lines, respectively, represent the extreme cases with only spin-dependent volume scattering or only spin-dependent interface scattering. The difference between the data point for a SVT with zero NiFe thickness and the cross of extrapolated curve for parallel alignment is due to the Pt/NiFe and Au/NiFe interfaces. T = 100 K. Taken from [22]*

.

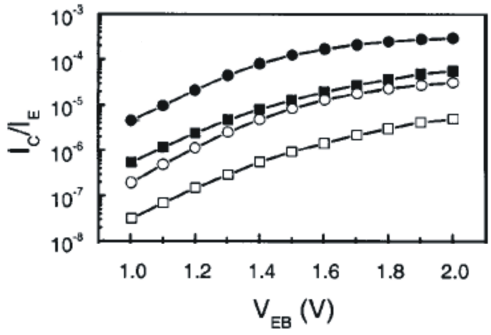

Figure 3.2: *Emitter bias dependence of the transfer ratio for an MTT with a CoFe (50 Å)/Cu (40 Å)/NiFe (50 Å) (circles) and a CoFe (50 Å)/Au (40 Å)/NiFe (50 Å) (squares) spin-valve base for parallel (solid symbols) and antiparallel (open symbols) alignment of the base magnetic moments. Taken from [38]*

.

transfer ratio as a function of emitter bias for a MTT with Cu/Al_2O_3 emitter, CoFe/Au(Cu)/NiFe spin-valve base and GaAs semiconductor as the collector is shown [taken from [38]]. The MTT with a CoFe/Cu/NiFe and CoFe/Au/NiFe spin-valve bases represented by circles and squares, respectively. Solid symbols are for parallel and open symbols are for antiparallel alignment of the base magnetic moments. It is clearly seen that the device with Cu spacer has 10 times higher transfer ratio for parallel and antiparallel alignment compared to the device with Au spacer. This is attributed to a better transmission at Cu/ferromagnet interfaces than Au/ferromagnet interfaces [38].

In this chapter, the aim is to study the transmission of hot-electrons at the (nonmagnetic metal)/ferromagnet interfaces in the SVT by changing the nonmagnetic metal spacer in the spin-valve base. For this goal, we report on the results of SVTs that has Cu/ferromagnet and Au/ferromagnet interfaces in the metal base. The study starts with analyzing the Schottky diodes of the SVTs that are used in this chapter. The Schottky barrier heights of the emitter and the collector of the devices are measured. Then, the transmission of hot-electrons is studied at Au/ferromagnet and Cu/ferromagnet interfaces by inserting Au and Cu as a spacer in the spin-valve base. Additional Cu layer is inserted between the spin-valve and the emitter diode in order to have all the interfaces with ferromagnets with Cu. Finally, the collector current, the magnetocurrent and the transfer ratio as a function of emitter current is investigated in a SVT with Si/Au/NiFe/Cu/Co/Cu/Si structure.

3.2 Experimental details

The typical structure of a SVT in this chapter consists of a n-Si/Au (3 nm) Schottky barrier as emitter, a n-Si/Cu(2 nm)//Cu(2 nm) schottky barrier as collector (where n denotes the doping type of silicon and "//"denotes the metal bonding) and a spin-valve base NiFe (5 nm)/NM/Co (2 nm) where NM denotes a nonmagnetic metal spacer. The device is realized by vacuum metal bonding in the Cu layer and is patterned by photolithography, dry and wet etching techniques as described previously in chapter 2.1. The active area of the emitter is 350 μm^2, the collector is 350 μm x 750 μm. The nonmagnetic metal spacer (NM) is changed to study the effect on the magnetocurrent and the transfer ratio. We have used Au, Cu and Cu/Au/Cu as NM. The device with Au(7 nm) spacer has 3 nm NiFe and 3 nm Co. The rest of the devices in this chapter have 5 nm NiFe and 2 nm Co. The magnetocurrent (MC) is defined as MC=(I_C^P - I_C^{AP})/I_C^{AP} where I_C^P (I_C^{AP}) refers to the collector current for parallel (antiparallel) states of spin-valve base. The transfer ratio is defined as I_C^P/I_E where I_E denotes the emitter current.

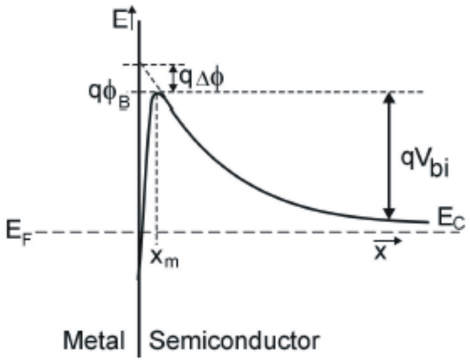

Figure 3.3: *Energy band diagram of a Schottky diode for a metal and an n-type semiconductor contact. E_F is the Fermi level, E is the energy, E_C is the conduction band minimum of the semiconductor, q is the charge, Φ_B is the Schottky barrier height, $\Delta\Phi$ is the energy lowering by image force effect, x is the position in the structure, x_m is the position of the Schottky barrier maximum in the semiconductor.*

3.3 Schottky diodes

The method of injection and collection of electrons determines many important properties of the SVT such as how many electrons can be injected in and collected from the device. The distribution and energy of electrons are also determined by the method of injection which effects how the electrons are transported in the metal base. It is important to understand how Schottky diodes work in order to see their effect on the properties of the SVT.

When a metal and a semiconductor are in contact, a Schottky diode is formed. In fig 3.3, the energy band diagram of a Schottky barrier is shown with no applied bias. $q\Phi_B$ is the Schottky barrier height which determines the energy with respect to E_F in the metal base of the electrons that are injected into the metal base of the emitter. E_F is the Fermi level. E_C is the conduction band minimum of the semiconductor. V_{bi} is the built in potential due to the contact. Due to the image force effects [39], the Schottky barrier height is lowered by $q\Delta\Phi$ and the barrier maximum is moved away from the interface to x_m. The Schottky barrier height $q\Phi_B$ is determined by the combination of the metal and the semiconductor. The typical values for n type Si and metal diodes are between 0.5 eV and 1.0 eV [39]. The thermionic emission theory [39] describes the current in a Schottky diode as:

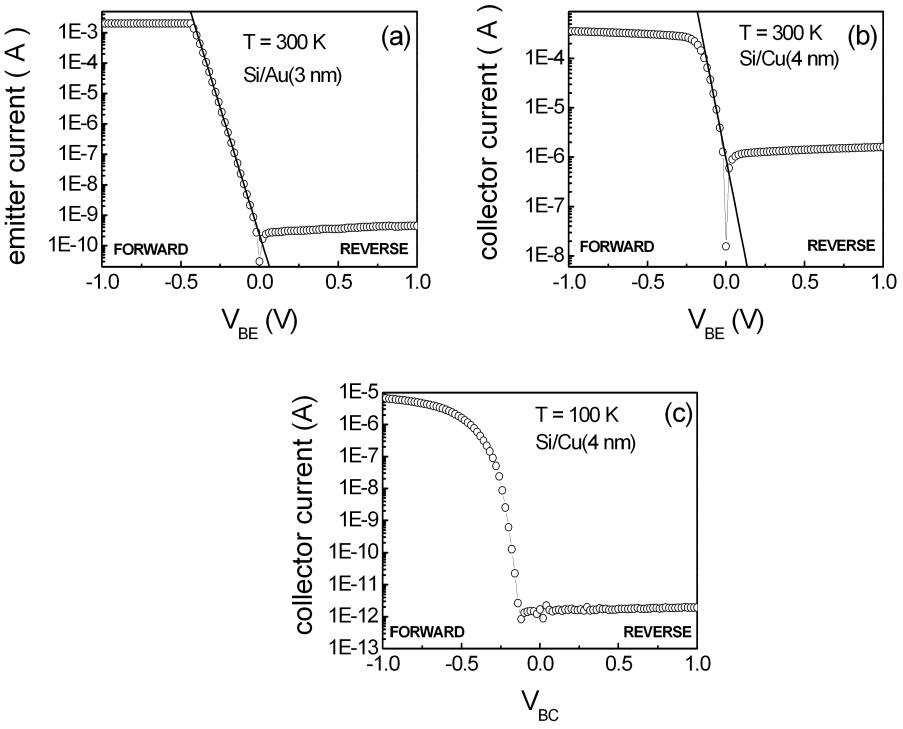

Figure 3.4: *(a) I-V characteristics of a typical Si/Au Schottky diode with an area of 350x350 μm^2 at 296 K. The compliance was set to 2 mA. The exponential region in forward bias is fitted by a solid line according to thermionic emission theory. (b) I-V characteristics of a typical Si/Cu Schottky diode with an area of 700x350 μm^2 at 296 K. The exponential region in forward bias is fitted by thermionic emission theory. (c) I-V characteristics of a typical Si/Cu Schottky diode with an area of 700x350 μm^2 at 100 K.*

	Au(3 nm)	Cu(4 nm)	Au(3 nm)/Cu(2 nm)	Au(7 nm)/Cu(2 nm)
Φ_B(eV)	0.80	0.64	0.67	0.72

Table 3.1: *Schottky barrier heights for four different Si metal contacts. T = 300 K.*

$$I_{diode} = AA^{**}T^2 \exp(-\frac{q\Phi_B}{kT})[\exp(\frac{qV}{nkT}) - 1] \tag{3.1}$$

where A is the diode area, A ** is the effective Richardson constant, T is the absolute temperature, q is the electron charge, Φ_B is the Schottky barrier height, k is the Boltzman constant, V is the applied voltage and n is the ideality factor.

In fig 3.4 (a), I-V characteristic of the Si/Au emitter diode of a SVT device which has Si/Au/ NiFe/Cu/Co/Cu//Cu/Si structure is plotted on a semi-log scale. It has a exponential characteristic in the forward bias and the compliance is set at 2 mA. The reverse bias has a very low current around 10^{-9} A. The exponential region of the diode can be fitted to thermionic emission theory current equation 3.1 to find the ideality factor. The Schottky barrier height can be calculated at zero bias by using equation 3.1. The Schottky barrier height is 0.805 eV which is the typical barrier height of Si/Au diodes and the ideality factor is 1.02. The ideality factor indicates the agreement with the thermionic emission theory and the experimental result. If the ideality factor is close to 1, it means that the electrons are emitted by thermionic emission. The emitter diode in SVT operates in forward bias. In fig 3.4 (b) and (c), the Si/Cu collector diode of the same SVT is shown at 296 K and 100 K respectively. It has a Schottky barrier height of 0.61 eV with an ideality factor of 1.05. This diode also shows thermionic emission. At low temperature the thermionic emission do not change so that the Schottky barrier height remains unchanged. At 0.25 V, the ohmic contact resistance starts to dominate where the exponential regime ends. Therefore, the compliance is not reached. At room temperature, the reverse bias current is around 10^{-6} A. The reverse bias current is due to the fact the Schottky barrier height is low enough that thermally activated electrons can overcome the barrier height. In the SVT, the collector diode is operated at zero bias. However, there is a shift to reverse bias direction due to the current passing in the base. The emitter current is 2 mA in most experiments. The transfer ratio is on the order of 10^{-4} so that only a small fraction of the current (0.5 μA) is collected by the semiconductor. Almost 2 mA of the current is collected by the contact to the metal base. Because of this current, there is a voltage drop. The voltage drop in the base shifts the operating voltage for the collector diode by about 0.2 V at 100 K. Therefore, the reverse bias current of the collector diode of the SVT is very important. The reverse bias current at such voltages should be much lower than the hot-electron current. The hot-electron collector current is expected to be around 10^{-7} A. Hence, the experiments are done at low temperature. In fig 3.4 (c), the reverse bias current at 100 K drops to 10^{-11} A or less. The forward bias current drops almost 1 order of magnitude because the contact resistance increases.

In table 3.1, the Schottky barrier heights of the diodes that are used in this chapter are given. Si/Au(3 nm), Si/Au(3 nm)/Cu(2 nm) and Si/Au(7 nm)/Cu(2

nm) are used as the emitter diodes. Si/Cu(4 nm) is used as the collector. The Si/Au(3 nm) diode has a Schottky barrier height of 0.80 eV. The Si/Cu(4 nm) diode has a Schotkky barrier height of 0.64 eV. The collector diode has a lower Schottky barrier height than the emitter current. The Si/Au(3 nm)/Cu(2 nm) and Si/Au(7 nm)/Cu(2 nm) Schottky diodes have Schottky barrier heights of 0.67 eV and 0.72 eV respectively. The barrier heights of these two diodes are in between the barrier heights of the Si/Au(3 nm) and the Si/Cu(4 nm) diodes. This indicates that Cu and Au intermixes so that the Schottky barrier is reduced. This has some consequences which will be discussed in the section 3.4.

3.4 Spin-valve transistors with Cu and Au spacer

In this section, the results of SVTs with different nonmagnetic spacers are shown. The effect of nonmagnetic spacer and interfaces on the magnetocurrent and the transfer ratio is studied.

Magnetocurrent

In fig 3.5, the magnetic field dependence of the collector current at I_E=2 mA of four SVT's with different spacers Au (10 nm), Au (7 nm), Cu (10 nm) and Cu (3 nm)/Au (4 nm)/Cu (3 nm) are shown. The SVTs in fig 3.5 (a), (c) and (d), have 5 nm $Ni_{80}Fe_{20}$ and 2 nm Co. In fig 3.5 (b), SVT has 3 nm $Ni_{80}Fe_{20}$ and 3 nm Co for the ferromagnetic layers. Data is taken at 100 K for devices in (b), (c), (d) and at 81 K for device in (a). When the Co and $Ni_{80}Fe_{20}$ magnetizations are aligned parallel at large fields (100 Oe), a high collector current is observed. As the field changes direction, first the magnetization of $Ni_{80}Fe_{20}$ switches resulting in an antiparallel magnetic alignment, and a low collector current is measured. When the field is further increased the Co magnetization switches in the direction of $Ni_{80}Fe_{20}$ magnetization such that a high collector current is achieved again. If the applied field is swept back again from -100 Oe to 100 Oe, the same behavior is observed. Fig 1(a) shows the collector current as a function of applied field for a SVT with Au (10 nm) spacer. The magnetocurrent is 350% and the transfer ratio is $1.2\text{x}10^{-4}$. The magnetocurrents are 384%, 308% and 256% for SVTs with Au (7 nm), Cu (10 nm) and Cu (2 nm)/Au (3 nm)/Cu (2 nm) spacers in fig 3.5 (b), (c) and (d). MC for devices in (a), (c) and (d) are somewhat lower than the MC of the SVT with Au (7 nm) spacer in (b). However, this is due to the fact that the SVT with Au (7 nm) spacer has 3 nm $Ni_{80}Fe_{20}$ and 3 nm Co while the SVT's in fig 3.5 (a), (c) and (d) have 5 nm $Ni_{80}Fe_{20}$ and 2 nm Co. The magnetocurrent can be calculated for these thicknesses using exponential dependence of the collector current on the hot-electron attenuation lengths, using well established values of 0.9 (1.0) nm for minority spin and 2.1 (4.3) nm for majority spin

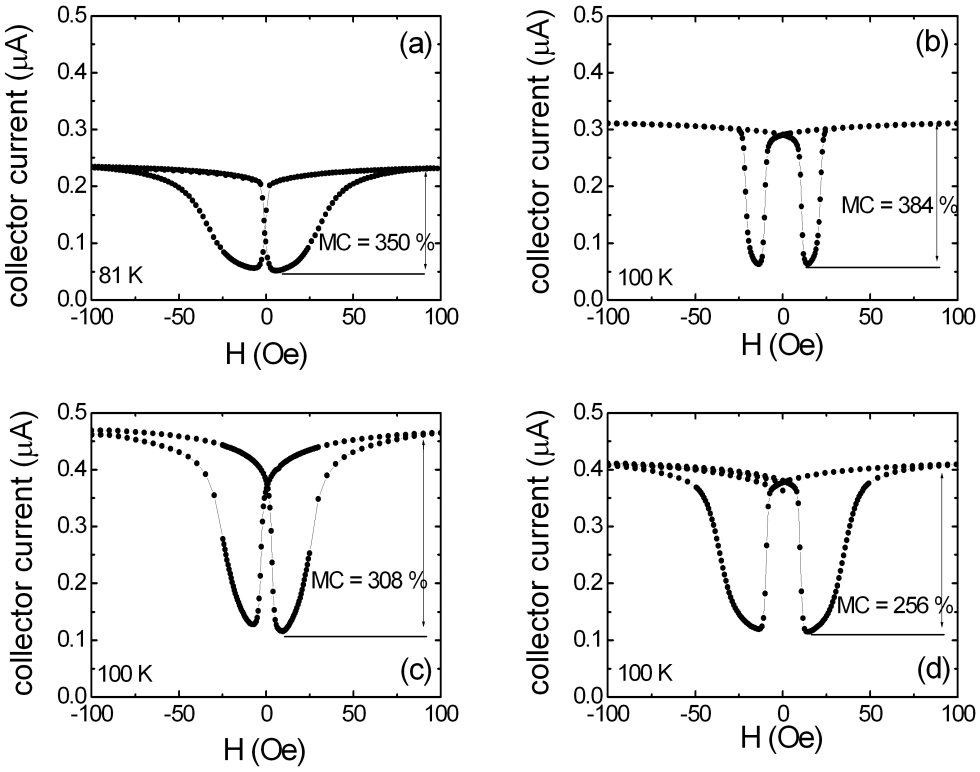

Figure 3.5: *Collector current as a function of magnetic field for a SVT with Si/Au/NiFe/NM/Co/Cu//Cu/Si structure where NM is (a)Au (10 nm),(b)Au (7 nm), (c) Cu (10 nm) and (d)Cu (3 nm)/Au (4 nm)/Cu (3 nm). NiFe is 5 nm and Co is 2 nm for devices in (a), (c) and (d). NiFe is 3 nm and Co is 3 nm for the device in (b). I_E = 2 mA. T = 100 K ((b), (c), (d)). T = 81 K ((a))*

in Co ($Ni_{80}Fe_{20}$) [13]. The calculated MC for the device in fig 3.5 (b) is 330%, while for the devices in (a), (c) and (d), a MC of 271% is calculated. Therefore, the difference in the magnetocurrents between fig 3.5 (b) and (a,c,d) is due to different thicknesses of ferromagnets in the devices. Note that there is also some difference in switching behavior of the ferromagnets between the four devices. While the layer growth could be different, also the coercivity of the ferromagnets are different because the thicknesses are not same. However, full or almost full antiparallel alignment is still obtained for all four devices.

Transfer ratio

The second important parameter to look at is the transfer ratio. It is $1.2\text{x}10^{-4}$ at I_E = 2 mA in fig 3.5 (a) for a SVT with Au (10 nm) spacer. In fig 3.5 (b), the

	Au(10 nm)	Au(7 nm)	Cu(10 nm)	Cu(3 nm)/Au(4 nm)/Cu(3 nm)
MC(%)	350	384	308	256
$\alpha(10^{-4})$	1.2	1.6	2.4	2.1

Table 3.2: *Magnetocurrent (MC) and transfer ratio α of SVT with different nonmagnetic(NM) spacers. The structure of SVTs is as Si/Au/NiFe/NM/Co/Cu//Cu/Si.*

transfer ratio is 1.6x10^{-4}. When the Au is replaced by Cu as in fig 3.5 (c), the transfer ratio is increased by a factor of 2.0 (1.5) to 2.4x10^{-4} compared to fig 3.5 (a)((b)). In a fourth device in fig 3.5 (d) in which Cu/Au/Cu spacer is used, the transfer ratio is 2.1x10^{-4} which is in between the transfer ratio of the devices in fig 3.5 (a) and (c). As mentioned above, the thicknesses of ferromagnets in fig 3.5 (b) and fig 3.5 (a,c,d) are different. However, using the exponential dependence of the collector current on hot-electron attenuation lengths as it is done for the magnetocurrent above, it can easily be calculated that the difference in transfer ratio is expected to be less that 3%. Therefore, the difference in thickness of the ferromagnets for both devices does not affect the transfer ratio. It is also important to mention that hot-electron attenuation length for Au and Cu are around 20 nm [40, 41, 42] which is larger than the thicknesses of the layers that are used here. Therefore, the hot-electron attenuation in the Au or Cu spacer has 5 times lower effect than the hot-electron attenuation in the ferromagnets on the transfer ratio. We therefore attribute the improvement in the transfer ratio to better transmission through Cu/FM interfaces compared to Au/FM interfaces. The transfer ratio for the device with Cu is 2.0 (1.5) times higher than the device with Au (10 nm) ((7 nm)) spacer, which is in sharp contrast to the factor of 10 difference reported in literature in MTT's with Cu and Au spacers [38]. In this respect it should be mentioned that for the SVT prepared by evaporation it has previously been established that Au/FM interfaces contribute to the attenuation by no more than a factor of 2.2 [22]. Improvement of the interface quality therefore can lead to an enhancement of the transfer ratio by a factor of 2.2 at best. Note that the device in fig 3.5 (d) has Cu/FM interfaces, which results in a higher transfer ratio than the SVT with Au spacers. However, it has a lower transfer ratio than the SVT with pure Cu spacer since there are two additional Au/Cu interfaces as well. For the SVT with Cu/Au/Cu spacer, we cannot rule out some intermixing of Au and Cu during the processing of the SVT in which the sample goes to temperatures of 390 K. In table 3.2, a summary of the devices that are discussed above are given. It is shown that by using Cu as nonmagnetic spacer, the transfer ratio can be improved by about a factor of 2 without losing much magnetic sensitivity compared to the SVT with Au(10 nm) spacer.

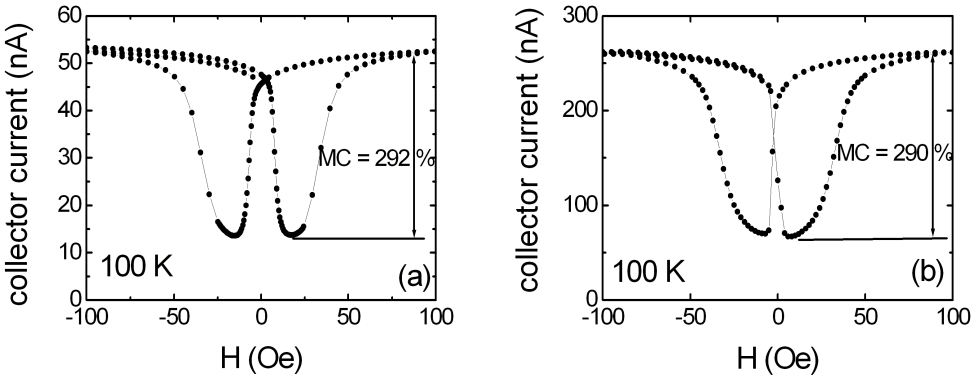

Figure 3.6: *Collector current as a function of magnetic field of a SVT with Si/Au(x nm)/Cu(2 nm)/NiFe(5 nm)/Cu(2 nm)/Au(3 nm)/Cu(2 nm)/Co(2 nm)/Cu(2 nm)//Cu(2 nm)/Si structure (a) x = 3 (b) x = 7. T = 100 K. I_E = 2 mA.*

	Si/Au(3 nm)	Si/Au(3 nm)/Cu(2 nm)	Si/Au(7 nm)/Cu(2 nm)
$\Delta\Phi_B$(eV)	0.16	0.03	0.08
MC(%)	256	292	290
$\alpha(10^{-4})$	2.1	0.27	1.3

Table 3.3: *MC and α of SVTs with different emitter diodes with NiFe/Cu/Au/Cu/Co spin-valve base and a Cu/Si collector diode. T = 100 K. I_E = 2 mA.*

3.5 Insertion of additional Cu/FM interfaces

In order to improve the transfer ratio more, all interfaces with ferromagnets could be with Cu by inserting Cu layer in between Si/Au emitter diode and NiFe. Hence, the device will have a Si/Au/Cu/NiFe/Cu/Au/ Cu/Co/Cu//Cu /Si structure. The spacer was chosen to have Au in between because ferromagnetic coupling is observed with pure Cu spacer. The coupling in fig 3.5 is not observed. However, a number of devices with Cu spacer which are not presented here, have shown to have strong coupling.

In fig 3.6 (a), the collector current as a function of magnetic field for a SVT with Si/Au(3 nm)/Cu (2 nm)/NiFe(5 nm)/Cu(3 nm)/Au(4 nm)/Cu(3 nm)/Co(2 nm) /Cu(2 nm)//Cu(2 nm)/Si is shown. The magnetocurrent is 292%. However, the transfer ratio is only 0.27x10^{-4}. The transfer ratio is lower than the device in fig 3.5 (c) without Cu after emitter diode. This is rather surprising since Cu/ferromagnet interface is shown to have better transmission than Au/ ferromagnet interface as discussed before. This must be caused by another fac-

Base	Φ_e(eV)	Φ_c(eV)	$\Delta\Phi_B$(eV)	α(x10^{-4})	MC(%)
Pt/s.v./Pt	0.88	0.86	0.02	0.01	213
Pt/s.v./Au	0.88	0.83	0.05	0.07	260
Pt/s.v./Cu	0.87	0.61	0.26	1.06	218
Au/s.v./Au	0.81	0.80	0.01	0.10	204
Au/s.v./Cu	0.82	0.69	0.13	1.18	230

Table 3.4: *Properties of SVTS with different combinations of emitter and collector diodes with NiFe/Au/Co spin-valve base. T = 290 K.* $I_E = 2mA$. *[24]*

tor. If the Schottky barrier heights of the device is measured, the emitter and the collector diode have Schottky barrier heights 0.67 eV and 0.64 eV respectively. The emitter diode barrier height is around 0.13 eV lower than what is expected from a Si/Au Schottky diode and it is just above (0.03 eV) that of the Si/Cu diode. It seems that Au and Cu have mixed and this lowered the Schottky barrier height. Therefore, the Schottky barrier height difference between the emitter and the collector is reduced. To overcome this problem, another device has been fabricated with emitter diode which has a Si/Au(7)/Cu(2) sturucture. The Au layer has been grown 7 nm so that it is thick enough to prevent Cu to be in contact with Si. In fig 3.6 (b), the collector current as a function of the magnetic field is plotted. The magnetocurrent is 290% and the transfer ratio is 1.3x10^{-4}. The transfer ratio is improved 5 times compared to the device in fig 3.6 (a). However, it is still lower than that of the device in fig 3.5 (c) with no Cu on emitter diode which has a transfer ratio of 2.4x10^{-4}. If the emitter and the collector Schottky barrier heights for the device is measured, the answer for the low transfer ratio is revealed. The emitter and the collector Schottky barrier heights are 0.720 eV and 0.64 eV respectively. Therefore, the emitter Schottky barrier height Φ_B is still lower than for Si/Au diode barrier height. In table 3.3, the table summarizes the results for the devices which has Si/Au(3 nm) (the device in fig 3.5 (d)), Si/Au(3 nm)/Cu(2 nm) (3.6 (a)) and Si/Au(7 nm)/Cu(2 nm) (3.6 (b)) emitter diodes. All three devices have NiFe/Cu/Au/Cu /Co spin-valve base and a Si/Cu(4 nm) collector diode. In the table, the magnetocurrent for all devices is close to each other since the spin-valve base is the same. The device with Si/Au emitter has a little bit lower MC which is because the antiparallel alignment for this device is not fully achieved. However, the transfer ratio for the devices with Si/Au(7 nm)/Cu(2 nm) and Si/Au(3 nm)/Cu(2 nm) emitter diodes is half and one fifth of the transfer ratio of the device with Si/Au(3 nm) emitter diode respectively.

In order to understand the effect of Schottky barrier heights on the magnetocurrent and the transfer ratio, we have a look at SVTs with different emitter

and collector diodes (table 3.4) that are reported before [24]. The spin-valve base is kept same for all. The magnetocurrents for all devices are between 200% and 260% since they have the same spin-valve base. However, the transfer ratio varies two orders of magnitude from device to device. The devices with Pt and Au collector are at least one order lower than the devices with Cu collector. This is due to larger number of states available in the collector semiconductor. The electrons which are injected at an energy just above the collector barrier (small $\Delta\Phi_B$), the density of states in the conduction band of the semiconductor collector is small. Therefore, only few electrons can be collected. When the energy of the injected electrons becomes larger (large $\Delta\Phi_B$), the density of states increases and more electrons can enter the semiconductor. The same trend is also observed for the devices in table 3.3.

3.6 The effect of emitter current on the properties of the Spin-valve transistor

The collector current in a SVT depends on several factors such as emission and collection of electrons by Schottky diodes, the Schottky barrier height difference between the collector and emitter diodes, quantum mechanical reflections at the collector, attenuation due to phonon scattering in the base at the emitter and the collector. The most important contributions to scattering comes from the scattering at the interfaces and spin-dependent scattering in the ferromagnets. All these factors can be expressed in the transfer ratio which is the proportionality constant in between the emitter current and the collector current. In the previous section, the transfer ratio is enhanced by using Cu as spacer which enables a better transmission at Cu/ferromagnet interfaces than Au/ferromagnet interfaces. In this section, the emitter current will be increased to see the effect of it on the collector current, the transfer ratio and the magnetocurrent.

In fig 3.7 (a), the emitter current dependence of the collector current (top panel), the magnetocurrent (middle panel) and the transfer ratio (bottom panel) of a SVT with Cu spacer are shown. For the collector current (top panel) results are shown when the Co and NiFe magnetizations are parallel (P) and when they are aligned antiparallel (AP). For both configurations, the collector current increases linearly with emitter current. A collector current of 64 μA is reached at 200 mA emitter current for parallel alignment. The magnetocurrent remains constant around 300 % as the emitter current increased. The transfer ratio of the SVT is 2.4x10^{-4} at 2 mA and as emitter current increased, the transfer ratio improves to 3.2x10^{-4} at 200 mA. We thus conclude that the main properties of the SVT, i.e. the transfer ratio and the magnetocurrent, remains unchanged and that the collector current scales linearly with the emitter current.

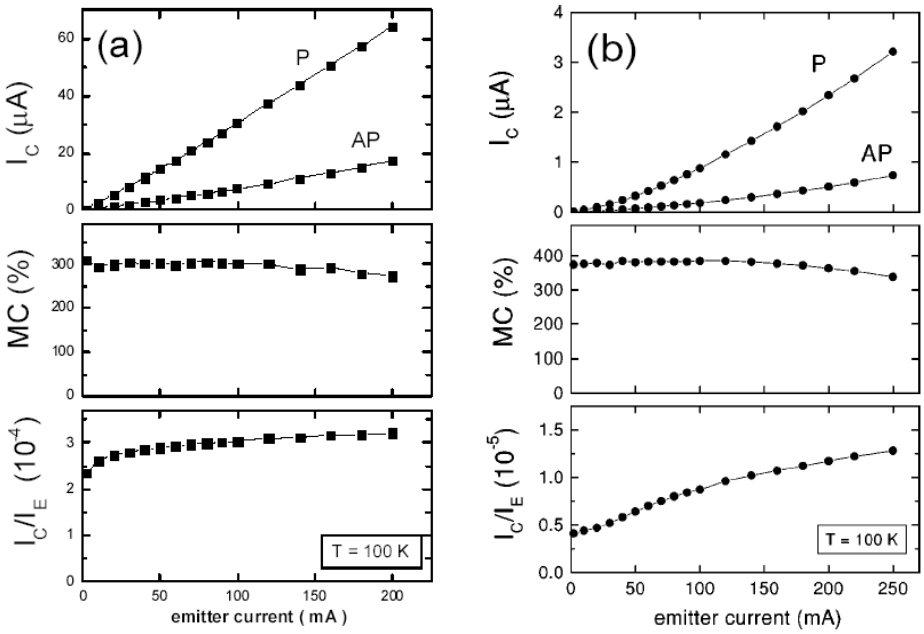

Figure 3.7: *The collector current (top panel), the magnetocurrent (middle panel) and the transfer ratio (bottom panel) as a function of emitter current for two different SVTs with a (a) Si/Au/NiFe/Cu/Co/Cu/Si (b) Si/Au/NiFe/Au/Co/Au/Si [43] structure. T=100 K.*

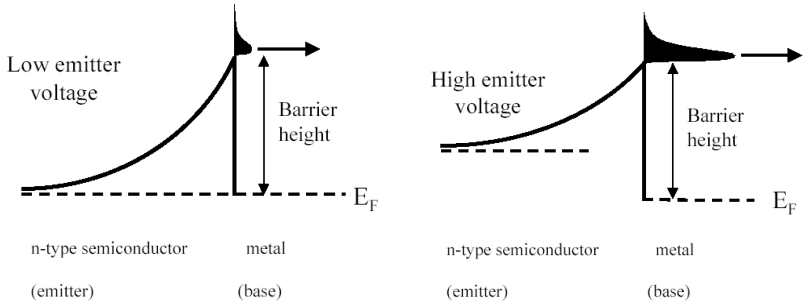

Figure 3.8: *Schottky diode energy band diagram with low bias (left) and high bias (right). E_F is the Fermi energy. The distribution of the hot-electrons over the Schottky barrier height maximum is shown. The peak of the hot-electron energy does not change for low and high bias. Only the number of electrons for high bias is more than the number of electrons for low bias.*

The results can be understood if the energy of the hot electrons that are used in the transport are considered. In fig 3.8, the picture of low and high bias are shown. To increase the emitter current the Fermi level of the silicon emitter is raised, such that more electrons are emitted over the Schottky barrier maximum. However, the Schottky barrier maximum with respect to Fermi level of the metal base is not significantly changed by the application of the emitter bias voltage for low and high bias. Therefore, the energy of the hot-electrons with respect to metal base is not changed, which results in an almost constant magnetocurrent and transfer ratio. A small increase in the transfer ratio at low bias (low emitter current) in fig 3.7 (a) is caused by the effect of image forces (which is not shown in fig 3.8) on the Schottky barrier height. In a Schottky diode, the barrier maximum enhancement is around 10-20 mV [39], which is small compared to the Schottky barrier height of about 0.8 eV for a Si/Au contact.

The increase in the transfer ratio due to the barrier maximum enhancement with respect to the metal base of the SVT can be seen better in a SVT which has Si/Au barriers for both emitter and collector. In that case, the hot-electon energy is comparable to the height of the collector Schottky diode. In this configuration, the electrons enter the states near the bottom of the conduction band of the collector Si and a slight change of the hot-electron energy will have a more strong impact on the transfer ratio. In fig 3.7 (b), this is observed for the SVT with Si/Au/NiFe/Au/Co/Au/Si structure. Especially at low emitter current, the collector current for both parallel and antiparallel configuration in not linear. The collector current starts in the nanoampere regime and reaches 4 μA at 200 mA. The increase for both alignment is similar therefore the MC remains contant around 400%. The striking parameter is the transfer ratio. Its value triples from 0.4x10^{-5} to 1.3x10^{-5} due to the Schottky barrier enhancement by the effect of image forces.

The magnetotransport characteristics of the SVT that is presented here depends on the emitter current or bias in a distinctly different way than for the MTT. The energy of the hot-electrons in the MTT increases as the emitter voltage increases. The spin-asymmetry of the hot-electron attenuation length for typical transition ferromagnets such as NiFe, CoFe, Co is reduced at higher hot-electron energy. Therefore, the MC of a MTT is significantly reduced at high emitter voltage (current). In contrast, it is shown here that for the SVT the emitter current can be increased without significant changes in the hot-electron energy such that the large MC is preserved.

3.7 Conclusion

The effect of nonmagnetic spacer on hot-electron transport has been presented in this chapter. It has been shown that the transfer ratio of the SVT can be im-

proved by using a spacer which offers a better transmission across the ferromagnet/nonmagnet interface. A second way to have a higher transfer ratio is also introduced. The amount of current that is injected from the emitter has been increased and higher transfer ratio as well as high collector currents are achieved with an almost constant magnetic sensitivity.

The investigation started by studying the Schottky diodes. The Si/Au and Si/Au/Cu Schottky diodes as the emitter and Si/Cu Schottky diode as the collector are used in this chapter. Si/Au has a barrier height of 0.80 eV. However, Si/Au/Cu Schottky diodes show a lower barrier height than Si/Au diode. This indicates that Au and Cu intermixes and Cu makes a contact with Si which lowers the Schottky barrier height in the emitter. Even 7 nm thick Au in Si/Au(7 nm)/Cu(2 nm) diode does not completely prevent the intermixing resulting in a 0.72 eV barrier height. The Si/Cu collector has a lower (0.65 eV) Schottky barrier height so that it has high reverse bias current around 10^{-6} A at room temperature. Hence, the measurements are done at low temperatures where the reverse bias current is around 10^{-11} A.

We have shown that a SVT with a NiFe/Cu/Co spin-valve base has a higher transmission than a SVT with a NiFe/Au/Co spin-valve base. The transfer ratio is 2 times higher for the former device which is in sharp contrast to the factor of 10 difference reported [38] in MTT's with Cu and Au spacers. The improvement is attributed to better transmission at Cu/ferromagnet interfaces than Au/ferromagnet interfaces. The magnetic sensitivity of both SVTs has high magnetic sensitivity above 250%. A third device with a Cu/Au/Cu nonmagnetic spacer has a transfer ratio between the transfer ratios of the devices with Au and Cu spacers. It shows that two more interfaces cause additional scattering sources. However, the transfer ratio for this device is still higher than the device with Au spacer. It has a comparable magnetocurrent with the first two SVTs.

Then, additional Cu/ferromagnet interfaces were inserted after Si/Au emitter in order to have Cu/NiFe/Cu/Au/Cu /Co/Cu structure in which ferromagnets have only interfaces with Cu. The SVTs' showed lower transfer ratio than NiFe/Cu/Co since the Schottky barrier height of emitter is reduced. This suggested that Au and Cu in Si/Au/Cu diode intermixes. Due to the lowered Schottky barrier height of the emitter diode, the hot-electron energy injected is closer to the value of the collector diode Schottky barrier height with respect to the metal base. Therefore, the hot-electrons enter the lower part of the conduction band of the collector semiconductor where less density of states is available. The enhancement in transmission of hot-electrons at interfaces due to the Cu/ferromagnet interface after the emitter diode is compensated by the lowered hot-electron energy. The magnetocurrent is as high as the SVTs with Si/Au/NiFe/Cu/Co/Cu/Si structure since the ferromagnets are kept the same.

The emitter current of a SVT with Si/Au/NiFe/Cu/Co/Cu//Cu/Si struc-

ture is changed to study the properties of the device such as the collector current, the transfer ratio and the magnetocurrent. An almost linear dependence of the collector current is observed and the collector current reaches values up to 64 μA. Since the increase is equally strong for parallel and antiparallel magnetic states of the spin-valve base, the resulting magnetocurrent is constant around 300% at low and high emitter current. There has been a slight improvement in the transfer ratio at high emitter current. This is due to the fact that the Schottky barrier maximum is enhanced because of the image forces. However, the enhancement is small compared to energy of the electrons.

Chapter 4

Hot-electron transport through Ta films and interfaces

In this chapter, hot-electron transport in a nonmagnetic metal Tantalum is studied with the SVT. A model is introduced for spin relaxation in Ta and spin-filtering at the Ta/ferromagnet interfaces. Transmission of hot-electrons in the Ta film and at the Ta/ferromagnet interface is discussed. Spin-transport in Ta is investigated in SVTs with NiFe/Ta/Co and NiFe/Au/Co/Ta spin-valve bases. The multilayers in the SVT are characterized structurally and magnetically with Transmission Electron Microscopy (TEM) and Vibrating Sample Magnetometer (VSM). The chapter ends with discussion of the spin relaxation in Ta and comparison with the model.

4.1 Introduction

Hot-electron spin-transport has been widely studied in nonmagnetic and ferromagnetic metal films and interfaces [44]. The spin transport in a ferromagnetic metal film depends on the magnetic ordering of the spins of the material, but it depends also on the energy of the carriers that are used in the transport. The ferromagnetic metals have an asymmetry in the density of states for the minority spin and majority spin. This leads to spin-dependent transport in the films [13] as well as at the interfaces formed with other metals [44]. Noble metals like Au and Cu, there is no spin-asymmetry in the density of states. Therefore, there is no spin-dependent scattering in Au and Cu. However, at interfaces with ferromagnetic metals, there might be spin-dependent transmission due to the mismatch of the density of states at the interface of the nonmagnetic and ferromagnetic metal.

Nonmagnetic metals are known to have long spin-relaxation lengths; 350 nm for Cu [45] and 600 nm for Al [46] at room temperature. The spin relaxation

lengths reported are much larger than the thicknesses in the hot-electron devices and techniques. In metals, the spin relaxation is due to the spin-orbit coupling [47, 48] via the impurity spin-flip scattering and the phonon-conduction electron scattering. Elliot has showed [47] that the elastic scattering time τ_e can be related to the spin relaxation time τ_{sr} with the spin-orbit interaction strength defined as $(\frac{\lambda}{\Delta E})^2$:

$$\frac{\tau_e}{\tau_s r} \propto (\frac{\lambda}{\Delta E})^2 \tag{4.1}$$

where λ is the atomic spin-orbit coupling constant for a specific energy band and ΔE is the average energy separation from the conduction band to the nearest band which is coupled via the atomic spin-orbit interaction constant. Yafet has shown that the equation 4.1 is temperature independent [48] which means that the spin relaxation time τ_{sr} follows the temperature dependence of the elastic scattering time τ_{el} that is proportional to to the temperature behavior of the resistivity. The temperature dependence of the resistivity for the clean metals is dominated by the electron-phonon scattering and follows the Bloch-Grüneisen relation [49] $(\tau_{sr})^{-1} \sim T^5$ for temperatures below the Debye temperature T_D and $(\tau_{sr})^{-1} \sim T$ for temperatures above the Debye temperature. It has been shown for the monovalent alkali and nobel metals that the Bloch-Grüneisen relation is followed [50, 51]. It is important to note that hot-electron transport is at energies above the Fermi level. Therefore, the Bloch-Grüneisen relation which is valid for the transport at Fermi level, may not hold for the hot-electrons. The polyvalent metals like Al, Be, Mg, and Pd do not obey the Bloch-Grüneisen relation. $(\frac{\lambda}{\Delta E})^2 = 3 \times 10^{-5}$ is for Al and $(\frac{\lambda}{\Delta E})^2 = 2.16 \times 10^{-2}$ is for Cu [50]. There is a 3 orders of difference in magnitude. However, the measured spin relaxation length for Al is comparable to the Cu. The discrepancy is resolved by Fabian and Das Sarma by considering the band structure effects [52, 53]. They have shown that the energy separation ΔE is decreased in small spin-hot-spot areas on the large Fermi surface making the spin-flip rate $(\tau_{sr})^{-1}$ 100 times faster than expected from Elliot-Yafet relation.

The hybrid structures in the spin-valve transistor (SVT) [2], the magnetic tunnel transistor (MTT) [35] and ballistic electron emission microscopy (BEEM) [21] contains spin-valve base with FM/NM/FM trilayer where FM and NM stands for ferromagnet and nonmagnetic metals. The carriers are injected above the Fermi energy by a tunnel barrier in MTT and BEEM and by a Schottky diode in SVT so that the carriers are called hot-carriers. The hot-carriers are collected by a Schottky diode formed by a nonmagnetic metal and semiconductor contact. Hot-electrons attenuate exponentially in ferromagnets such as NiFe, Co and CoFe in a way that the minority electrons attenuate more than the majority electrons. No spin asymmetry in hot-electron attenuation in Au, Cu is expected. The

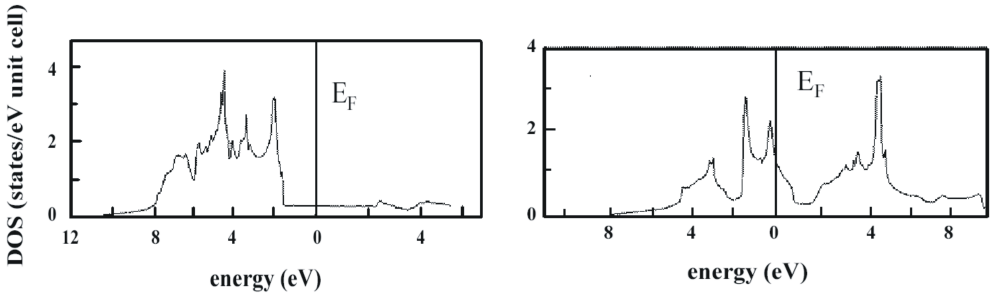

Figure 4.1: *Total density of states of Au (left) and Ta (right). The line indicates the fermi level E_F. The density of states in Ta is almost 5 times higher than the density of states in Au between E_F and $E_F + 1eV$. Taken from [54]*

reported attenuation lengths in Au and Cu are around 20 nm [40, 41, 42] which are very long compared to the attenuation lengths (2-5 nm) in Co, NiFe [13]. The details have been discussed in more detail in section 3.1 in this thesis. The hot-electron transmission at Au/ferromagnet and Cu/ferromagnet interfaces have been also presented in section 3.4.

One of the motivation to study spin transport in tantalum is that the tantalum is a nonmagnetic transition metal. It differs from Au and Cu in terms of its density of states. In fig 4.1 (a), the total density of states for Au is shown. The energy range that is relevant for the SVT is between 0.6-0.9 eV above the Fermi level. The energies above the Fermi level have a very small density of states available in contrast to the density of states of Ta in fig 4.1 (b). Therefore, Ta has more available density of states than Au. The high number of available density of states in Ta is due to empty d-states of Ta. The d-states of Au is located below the Fermi level between 2 eV and 8 eV. The d-states of Ta is located between 4 eV below the Fermi level and 6 eV above the Fermi level. The s-states for both material are very broad. The density of s-states is at least 5 times lower than the d-states in both materials. The hot-electron scattering in the SVT is an inelastic scattering via Coulomb interaction of a hot-electron and an electron below the Fermi level. If there is a spin-asymmetry in the density of states like in Co and NiFe, the scattering rate for the minority and majority spins is different which results in an asymmetry in the hot-electron attenuation lengths. The spin-asymmetry in density of states in Ta does not exist. However, hot-electron spin transport in Ta could be different than Au and Cu because Ta has larger available density of states above the Fermi level than Au and Cu. This may result a higher inelastic decay rate for hot-electrons in Ta compared to Au and Cu. The spin-relaxation in nonmagnetic metals is due to the spin-orbit coupling via the momentum (elastic) scattering. There are many states available in Ta for hot-electrons to scatter into elastically at SVT operation energies unlike Au and Cu

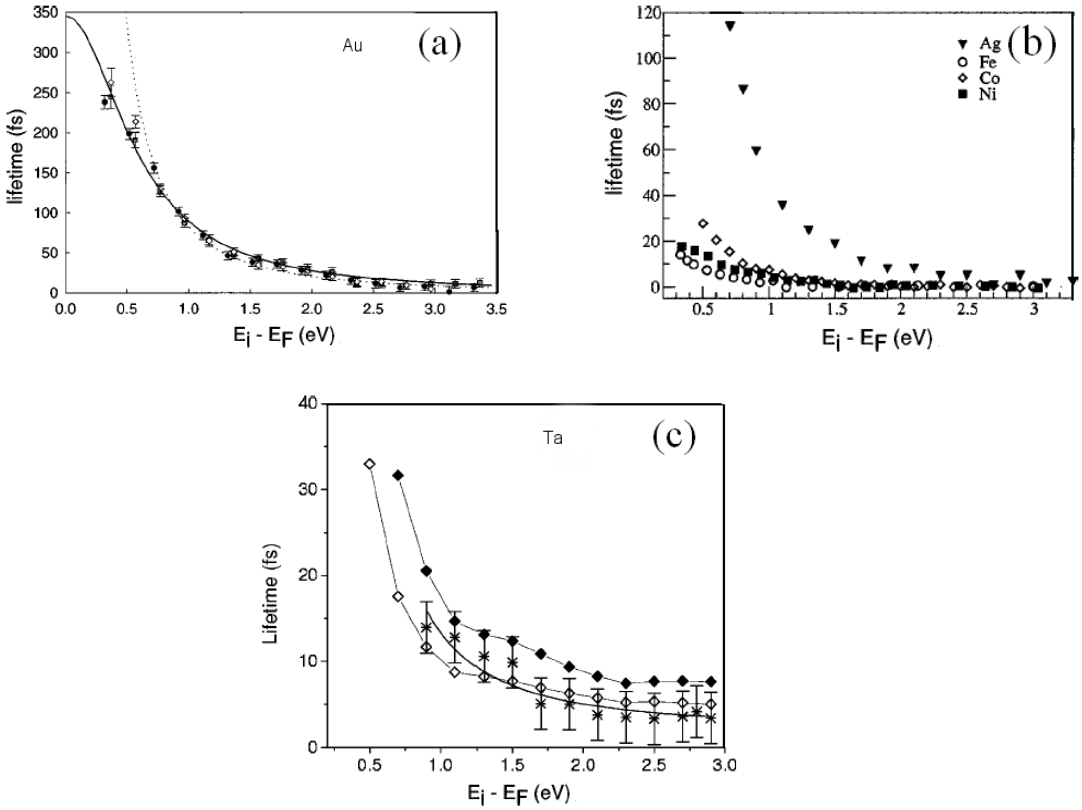

Figure 4.2: *Electron lifetimes as a function of electron energy measured by time-resolved two-photon emission for (a) Au(111) (squares, circles are experimental data for films with thicknesses 15 nm, 50 nm and 300 nm, respectively.)(taken from [55]). The solid line and the dotted line are theoretical fits. (b) Ag, Ni, Co, Fe (taken from [56]) (c) Ta (stars are experimental data). Solid diamonds are theoretical averaged GW lifetimes, open diamonds are theoretical averaged GW+T lifetimes. Thick solid line is a guide for the eye(taken from [57]).*

which may lead to spin-relaxation lengths shorter than Au and Cu. The density of states in Ta look like the density of states for minority spin in Co (or NiFe) where many d-states are empty. Therefore, at the Ta/ferromagnet interfaces, the minority spin may have higher transmission probability than the majority spin which do not have as many states available as the minority spin in Co (or NiFe).

It is important to note that the hot-electron attenuation lengths in a SVT is a sum of many factors. One of these factors is the physical mean free paths for elastic and inelastic scattering of electrons in the metals and the transmission factor at the interfaces in the metal base. By replacing Au with Ta, the scat-

tering mechanism is changed. The other factors like emission and collection of the hot-electrons are kept same. In fig 4.2, the reported electron lifetimes as a function of energy of the electrons with Time-resolved two-photon photoemissin TR-TPPE [58] for Au (top) [55], Ag, Fe, Co, Ni (middle) [56] and Ta (bottom) [57] are shown. The Au and Ag which are nobel metals which do not have empty d-states, have longer electron lifetimes than the ferromagnetic metals Co, Fe and Ni which have empty d-states. The Ta is a nonmagnetic metal but it has empty d-states above the Fermi level like the ferromagnetic metals. The electron lifetimes in Ta are comparable to the electron lifetimes in ferromagnetic metals. Therefore, the hot-electron attenuation lengths is expected to be shorter than Au and Cu.

The samples in this chapter are prepared in the same way as described in the section 3.2 in chapter 3. First a model will be discussed for SVTs without any Ta in it that has no spin-dependent scattering at the interfaces and no spin-relaxation. Then the spin-dependent transmission at the Ta/ferromagnets and spin relaxation in Ta will be introduced. After discussing the theoretical aspect of the spin-transport, hot-electron scattering in Ta will be reported in SVTs with NiFe/Ta/Co spin-valve base. The experimental results have two parts. In the first part, the transmission of hot-electrons in Ta is presented. In the second part, the magnetocurrent for the devices with NiFe/Ta/Co and NiFe/Au/Co/Ta spin-valve bases are studied. The results for magnetocurrent are discussed on the basis of the model including structural and magnetic characterization. The chapter ends with a conclusion.

4.2 The model for spin-transport in Ta

In this section, a model will be used to describe spin transport in Ta films and at Ta/ferromagnet interfaces. The model is derived from the hot-electron spin-transport in the spin-valve transistor (SVT) [13]. Therefore, the hot-electron spin-transport in a SVT without Ta will be discussed first. The structures that are considered are n-Si/Au/NiFe/Au/Co/Cu// Cu/n-Si, n-Si/Au/NiFe/Ta/Co/Cu//Cu/n-Si and n-Si/Au/NiFe/Au/ Co/Ta/Cu//Cu/n-Si and the spin-valve base of these structures are drwan in fig 4.3. The first structure (top) is a device without Ta film which has no spin-relaxation and no spin dependent transmission at the FM/Au and the FM/Cu interfaces. The second structure (middle) has Ta between the Co and the Si/Cu collector diode. With this structure, the transmission at the Co/Ta interface will be studied while spin relaxation in the Ta us not relevant. In the third structure (bottom), the Ta film is inserted between ferromagnets so that the spin relaxation in Ta will be investigated.

The difference in the collector current for parallel I_C^P and antiparallel I_C^{AP} configuration of the base magnetic moments originates from the spin asymmetry in

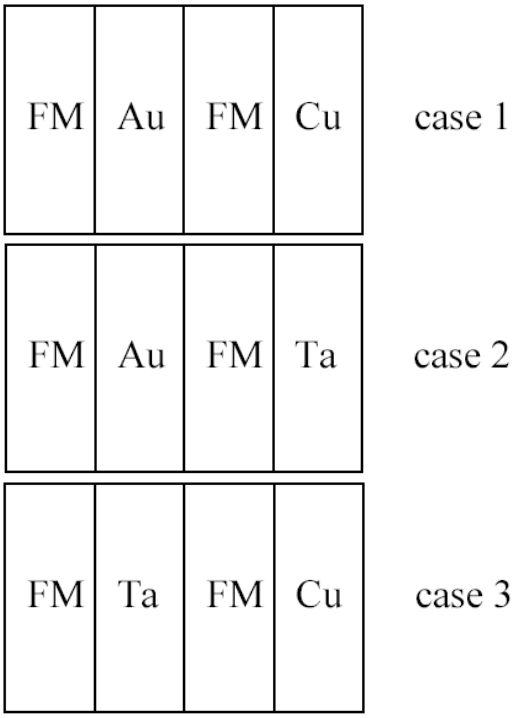

Figure 4.3: *The spin-valve base of the SVTs with Si/Au emitter and Si/Cu collector. No spin relaxation and no spin dependent transmission is expected for the structure at the top. In the middle, spin dependent transmission at the Co/Ta interface is discussed. In the structure at the bottom the spin relaxation and the spin-dependent transmission at the Ta/Co interface is taken into account in the model.*

hot-electron attenuation length in the ferromagnets as discussed in section 3.1. The collector current can be written for both configurations in a SVT with n-Si/Au/NiFe/Cu/Co/Cu//Cu/n-Si structure as:

$$I_C^P \propto T_{NiFe}^M T_{Co}^M + T_{NiFe}^m T_{Co}^m. \tag{4.2}$$

$$I_C^{AP} \propto T_{NiFe}^M T_{Co}^m + T_{NiFe}^m T_{Co}^M. \tag{4.3}$$

where T^M and T^m are the transmission of majority (M) and minority (m) spin hot electrons. They can be expressed as:

$$T_{FM}^M = \Gamma_{in}^M \exp(-\frac{t_{FM}}{\lambda_{FM}^M})\Gamma_{out}^M. \tag{4.4}$$

$$T^m_{FM} = \Gamma^m_{in} \exp(-\frac{t_{FM}}{\lambda^m_{FM}})\Gamma^m_{out}. \tag{4.5}$$

where t_{FM} is the film thickness, λ^M_{FM} and λ^m_{FM} the hot-electron attenuation lengths for majority and minority spin and FM denotes the ferromagnet. The Γ_{out} and Γ_{in} denote the transmission across the interface of the ferromagnet with the nonmagnetic metal at each side. An unpolarized hot-electron current is injected into spin-valve base by the n-Si/Au emitter. The current is polarized after transmission of a film FM and the transmission polarization can be expressed as:

$$P_{FM} = \frac{T^M_{FM} - T^m_{FM}}{T^M_{FM} + T^m_{FM}}. \tag{4.6}$$

Finally, the magnetocurrent (MC) can be written in terms of the collector current and the transmission polarization as:

$$MC = \frac{I^P_C - I^{AP}_C}{I^{AP}_C} = \frac{2P_{NiFe}P_{Co}}{1 - P_{NiFe}P_{Co}}. \tag{4.7}$$

It is important to note that the attenuation in the nonmagnetic metals in the base of the SVT are ignored due to the fact that the attenuation length in Au and Cu [40, 41, 42] is much higher than the typical thicknesses of Au and Cu used. In addition to this, it is known for Au and Cu that there is no spin-asymmetry in the attenuation lengths and spin-relaxation of hot-electrons is hundreds of nm **[?]**.

Three cases will be discussed corresponding to the structures in fig 4.3. The first case is that the there is no spin-dependent transport at the interfaces for the devices with Au and Cu such that $\Gamma^M_{in} = \Gamma^m_{in}$ and $\Gamma^M_{out} = \Gamma^m_{out}$ where M (m) stands for majority (minority) spin. The second case is that there is spin-dependent transport at the interfaces for the devices with NiFe/Au/Co/Ta spin-valve base such that $\Gamma^M_{Ta/Co} \neq \Gamma^m_{Ta/Co}$. The third case is that there is spin relaxation in Ta and spin-dependent transport at Ta/ferromagnet interfaces for the devices with NiFe/Ta/Co spin-valve base.

Case 1

The device with n-Si/Au/NiFe/Cu/Co/Cu//Cu/n-Si structure has no spin-dependent transport at Au,Cu/ferromagnet interfaces ,i.e., $\Gamma^m_{in} = \Gamma^M_{in}$ and $\Gamma^m_{out} = \Gamma^M_{out}$. The transmission polarization solely depends on the exponential decay of

the current in the ferromagnets. The equation for transmission polarization can be written as;

$$P_{FM} = \frac{\exp(-\frac{t_{FM}}{\lambda^{M}_{FM}}) - \exp(-\frac{t_{FM}}{\lambda^{m}_{FM}})}{\exp(-\frac{t_{FM}}{\lambda^{M}_{FM}}) + \exp(-\frac{t_{FM}}{\lambda^{m}_{FM}})}. \tag{4.8}$$

which can be used in equation 5.7. The structures that are discussed in chapter 3 belongs to this case. Spin-dependent transport transmission is only in the ferromagnets.

Case 2

When Ta is used in the metal base, spin-dependent transport at the interfaces might be expected for the reasons that are discussed in the introduction of this chapter. Therefore, spin-dependent transmission at the Ta/Co interface should be considered. The structure that is considered in this case is n-Si/Au/NiFe/Au/Co/Ta/Cu//Cu/n-Si. The spin relaxation in Ta is not considered in this case since the spins are filtered by NiFe and analyzed by the Co film. In this case, the transmission polarization of NiFe is expressed by the exponentials as in the case 1. But the polarization of Co must take into account the spin-dependent scattering at the Ta/Co interface. Therefore, the transmission polarizations can be written as:

$$P_{NiFe} = \frac{\exp(-\frac{t_{NiFe}}{\lambda^{M}_{NiFe}}) - \exp(-\frac{t_{NiFe}}{\lambda^{m}_{NiFe}})}{\exp(-\frac{t_{NiFe}}{\lambda^{M}_{NiFe}}) + \exp(-\frac{t_{NiFe}}{\lambda^{m}_{NiFe}})}. \tag{4.9}$$

$$P_{Co} = \frac{\exp(-\frac{t_{Co}}{\lambda^{M}_{Co}})\Gamma^{M}_{Co/Ta} - \exp(-\frac{t_{Co}}{\lambda^{m}_{Co}})\Gamma^{m}_{Co/Ta}}{\exp(-\frac{t_{Co}}{\lambda^{M}_{Co}})\Gamma^{M}_{Co/Ta} + \exp(-\frac{t_{Co}}{\lambda^{m}_{Co}})\Gamma^{m}_{Co/Ta}} \tag{4.10}$$

where $\Gamma^{M}_{Ta/Co} \neq \Gamma^{m}_{Ta/Co}$.

Case 3

When Ta is used as a spacer in the spin-valve base as in the device with n-Si/Au/NiFe/Ta/Co/Cu//Cu/n-Si structure, more complicated case is observed. In this case, the spin relaxation must be taken into account since some of the spin information will be lost in the Ta film before it is analyzed by the Co film. It is illustrated in fig 4.4 for no spin relaxation in nonmagnetic spacer (Au or Cu) on the top and for spin relaxation in nonmagnetic spacer (Ta) on the bottom. The NiFe is the polarizer and the Co is the analyzer. The spin information

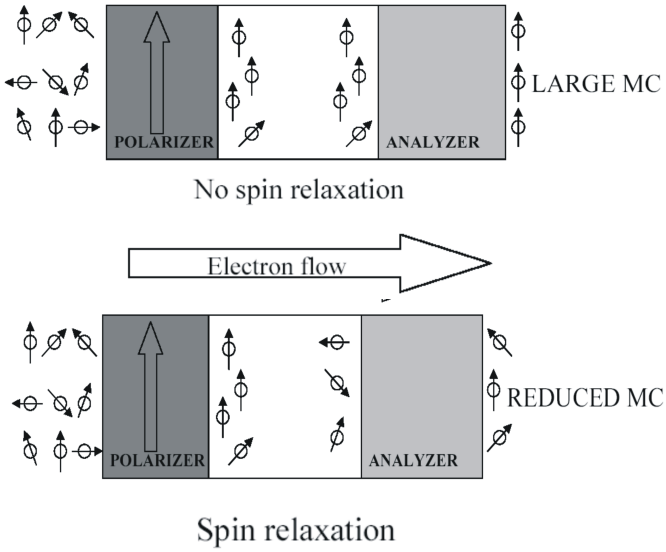

Figure 4.4: *Schematic diagram of the spin transport in spin-valve base with no spin relaxation in nonmagnetic metal spacer (top) and spin relaxation in the nonmagnetic metal spacer (bottom).*

of the electron is lost due to the spin relaxation in Ta which reduces the magnetocurrent. In this case, the transmission polarizations of the ferromagnets can be written as:

$$P_{NiFe} = \frac{\exp(-\frac{t_{NiFe}}{\lambda^M_{Co}})\Gamma^M_{NiFe/Ta} - \exp(-\frac{t_{NiFe}}{\lambda^m_{NiFe}})\Gamma^m_{NiFe/Ta}}{\exp(-\frac{t_{NiFe}}{\lambda^M_{NiFe}})\Gamma^M_{NiFe/Ta} + \exp(-\frac{t_{NiFe}}{\lambda^m_{NiFe}})\Gamma^m_{NiFe/Ta}} \tag{4.11}$$

$$P_{Co} = \frac{\Gamma^M_{Ta/Co}\exp(-\frac{t_{Co}}{\lambda^M_{Co}}) - \Gamma^m_{Ta/Co}\exp(-\frac{t_{Co}}{\lambda^m_{Co}})}{\Gamma^M_{Ta/Co}\exp(-\frac{t_{Co}}{\lambda^M_{Co}}) + \Gamma^m_{Ta/Co}\exp(-\frac{t_{Co}}{\lambda^m_{Co}})} \tag{4.12}$$

where $\Gamma^M_{Co/Cu} = \Gamma^m_{Co/Cu}$ and $\Gamma^M_{Co/Au} = \Gamma^m_{Co/Au}$. The magnetocurrent can be rewritten using the transmission polarization in equations 4.11 and 4.12 and inserting an exponential spin relaxation term in between the transmission polarizations as;

$$MC = \frac{2P_{NiFe}\exp(-\frac{t_{Ta}}{\lambda_{SR}})P_{Co}}{1 - P_{NiFe}\exp(-\frac{t_{Ta}}{\lambda_{SR}})P_{Co}}. \tag{4.13}$$

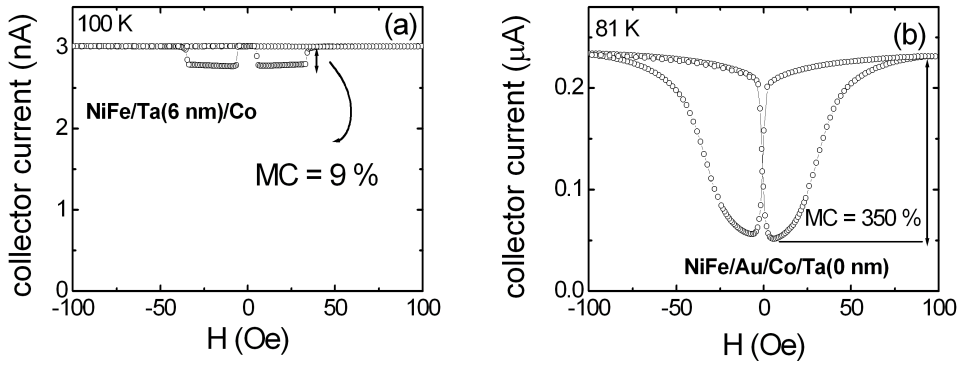

Figure 4.5: *The collector current as a function of magnetic field with Si/Au(3 nm)/NiFe(5 nm)/NM/Co(2 nm)/Cu(2 nm)//Cu(2 nm)/Si structure where NM is (a) Ta (6 nm) (I_E = 20 mA. T = 100 K) (b) Au (10 nm) (I_E = 2 mA. T = 81 K).*

where t_{Ta} is the Tantalum film thickness and λ_{SR} is the spin relaxation length in the Tantalum.

4.3 Hot-electron transmission in Ta

The hot-electron scattering in the spin-valve transistor has two major contributions. The spin-dependent inelastic scattering in the ferromagnets and elastic spin independent scattering at the interfaces in the metal base [13] which is discussed in more detail in section 3.1. Using Cu as nonmagnetic spacer instead of Au resulted in a better transmission across the interfaces. In this section, the hot-electron scattering in Ta and at Ta/ferromagnet interfaces will be studied in SVTs with Si/Au(3)/NiFe(5)/Ta(x nm)/Co(2 nm)/Cu(2 nm)// Cu(2 nm)/Si structure.

The collector current for the device with Si/Au(3)/NiFe(5)/Ta(6 nm)/Co(2 nm)/Cu(2 nm)//Cu(2 nm)/Si at 100 Oe in parallel alignment is 3 nA in fig 4.5 (a). The transfer ratio is calculated to be $1.5\text{x}10^{-7}$. If the transfer ratio is compared to the device with Si/Au(3)/NiFe(5)/Au(10 nm)/Co(2 nm)/Cu(2 nm)// Cu(2 nm)/Si structure in fig 4.5 (b), the transfer ratio of the device with Ta spacer is three orders of magnitude smaller than the device with Au spacer. The difference in transfer ratio could originate from the bulk of the Ta film or the Ta/ ferromagnet interfaces. A series of devices with Si/Au(3)/NiFe(5) /Ta(x nm)/Co(2 nm)/Cu(2 nm)// Cu(2 nm)/Si structure is fabricated to find out the contributions coming from both sources. The Ta thickness is varied from 2 nm to

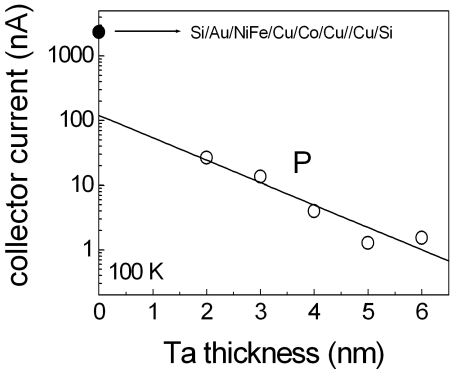

Figure 4.6: *The collector current as a function of Ta thickness for Si/Au(3 nm)/NiFe(5 nm)/Ta(x nm)/Co(2 nm)/Cu(2 nm)/Cu(2 nm)//Cu(2 nm)/Si. The line is an exponential fit of the collector current as a function of Ta thickness. The open circles are the experimental data for parallel alignment (P) of the magnetic moments of Co and NiFe. I_E = 10 mA. T = 100 K. The closed circle is the experimental data for Si/Au(3 nm)/NiFe(5 nm)/Ta(x nm)/Co(2 nm)/Cu(2 nm)/Cu(2 nm)//Cu(2 nm)/Si.*

6 nm. In fig 4.6, the collector current for parallel alignment of the base magnetic moments of the devices as a function of Tantalum thickness is plotted on a semi-log scale at 10 mA of emitter current(open circles). Data is taken at 100 K. The data point at zero Ta thickness (closed circle) is the device in fig 3.5 in section 3.4 with Si/Au(3 nm)/NiFe(5 nm)/Cu(10 nm)/Co(2 nm)/Cu(2 nm)//Cu(2 nm)/Si structure. The data shows that the collector current drops exponentially with respect to Ta thickness and the collector current I_C^P as a function of Ta thickness can be written as:

$$I_C^P(t_{Ta}) = I_C^P(0)\exp(-\frac{t_{Ta}}{\lambda_{Ta}}) \tag{4.14}$$

where $I_C^P(0)$ is the current when the solid line intersects the collector current axis at zero Ta thickness, t_{Ta} is the Tantalum film thickness and λ is the hot-electron attenuation length in Ta. The data fits with the exponential line in 4.6 very well. The hot-electron attenuation length λ in Ta is found to be 1.3 nm from the fit. To have an idea about the Ta/ferromagnet interface, in 4.6 the exponential fit and the data point at zero tantalum thickness should be considered. At zero tantalum thickness, the contribution from hot-electron attenuation in Ta is zero. Therefore, the difference between the extrapolated point (120 nA) and the data point (2350 nA) with a NiFe/Cu/Co spin-valve base

originates from the interface scattering difference between Cu/ferromagnet and Ta/ferromagnet interfaces. The scattering at Ta/ferromagnet is 19.6 times higher than Cu/ferromagnet interface.

4.4 Spin-transport through Ta films and Ta/FM interfaces

In this section the experimental results on hot-electron spin-transport in tantalum and at Ta/ferromagnet interfaces will be presented. In the first section, a series of devices with Si/Au(3 nm)/NiFe(5 nm)/Ta(x nm)/Co(2 nm)/Cu(2 nm)//Cu(2 nm)/Si structure will be shown for spin-transport in Ta. The magnetocurrent depends on the thickness of the Ta film. In the second part of the section, the Ta film is inserted between the Co and the Si/Cu collector diode and Au is used as the spacer. It is shown that the magnetocurrent does not depend on the thickness of the Ta film in this configuration of the layers in the SVT.

Magnetocurrent with Ta spacer

Hot-electron spin-transport in Ta is studied in SVTs which has a Si/Au(3 nm)/NiFe(5 nm)/Ta(x nm)/Co(2 nm)/Cu(2 nm)//Cu(2 nm)/Si structure. In fig 4.7 (a), the SVT with 6 nm Ta spacer collector current as a function of magnetic field is plotted. Data is taken at 82 K. The transfer ratio is 1.5x10^{-7}. The transfer ratio is discussed in detail in section 4.2. The magnetocurrent is 9 %. It is important to mention that magnetocurrent in a SVT is due to the spin-asymmetry of the hot-electron attenuation lengths in ferromagnets. The devices in chapter 3 has no Ta in it and they have magnetocurrent around 350 %. The drop in MC is surprising for a nonmagnetic metal like Ta. In order to investigate further, a series of devices are fabricated with different Ta thicknesses in the spacer of the spin-valve base of the SVT. The results are shown in fig 4.7 (b), (c) and (d). The magnetocurrents are 10%, 13% and 26% and the transfer ratios are 1.28x10^{-7}, 4x10^{-7} and 13.6x10^{-7}, respectively. The magnetocurrent is very low in all devices in fig 4.7. The parallel and antiparallel alignment of the base magnetic moments are very well defined. The switching points for NiFe and Co are different for all devices. The reason for this behaviour is that the coupling of NiFe and Co is higher for the devices which has a thinner Ta. If the magnetocurrent is plotted as a function of Ta thickness in fig 4.8, it can be seen that the MC depends on the Ta thickness. It indicates that there is spin-dependent transport in Ta. However, the contribution of Ta/ferromagnet interfaces to the magnetocurrent cannot be ruled out.

Ta/ferromagnet interfaces

In the previous section, the MC is effected by two factors which are the contribution from the film and the Ta/ferromagnet interfaces. There is an apparent

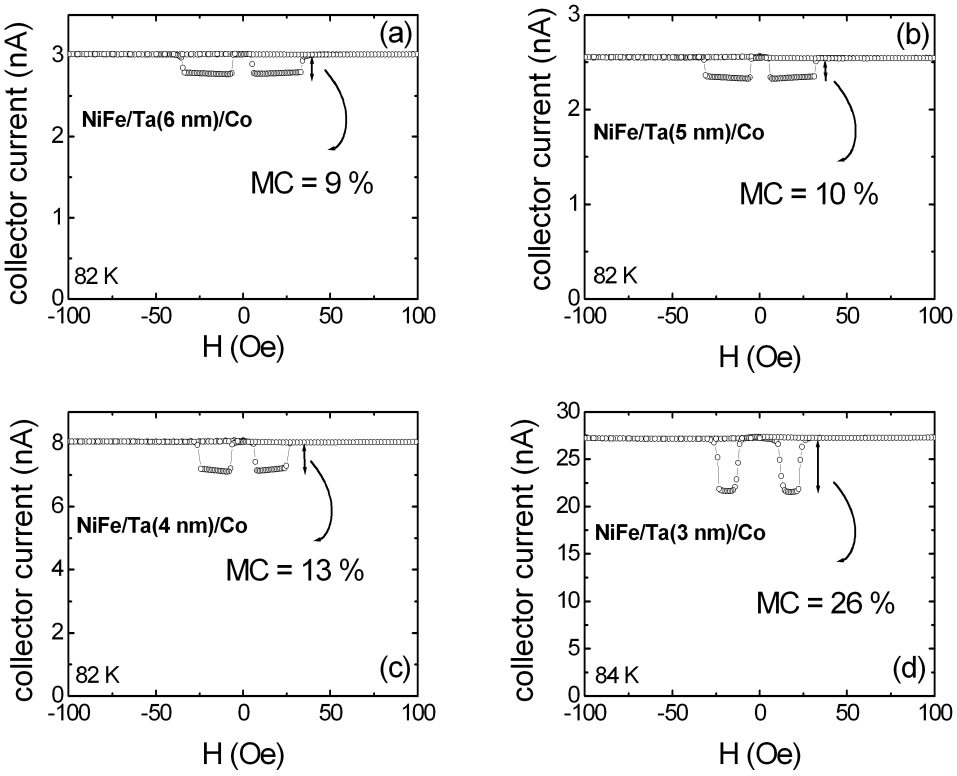

Figure 4.7: *The collector current as a function of magnetic field with Si/Au(3 nm)/NiFe(5 nm)/Ta(x)/Co(2 nm)/Cu(2 nm)//Cu(2 nm)/Si structure where x = (a) 6 nm (T = 100 K) (b) 5 nm (T = 82 K) (c) 4 nm (T = 82 K)(d) 3 nm (T = 84 K). I_E = 20 mA.*

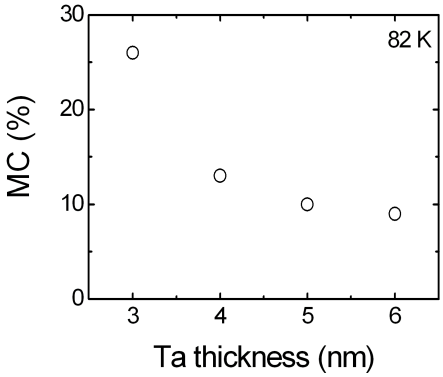

Figure 4.8: *The magnetocurrent as a function of tantalum thickness for SVTs with Si/Au(3 nm)/NiFe(5 nm)/Ta(x nm)/Co(2 nm)/Cu(2 nm)//Cu(2 nm)/Si structure. T = 82 K.*

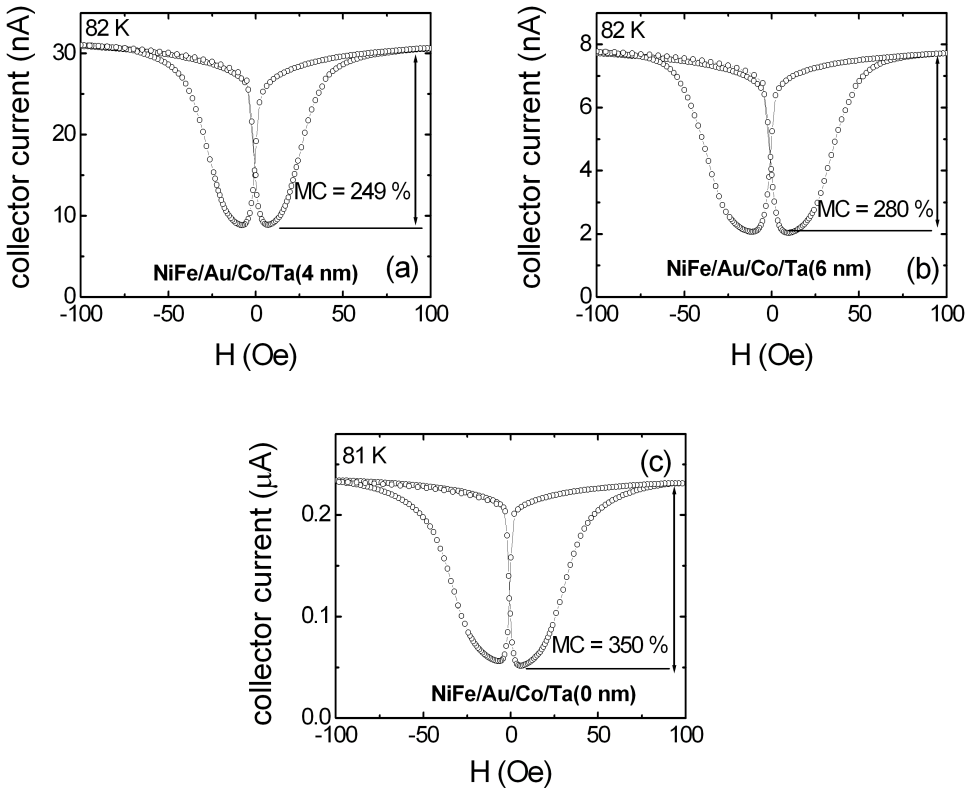

Figure 4.9: *The collector current as a function of magnetic field with Si/Au(3 nm)/NiFe(5 nm)/Au(10 nm)/Co(2 nm)/Ta(x)/Cu(2 nm)//Cu(2 nm)/Si structure in (a) x = 4 nm (I_E = 10 mA) (b) x = 6 nm (I_E = 10 mA) (c) x = 0 nm (I_E = 2 mA).*

thickness dependence. In this section, the Ta/ferromagnet interface affect will be studied. The thickness dependence can be due to spin relaxation in Tantalum since there is no spin asymmetry in density of states. In spin relaxation, the energy of the hot-electrons are not affected much. Spin relaxation happens due to momentum interaction [44]. To isolate the interface effect, a new layer sequence is needed. For this purpose, SVTs with Si/Au/NiFe/Au/Co/Ta/Cu//Cu/Si structure is used. The spins are already analyzed in this configuration. Therefore, the orientation of spins does not matter anymore. However, if there is any spin-dependent transmission at Ta/Co interface, it can be observed in the magnetocurrent.

In fig 4.9 (a), the collector current as a function of magnetic field for a SVT with Si/Au(3 nm)/NiFe(5 nm)/Au(10 nm)/Co(2 nm)/Ta(4 nm)/Cu(2 nm)//Cu(2 nm)/Si structure is plotted. The transfer ratio is 4.0x10-7. The magne-

tocurrent is 249%. The MC for Si/Au(3 nm)/NiFe(5 nm)/Ta(4 nm)/Co(2)/Cu(2 nm)//Cu(2 nm)/Si device in fig 4.7 (c) is 13%. The difference in MC for the same Ta thickness is very large. However, if the MC of the SVT in fig 4.9 (a) is compared with the SVT that has no Ta in fig 4.9 (c), the MC is still 100% less. Let's have a look for a device with thicker Ta. In fig 4.9 (b), the collector current as a function of magnetic field for a SVT with Si/Au(3 nm)/NiFe(5 nm)/Au(10 nm)/Co(2 nm)/Ta(6 nm)/Cu(2 nm)//Cu(2 nm)/Si structure is plotted. The transfer ratio is 1.5x10-6. The magnetocurrent is 280%. The MC of the SVT with 6 nm Ta as the spacer is 9%. In order to analyze the results, the structural and magnetic characterization of the multilayers have to be done. In literature, it is reported that Ta and ferromagnets can mix so that the effective magnetic film thicknesses could be lowered. Then, low magnetocurrent in the devices in fig 4.9 (a) and (b) could be explained by the mixture.

4.5 Structural and magnetic characterization

Inserting Ta layer in the metal base of the SVT reduces the magnetocurrent as discussed in section 4.4. If there is a intermixing of Ta and ferromagnets resulting in magnetically dead volume in ferromagnets, this could also be a possible explanation for the reduced MC, because the polarizations of NiFe and Co in the cases 2 and 3 in the section 4.2 will be reduced. It is reported in literature that when Ta deposited on NiFe and Co, the magnetic moment of the as-deposited NiFe and Co films are reduced [59, 60]. The reduction in magnetic moment was attributed to the intermixing at the NiFe/Ta and Co/Ta interfaces. The amount of intermixing is calculated to be 1 nm for NiFe and 0.5-1.0 nm for Co. If the samples with NiFe/Ta are annealed to 600 K, the intermixing increases to 1.2 nm [60]. Kowalewski et al shows that using Korringa, Kohn and Rostoker coherent potential approximation (KKR-CPA) method, the average magnetic moment vanishes at 12 % Ta concentration in Ni-rich Ni-Ta alloys in the ideal random alloy limit.

For the SVTs with Si/Au/NiFe/Ta/Co/Cu//Cu/Si and Si/Au/NiFe/Au/Co/Ta/Cu//Cu/Si structures that we have fabricated, the magnetocurrent is found to be 108 % and 117 % using the polarizations in case 1 in the model section 4.2. In this model, the transmission at the interfaces are spin-independent. If spin-dependent transmission at the interfaces are introduced, the intermixing could explain the reduction in the MC for the SVT with Si/Au/NiFe/Ta/Co/Cu//Cu/Si structure. To analyze the possibility of intermixing, transmission electron microscopy (TEM) and vibrating sample magnetometer (VSM) are used for structural and magnetic characterization.

In fig 4.10, the cross section TEM of Si/NiFe(5 nm)/Ta(6 nm)/Co(2 nm)/Cu(4

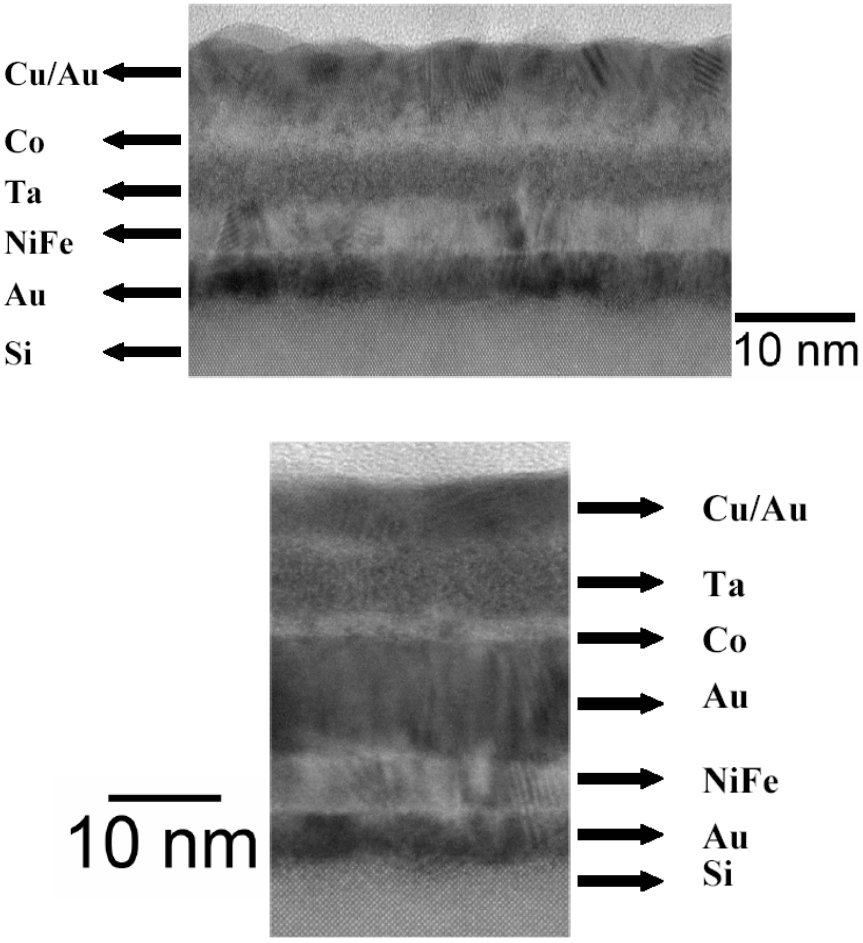

Figure 4.10: *Cross sectional transmission electron microscopy images of Si/Au(3 nm)/NiFe(5 nm)/Ta(6 nm)/Co(2 nm)/Cu(4 nm)/Au(5 nm) (left) and Si/Au(3 nm)/NiFe(5 nm)/Au(10 nm)/Co(2 nm)/Ta(6 nm)/Cu(4 nm)/Au(5 nm) (right) structures.*

nm)/Au(5 nm) (left) and Si/NiFe(5 nm)/Au(10 nm)/Co(2 nm)/Ta(6 nm)Cu(4 nm)/Au(5 nm) (right) structures are shown. In both TEM pictures, each layer can be easily observed until the Cu/Au cap layer in which the Au and Cu are indistinguishable. In fig 4.10, the structure on the left shows that Ta and NiFe are equal in thickness. The thicknesses obtained from the TEM images are 4.5 ± 0.3 nm for NiFe and Ta, 1.6 ± 0.1 nm for Co. NiFe is 0.5 nm, Ta 1.5 nm and Co 0.4 nm thinner than the aimed thicknesses. It is possible that the Ta intermixed with Co and NiFe. However, at the NiFe/Ta and Ta/Co interfaces there is no sign of intermixing. It is important to note that even though the Co layer is very thin it is continuous. If there has been shortcuts, this would also reduce the MC since the hot-electrons would not pass through the ferromagnetic Co layer. In fig 4.10 on the right, the Co layer on top of Ta layer is also continuous even though it is very thin. The thicknesses of the Ta and Co are slightly lower than expected as in the structure on the left. At the Co/Ta interface, it is not possible to see any sign of intermixing.

The TEM images do not show a conclusive result about the intermixing of Ta and NiFe (Co). The magnetic moments of the layers with Ta and without Ta could give an evidence about mixture. For this purpose, 4 samples are grown. Two samples with Si/Au(3 nm)/NiFe(5 nm)/Au(10 nm) and Si/Au(3 nm)/Co(2 nm)/Cu(4 nm)/Au(5 nm) structure are control samples which do not contain Ta. The thicknesses of ferromagnets and the layer sequence are chosen to have the same as in the SVTs. Two more samples with Si/Au(3 nm)/NiFe(5 nm)/Ta(6 nm)/Au(10 nm) and Si/Au(3 nm)/Co(2 nm)/Ta(6 nm)/Cu(4 nm)/Au(5 nm) structures are deposited. In fig 4.11 (a), the magnetic moment as a function of applied field in the plane of the sample is plotted for Si/Au(3 nm)/Co(2 nm)/Cu(4 nm)/Au(5 nm) and Si/Au(3 nm)/Co(2 nm)/Ta(6 nm)/Cu(4 nm)/Au(5 nm) structures. The structure with Ta film shows a lower saturation magnetization. It indicates that Co and Ta intermixes so that the mixed layer is magnetically dead. The amount of magnetically dead Co is found 14% of the the sample with Si/Au/Co/Cu/Au structure. For a 2 nm Co film, it corresponds to 2.8 $\mathring{A}$. In fig 4.11 (b), the magnetic moment as a function of applied field in the plane of the sample is plotted for Si/Au(3 nm)/NiFe(5 nm)/Au(5 nm) and Si/Au(3 nm)/NiFe(5 nm)/Ta(6 nm)/Au(5 nm) structures. The saturation magnetization for both samples are equal. There is no intermixing of Ta and NiFe.

There are indications of intermixing of Co and Ta from TEM images for devices with Si/Au/NiFe/Ta/Co/Cu//Cu/Si and Si/Au/NiFe/Au/Co/Ta/Cu//Cu/Si structures and from hysteresis loops of Si/Au/Co/Ta/Cu/Au structure. The intermixing of Ta and NiFe can be ruled out by the hysterisis loops of Si/Au/NiFe/Ta/Au structure which do not show any magnetic moment reduction compared to Si/Au/NiFe/Au structure. The intermixing of Co and Ta deduced from this section is not high enough to explain the reduction in the MC especially for the device with Si/Au/NiFe/Ta/Co/Cu//Cu/Si. Therefore, the

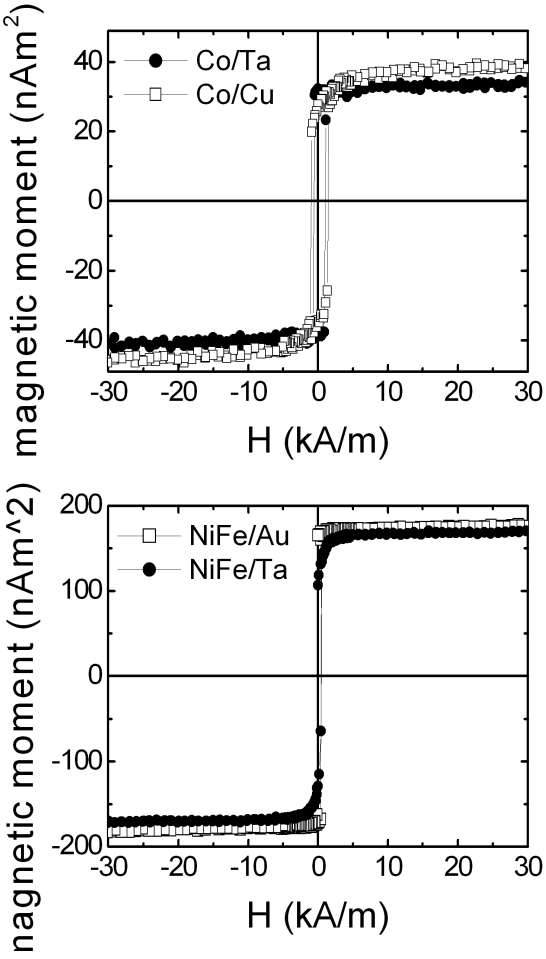

Figure 4.11: *(a)The magnetic moment of Si/Au(3 nm)/NiFe(5 nm)/Au(5 nm) and Si/Au(3 nm)/NiFe(5 nm)/Ta(6 nm)/Au(5 nm) as a function of magnetic field in the plane of the multilayer. (b)The magnetic moment of Si/Au(3 nm)/Co(2 nm)/Cu(4 nm)/Au(5 nm) and Si/Au(3 nm)/Co(2 nm)/Ta(6 nm)/Cu(4 nm)/Au(5 nm) as a function of magnetic field in the plane of the multilayer. T = 296 K.*

quantification with the model is needed to address the reduced magnetocurrent.

4.6 Discussion on the origin of reduced magnetocurrent with Ta

In this section, the experimental results will be compared with the theoretical model developed in section 4.2. Then, the physics of the spin-transport in Ta and at Ta/ferromagnet interface is discussed.

The magnetic moment measurements have to be considered to find out the effective magnetic Co layer in the SVT before the comparison with the model. It is found to be 86% of the Co layer in section 4.5. For 2 nm Co, the effective Co layer becomes 1.7 nm due to mixing of Co and Ta layer. The SVT with Si/Au/NiFe/Au/Co/Ta/Cu//Cu/Si structure is first compared with the model since the spin relaxation in Ta can be ignored in this configuration. Spins are already analyzed by the Co layer because collection by transmission across Si/Cu is not spin-dependent. The case 2 in the model section 4.2 can be applied to the SVT Si/Au/NiFe/Au/Co/Ta/Cu//Cu/Si structure. By using the equations 4.9, 4.10 and 5.7, the magnetocurrent is calculated and plotted as a function of the Co/Ta interface spin transmission spin asymmetry $\frac{\Gamma_m}{\Gamma_M}$ in fig 4.12 where $\Gamma_{m(M)}$ for minority (majority) is the transmission across Co/Ta interface. The hot-electron attenuation lengths for majority(minority) spin that are used for the calculation are 4.3 nm (1.0 nm) in NiFe and 2.3 nm (0.8 nm) in Co. The calculated MC (solid line) for $\Gamma_m = \Gamma_M$ is 275% instead of 350% found for SVTs with 5 nm NiFe and 2 nm Co (case 1) since the effective magnetic Co layer thickness is 1.7 nm ,i.e., the volume and the interface contribute oppositely to the spin asymmetry. When the transmission of minority spin at Ta/Co interface is higher than the transmission of majority spin ($\frac{\Gamma_m}{\Gamma_M} > 1$), the MC starts to decrease since the majority spin in the ferromagnets have higher transmission than minority spin. When the tranmission for the majority spin at Ta/Co interface is higher than minority, the MC starts to increase above 275 % adding up to the contribution from the "bulk"of ferromagnets. Two data points (circles) from fig 4.9 are inserted in 4.12. The experimental data corresponds to $\frac{\Gamma_m}{\Gamma_M} =$ 1.0 and 1.1 for the SVT with Si/Au/NiFe/Au/Co/Ta(6 nm)/Cu//Cu/Si and Si/Au/NiFe/Au/Co/Ta(4 nm)/Cu//Cu/Si, respectively. From this figure, the interface transmission spin asymmetry at Ta/Co interface can be found by averaging the two data points for magnetocurrent and the average corresponds to $\frac{\Gamma_m}{\Gamma_M} = 1.03$. The result for the Co/Ta interface transmission is similar to that of Au/NiFe interface transmission ($\frac{\Gamma_m}{\Gamma_M} = 0.8 \pm 0.2$ [22]) within the error bar.

Since the spin-dependence of the interface transmission at the Co/Ta interface is determined to be small, we conclude that the strong MC reduction must be due to spin relaxation in Ta in SVT with Si/Au/NiFe/Ta/Co/Cu//Cu/Si

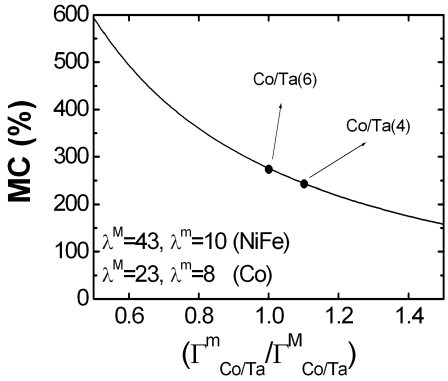

Figure 4.12: *The calculated magnetocurrent as a function Co/Ta interface transmission spin-asymmetry (the ratio of minority spin transmission to majority spin transmission at the Co/Ta interface) for a SVT with Si/Au(3 nm)/NiFe(5 nm)/Au(10 nm)/Co(1.7 nm)/Cu(2 nm)//Cu(2 nm)/Si. The Co layer is taken to be 1.7 nm since Ta and Co mixes which is magnetically dead layer. The circles are experimental data for SVTs with Ta inserted between Co and Cu.*

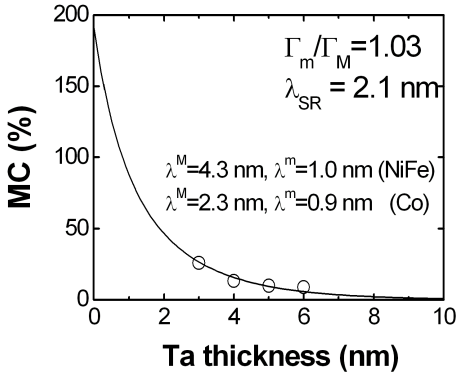

Figure 4.13: *Magnetocurrent as a function of Ta thickness for SVTs with Si/Au(3 nm)/NiFe(5 nm)/Ta(x nm)/Co(2 nm)/Cu(2 nm)//Cu(2 nm)/Si structure. The line is calculated MC and the circles are experimental data.*

structure. The equation 4.13 for the magnetocurrent in section 4.2 (case 3) can be used by using the Co/Ta interface transmission ratio $\frac{\Gamma_m}{\Gamma_M} \propto 1.03$ and a certain spin-relaxation length in Ta. The calculated magnetocurrent as a function of Ta thickness is plotted in fig 4.13 with the experimental data (circles). The spin-dependent transmission at the NiFe/Ta interface is assumed to be the same as the Co/Ta interface. The magnetocurrent at zero tantalum thickness is around 190% due to the spin-dependent transmission at the Ta/ferromagnet interfaces and the intermixing of the Co with tantalum which reduces the effective magnetic Co layer. As the Tantalum thickness increase, the magnetocurrent decreases exponentially. The spins relax so fast before they reach the Co film that even for 2 nm Ta thickness the magnetocurrent reduces to 50% and it is almost zero at 8 nm Ta thickness. The spin relaxation length λ_{SR} can be extracted from the fit. Spin relaxation length λ_{SR} in Ta is found to be 2.1 $\pm$ 0.3 nm. The spin relaxation length in Ta which is a nonmagnetic metal is very short compared to Au and Cu which are reported [45] to have spin relaxation lengths in the order of hundreds of nm.

In metals, the spin relaxation is due to the spin-orbit coupling [47, 48] via the impurity spin-flip scattering and the phonon-conduction electron scattering. The spin relaxation length that is found in Tantalum is mostly due to the phonon scattering since the mechanism that dominates at low temperatures (below 20 K) is impurity scattering and at high temperatures (above 20 K) the phonon induced spin relaxation [61]. To calculate the elastic scattering length in Tantalum, inelastic scattering length can be calculated by using the inelastic scattering time from TR-TPPE and use Matthiessens' rule $\frac{1}{\lambda_{Ta}} = \frac{1}{\lambda_{el}} + \frac{1}{\lambda_i}$ where λ_{Ta} is the measured attenuation length in Tantalum which is found to be 1.3 nm in section 4.3, λ_{el} is elastic scattering length and λ_i is the inelastic scattering length. The inelastic lifetime τ_i of electron in Tantalum at 0.9 eV is around 15 fs from fig 4.2. The inelastic scattering length can be calculated by $\lambda_i = \upsilon\tau_i$ where υ is the velocity of the hot-electron in the s-band and it is approximately 2 nm/fs. The inelastic scattering length λ_i is calculated from this equation to be 30 nm in Ta. From Matthiessens' rule, elastic scattering length λ_{el} is calculated to be 1.4 nm. Now, the ratio of the elastic scattering length λ_{el} to the phonon induced spin relaxation length is calculated to be 6.7x10^{-1}. This is 2 orders lower than the ratio for the Cu. The reason could be related to the density of states. Tantalum has many available states in d band for scattering processes which is a localized band. The momentum change in scattering process for the d-band would be higher than the momentum change in a s-band for the same energy change. Therefore, less number of momentum scattering is needed to relax a spin of a hot-electron in Ta than Cu in formula.

4.7 Summary

The spin-valve transistor is used to study the hot-electron transport in Tantalum. We have introduced a model to describe the spin transport in Ta and at the Ta/ferromagnets. Then, hot-electron transmission in Ta and Ta/ferromagnet interfaces are presented. Experimental results on the spin transport in Ta and the Ta/ferromagnet interfaces are followed by the structural and magnetic characterization of the metalic layers in the base of the device. Finally, the model is used to explain the spin transport behavior in Ta and at the Ta/ferromagnet interfaces.

The hot-electron transport in the SVT is very well established. However, it is based on the assumption that the spin relaxation length of the nonmagnetic layers (Au, Cu) are much more longer than the thicknesses that are used in the SVT. The model is expanded to a more general expression including spin relaxation effect on the magnetocurrent. Three cases are introduced. The first case is related to the devices with no spin relaxation and no spin dependent scattering at the ferromagnet/nonmagnetic metal interfaces which is valid. Second case includes the spin dependent scattering at Ta/Co interface. Finally, a complete picture is presented for the SVT with Si/Au/NiFe/Ta/Co/Cu//Cu/Si structure which has spin relaxation in Tantalum and spin-dependent scattering at the Ta/ferromagnet interfaces.

The hot-electrons in Ta attenuates in a very short length unlike the nonmagnetic metals like Au and Cu. The attenuation length in Ta is found to be 1.3 nm. The transmission at Ta/ferromagnet interfaces is 19.6 times lower than the Cu/ferromagnet interfaces. The short hot-electron attenuation length in Ta is attributed to large available density of states in partially empty d band which increases the scattering probability of a hot-electron as it is observed in the ferromagnets. The short inelastic lifetime length for Tantalum measured by time-resolved two photon photoemission (TR-2PPE) is in good agreement with our short attenuation length which is a sum of the elastic and inelastic scattering events.

Then, hot-electron spin-transport in Ta films and at Ta/ferromagnet interfaces are studied. It is shown that the MC depends on the thickness of tantalum spacer layer in the spin-valve base of the SVT. While a SVT with Au or Cu spacer has magnetocurrent 300 %, the magnetocurrent for SVT's with Ta (3 nm) spacer is 26 %. The MC drops to 9% for 6 nm Ta thickness in the spacer layer. The magnetocurrent has a weak dependence on the Ta/ferromagnet interface transmission. The MC is 280% for a device with Si/Au(3 nm)/NiFe(5 nm)/Au(10 nm)/Co(2 nm)/Ta(6 nm)/Cu(2 nm)//Cu(2 nm)/Si structure. It is still 80% lower than 350% indicating that the minority spin transmission is a little bit higher than the majority transmission.

Structural and magnetic characterization is done by transmission electron

microscopy and vibrating sample magnetometer in order to investigate the possibility of mixture of NiFe or Co with Ta. The TEM shows continuous tantalum layers for SVTs with NiFe/Ta/Co and NiFe/Au/Co/Ta spin-valve bases without any conclusive indication of mixture. The saturation magnetic moment of Si/Au(3 nm)/NiFe(5 nm)/Au(5 nm) and Si/Au(3 nm)/NiFe(5 nm)/Ta(6 nm) /Au(5 nm) are equal which proves to have no mixing of NiFe and Ta. However, the saturation magnetic moment of Si/Au(3 nm)/Co(2 nm)/Cu(4 nm)/Au(5 nm) is higher than the saturation magnetic moment of i/Au(3 nm)/Co(2 nm)/Ta(6 nm)/Cu(4 nm)/Au(5 nm). The calculations give intermixing of 14% of Co with Tantalum making 0.28 nm of Co magnetically dead for a 2 nm Co layer.

Finally, we have found no significant spin-dependent transmission at Ta/Co interface where the ratio of the transmission factor for majority spin to minority spin is almost 1.0. Then, spin-relaxation in Ta is found to be 2.1 ± 0.3 nm in Ta. It is argued that the main relaxation process is due to the spin-orbit coupling. It has been calculated that a hot-electron should scatter elastically 20 times before it relaxes which is 2 orders faster than Cu or Al. This is attributed to the localized partially empty d density of states in Ta which has a bigger momentum change for an elastic scattering event than a s band that has a broader distribution.

Chapter 5

Hot-hole transport in a p-type spin-valve transistor

While in the previous two chapters the spin-dependent hot-electron transport in the spin-valve transistor (SVT) was discussed, in this chapter we use a SVT with p-type semiconductor in order to study the transport of non-equilibrium holes with energies below E_F. The attenuation lengths for hot-holes are studied in Co. It is shown that in a SVT with NiFe/Au/Co spin-valve the hot-hole transport is spin-dependent. We present a model to compare and discuss possible mechanisms for the spin-dependent hot-hole transmission in ferromagnets at the end of the chapter.

5.1 Introduction

Hot-electron transport in ferromagnets such as Co, Ni and Fe has shown that electrons above the Fermi level have a spin-dependent transmission in the magnetic materials. In fig 5.1 (a), the density of states for Co is shown. There is an asymmetry in the density of states above the Fermi level where there are more empty states for minority spin than for the majority spin. Therefore, the minority spin (hot) electrons that are travelling at energies above Fermi level have higher number of states to scatter into than the majority spin hot-electrons according to Fermi's golden rule. This results in a shorter inelastic lifetime for the minority spin than for the majority spin [13, 62, 63, 64, 65]. The attenuation lengths for transition metal ferromagnets were determined ranging between 2.5 to 8 nm for majority spin, while the minority spin attenuation length is 2-6 times shorter than that of the majority spin [20, 22, 25]. Spin-waves are also investigated which is another source of spin-asymmetry for the attenuation lengths. The role of interfaces are discussed in chapter 3 and in literature [38, 22, 66].

Although the hot-electron spin-dependent transport above the Fermi level

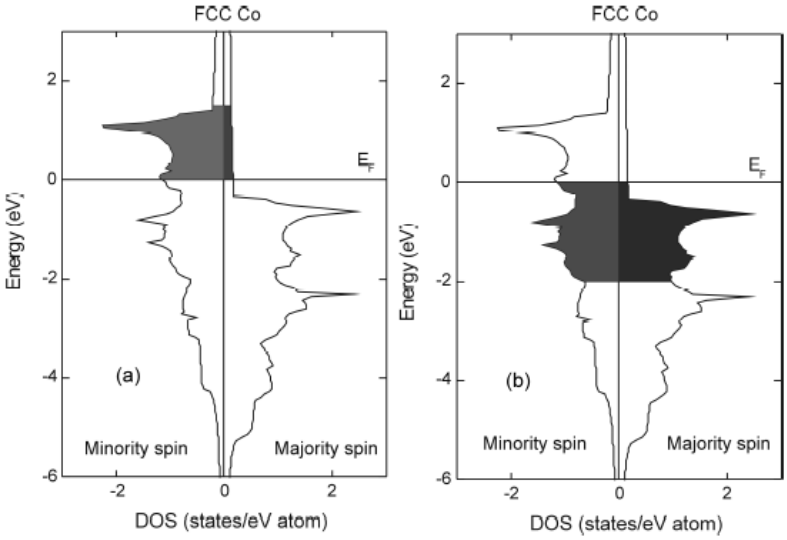

Figure 5.1: *Spin-resolved density of states of fcc Co. (a) the dark (light) area is the empty states available for the minority (majority) hot-electrons of energy between E_F and E_F+2.0 eV to scatter into. (b) the dark (light) area is the empty states available for the minority (majority) hot-holes of energy between E_F and E_F+2.0 eV to scatter into.*

has been studied widely, this is not so for hot-holes below the Fermi level. To complete the picture of transport of non-equilibrium carriers, an investigation of hot-holes is required. The spin asymmetry in the attenuation lengths of hot-electrons is understood by the density of states of the transition magnetic ferromagnets as discussed for Co. With respect to holes, we can see in fig 5.1 (b) that there is an asymmetry between majority and minority spin between E_F and $E_F - 0.4$ eV. Between $E_F - 0.4$ eV and $E_F - 2.0$ eV, the available density of states for both spin channels are comparable. However, spin-dependent hot-hole transport is observed by ballistic hole magnetic microscopy (BHMM) [67, 18] for hot-holes with energies between $E_F - 0.3$ eV and $E_F - 2.0$ eV. For the structures that have NiFe(1.8 nm)/Au(7 nm)/Co (1.8 nm) spin-valve base, 130 % of magnetocurrent (relative change in the collector current under applied field) was reported for holes with injection energy of $E_F - 2.0$ eV. The magnetocurrent is higher than one can expect from the band structure in which a significant asymmetry of the DOS is absent below E_F. The attenuation lengths for holes at energy of $E_F - 2.0$ eV found by BHMM are around 1 nm [18]. This is very short, as can be expected because there are many states available for the hot-holes to scatter into.

In this chapter, we use SVT to study the hot-hole transport in ferromagnets.

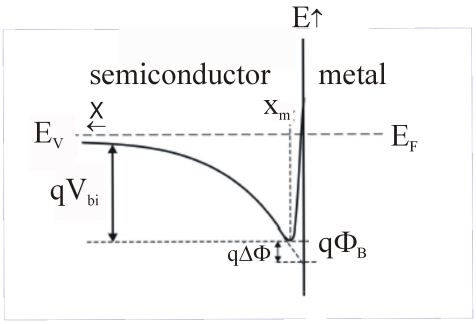

Figure 5.2: *Energy band diagram of a Schottky diode for a metal and an p-type semiconductor contact. E_F is the Fermi level, E is the energy, E_V is the valence band maximum of the semiconductor, q is the charge, Φ_B is the Schottky barrier height, $\Delta\Phi$ is the energy lowering by image force effect, x is the position in the structure, x_m is the position of the Schottky barrier maximum in the semiconductor.*

The spin-valve transistor differs from the BHMM in current injection. BHMM uses an STM tip to inject hot carriers by tunnelling through vacuum. The energy of the holes can be tuned by changing the applied bias between the sample and the tip. The SVT incorporates Schottky diodes. Therefore, the energy of the holes are fixed at the barrier height of the emitter diode. The SVT has an advantage that the emitter current can be increased without effecting the magnetic field dependence of the collector current so that a wide range of thicknesses of ferromagnets can be studied, whereas BHMM suffers from reduced signal to noise ratio for thicker films. The low signal is due to two reasons. One is that there is a limit for the tunnel current (in nA range) that can be applied in BHMM. The second reason is that the collector current signal drops exponentially with the thickness of the ferromagnets in the base. Another important difference is that the energy of the hot-holes for SVT is limited to the Schottky barrier heights. Hence, the energy of the hot-holes cannot be tuned as it can be done in BHMM.

One of the motivation of this chapter is to understand spin-dependent hot-hole transport at ferromagnet/nonmagnetic metal interfaces and in bulk of the ferromagnets. For example, why such large effects in BHMM are observed even though there is no significant spin asymmetry in the band structure of Co DOS. A specific aim is to quantify the interface contribution and hot-hole attenuation lengths in ferromagnets. The reason we want to use SVT is that it offers a different geometry which enables us to study thicker films than BHMM. Another

motivation to study the hot-hole spin transport is that in conventional electronics both holes and electrons are used as the carriers which enables us to have low power consumption devices. Therefore, the emerging field of spintronics [44, 4] needs to have the understanding of spin-dependent transport of electrons and holes to be an alternative future for electronics.

We will first describe the energy band diagram of the SVT with hot-holes. Then, the Schottky diodes that are needed for hot-hole injection and collection are presented. Hot-hole transport study has two parts. In the first part, the hot-hole transmission in Co is studied. Secondly, the spin-dependent hot-hole transport is investigated in SVTs with NiFe/Au/Co spin-valve base with varying thickness of the Co film. We introduce a model to understand spin-dependent hot-hole transmission in NiFe/Au/Co spin-valve base. A comparison of the model and the experiments are done in section 5.5. The chapter ends with a discussion and a conclusion.

5.2 The spin-valve transistor with hot-holes

The spin-valve transistor uses Schottky diodes as the collector and emitter. When a p-type semiconductor and a metal is brought in contact as in fig 5.2, the Fermi levels are aligned in a way that a Schottky barrier is formed. $q\Phi_B$ is the Schottky barrier height which determines the energy of the holes with respect to E_F in the metal base that are injected. E_F is the Fermi level. E_V is the valence band maximum of the semiconductor. V_{bi} is the built in potential due to the contact. The Schottky barrier height $q\Phi_B$ is determined by the combination of the metal and the semiconductor. The typical values for p type Si and metal diodes are between 0.6 eV and 0.3 eV [39].

In order to study hot-hole transport in the spin-valve transistor, the SVT that operates with hot-electrons is modified. The silicon that are used for collector and emitter is chosen to be p-type. The energy band diagram of the p-type SVT is illustrated in fig 5.3. In the metal base there is a spin-valve base consisting of two ferromagnets separated by a nonmagnetic metal. The non-magnetic metal at the emitter diode is chosen such that it has a higher Schottky barrier height than the collector diode. The hot-holes that are injected from emitter pass through the metal base. At the collector silicon, the hot-holes that have enough energy and the right momentum are collected. A hot-hole can scatter inelastically with a hole above the Fermi level. The incoming hot-hole loses energy and the hole above the Fermi level is excited to the energies below the Fermi level. The holes that have energy less than the Schottky barrier height of the collector diode are transported by an electrical contact in the metal base. If the holes have spin-dependent attenuation lengths in the ferromagnetic metals, the collector current will depend on the relative orientation of the magnetic moments of the

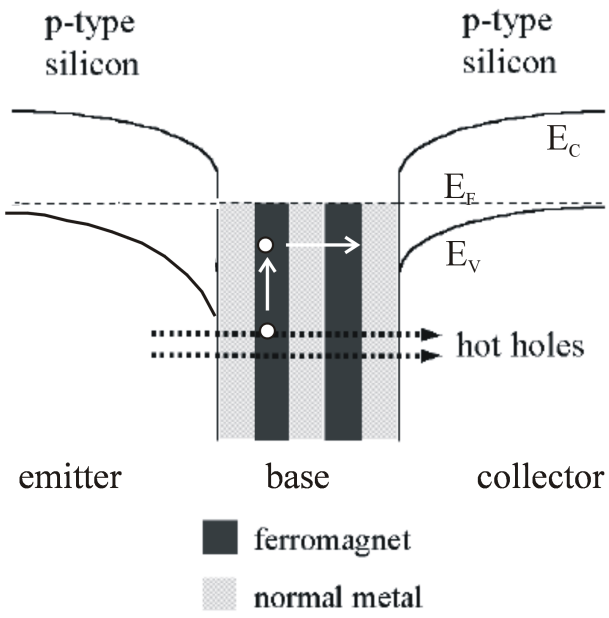

Figure 5.3: *Schematic energy band diagram of the spin-valve transistor. A spin-valve base with ferromagnet/normal metal/ferromagnet is sandwiched in between "p-Si/normal metal"diodes. Hot-holes are injected from a Schottky diode, transported spin-dependently through the spin-valve base and collected by another Schottky diode.*

ferromagnetic metals.

The structure of SVTs in this chapter is p-Si/Au/NiFe/Au/Co/Cu//Cu/p-Si where p-Si stands for p-type silicon (100) which is doped with boron and "//"is the metal vacuum bonding that is realized in the deposition setup. The p-Si substrates are cleaned to have hydrogen terminated surfaces before the deposition in the molecular beam epitaxy (MBE). Then, devices with $350\mu m^2$ emitter and $350x750\mu m^2$ collector area are fabricated by photolithography, dry and wet etching techniques with a process that is similar to that described in chapter 2.1.

5.3 Schottky diodes

It is important to choose proper nonmagnetic metal for the Schottky diode. It must have three characteristics. The first one is that the nonmagnetic metal should form a good quality Schottky barrier. The second characteristics is that the growth of the metal should be smooth. Since the subsequent metal base is

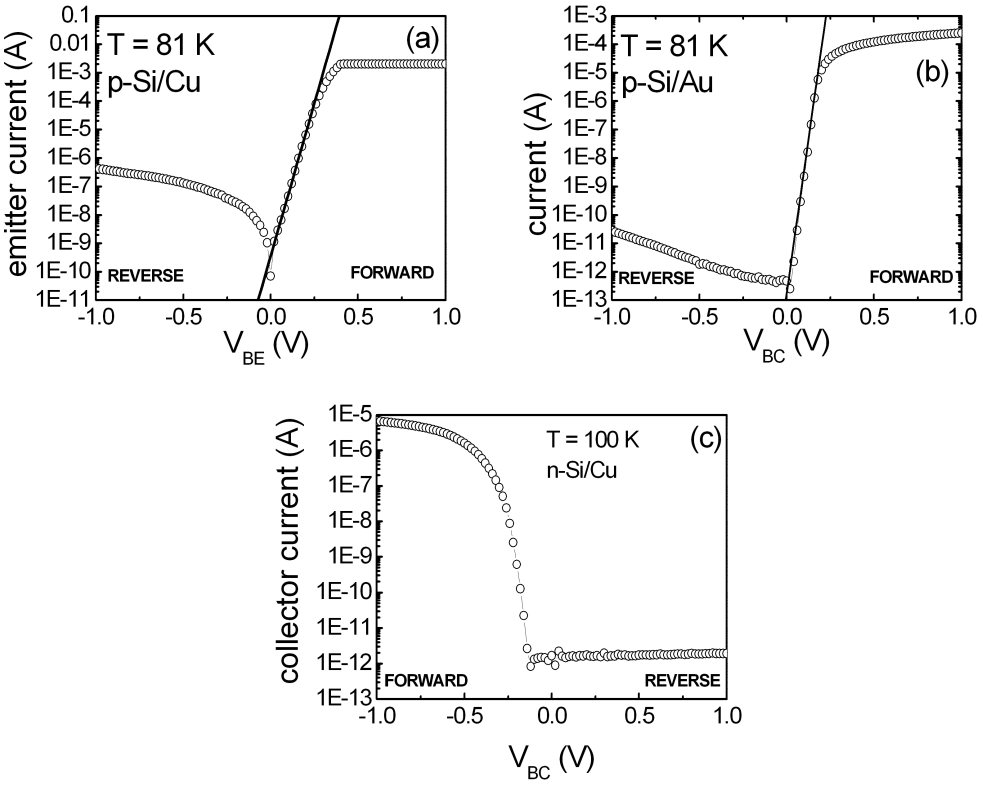

Figure 5.4: *(a) I-V characteristics of a typical p-Si/Cu Schottky diode with an area of 350x350 μm^2 at 81 K. There is a compliance current set to 2 mA in the forward bias. (b) I-V characteristics of a typical Si/Au Schottky diode with an area of 700x350 μm^2 at 81 K. (c) For comparison, I-V characteristics of a typical n-Si/Cu Schottky diode with an area of 700x350 μm^2 at 100 K.*

grown on the Schottky diode, the smoothness of first layer will determine the growth of the rest of the metal stacks. The third criteria is that the metal should have long hot-hole mean free paths. Large hole transmission in Au is found for hot-hole energies between E_F-0.29 eV in BHMM [19] and E_F-1.2 eV which is in agreement with the long inelastic lifetime of hot-holes in Au [68]. Au is a good choice since it grows smooth on silicon and forms a nice Schottky barrier on silicon. The expected barrier height for p-Si/Au is around 0.29 eV [39] which has important consequence. Due to low Schottky barrier height, the leakage current is very high at room temperature. Therefore, the measurements has to be done at low temperature. A second metal, Cu, for the Schottky diode is chosen since one of the Schottky barrier heights of the SVT must be higher than the other. The expected barrier height for p-Si/Cu is around 0.5 eV [39]. It is also calculated that

Cu has a long inelastic lifetime of hot-holes [68] like Au.

In fig 5.4 (a), I-V characteristic of the p-Si/Cu emitter diode of a SVT device which has a p-Si/Au/NiFe/Au/Co/Cu//Cu/p-Si structure is plotted on a semi-log scale, using a compliance of 2 mA in the forward bias. The forward bias has a exponential characteristics. The reverse bias has a current around 10^{-7} A. The transport across Schottky diodes are well explained by the thermionic emission theory as it is described in more detail in chapter 3.3. The barrier height and the ideality factor can be extracted to be 0.51 eV and 1.04, respectively by fitting the exponential region with the thermionic emission theory. The barrier height for p-Si/Cu diode are also measured by ballistic hole magnetic microscopy (BHMM) [19] to be 0.49 eV which is consistent with the barrier heights in the p-SVT. The samples are grown in the same MBE system on identical p-type silicon substrates. In fig 5.4 (b), I-V characteristic of the p-Si/Au collector diode of the same p-SVT is shown. The forward bias has an exponential regime from 0 V to 0.2 V. The contact resistance dominates in voltages higher than 0.2 V. The reverse bias has a current around 10^{-13} A at 0 V. It increases to 10^{-11} A as the voltage increased to 1 V. Leakage current due to the edge damage during the process contributes to the reverse bias current which shows itself as an increase in the reverse bias current with the applied bias. The Schottky barrier height and the ideality factor of the collector diode p-Si/Au is found by the thermionic emission theory fit and found to be 0.31 eV and 1.05, respectively. The Schottky barrier height was also measured with BHMM [19] to be 0.29 eV. In fig 5.4 (c), n-Si/Cu diode is shown for comparison. The carriers in this diode are electrons since the semiconductor used is an n-type silicon. The voltage polarity of the p-Si/Au(Cu) diode and the n-Si/Cu is opposite since the carriers in the former are holes rather than electrons.

5.4 Hot-hole transport in Co

In the previous section, the emitter and collector diodes of the SVTs with p-Si/Au/NiFe/Au/Co/Cu//Cu/p-Si structure are discussed. The p-Si/Cu and p-Si/Au Schottky diodes are used to inject and collect hot-holes respectively. In this section first, hot-hole attenuation lengths in Co will be investigated and then spin-dependent hot-hole transmission in Co is discussed in SVTs that have a NiFe/Au/Co spin-valve base.

Hot-hole transmission in Co

In order to study hot-hole transmission in Co, we have prepared a series of devices with different Co thicknesses. The devices have p-Si/Au(3 nm)/NiFe(3 nm)/Au(10 nm)/Co(2.0-7.5 nm)/Cu(2 nm)//Cu(2 nm)/p-Si structure. The collector current is measured for the case when the magnetic moments of the Co

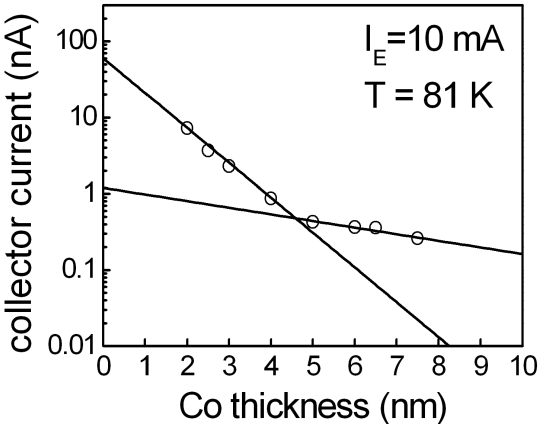

Figure 5.5: *The collector current as a function of Co thickness in devices with p-Si/Au(3 nm)/NiFe(3 nm)/Au(10 nm)/Co(x)/Cu(2 nm)//Cu(2 nm)/p-Si structure where x is the thickness of Co in nm. The circles are experimental data. The lines are exponential fits for two different attenuation length. The emitter current is 10 mA. T = 81 K.*

and the NiFe layer are parallel using an applied field of -100 Oe. The emitter current is 10 mA and the temperature is 81 K. The results are plotted as a function of Co thickness in fig 5.5 in a semi-log scale where the circles are the experimental data. As the Co thickness increases, the collector current decreases. However, the decrease is not a single exponential as it is observed in hot-electron transmission in Co [22]. Instead for hot-holes in Co, there are two regions (below and above approximately 4.5 nm Co thickness) observed where the data can be fitted with only one exponential each with a different slope as indicated by the solid lines. We will come back to the interpretation of this after describing magnetocurrent and model.

The transfer ratio of the devices defined as I_C/I_E can be calculated by using the experimental data points in fig 5.5. The transfer ratio is a useful parameter to measure how many of the injected hot-holes are collected. It also allows us to make comparisons between the transmission of hot-holes and hot-electrons. The transfer ratio is 7.24×10^{-7} for the device with 2 nm Co. It drops to 0.26×10^{-7} for the device with 7.5 nm Co. The transfer ratio for hot-electrons for the n-type SVTs with 3 nm Co and the same 3 nm $Ni_{80}Fe_{20}$ as for the p-type devices is around 10^{-4}. There is a three orders of magnitude difference in the transfer ratio of hot-electron transmission and hot-hole transmission in the SVT.

Spin-dependent hot-hole transport in SVTs with NiFe/Au/Co base

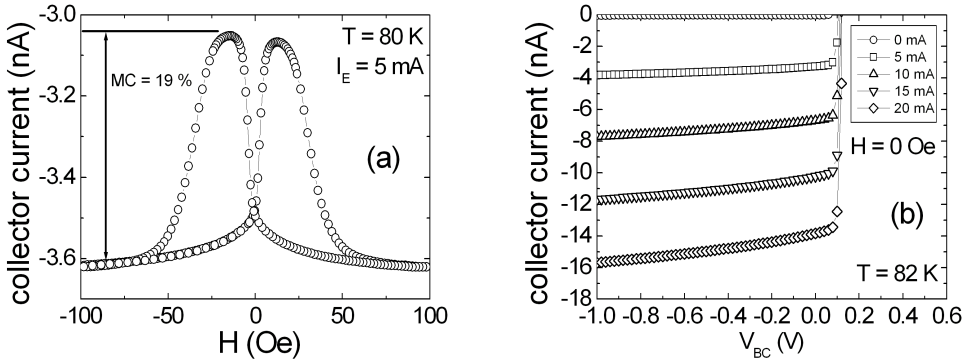

Figure 5.6: *(a) The collector current as a function of magnetic field of a device with p-Si/Au(3 nm)/NiFe(3 nm)/Au(10 nm)/Co(2 nm)/Cu(2 nm)//Cu(2 nm)/p-Si structure. $I_E = 5mA$. T = 80 K. (b) The collector current as a function of applied bias across the collector diode for different emitter currents for the same device as in (a). No applied magnetic field. T = 82 K.*

In order to study hot-hole transport, p-type SVT with NiFe/Au/Co spin-valve base is prepared as described in section 5.2. In fig 5.6 (a), the collector current as a function of magnetic field for a SVT with p-Si/Au(3 nm)/NiFe(3 nm)/Au(10 nm)/Co(2 nm)/Cu(2 nm)//Cu(2 nm)/p-Si structure is plotted for 5 mA emitter current at 80 K. Since the charge carriers are holes which have positive charge, the collector current is measured negative rather than positive where $I_C<0$ corresponds to holes flowing from base to the collector Si. When the magnetic moment of the Co and NiFe are parallel (antiparallel) at +100 (-14) Oe, the collector current is -3.62 nA (-3.05 nA). The hot-hole current clearly depends on the magnetic field which indicates that the transmission of hot-holes in both ferromagnetic metals is spin-dependent. The magnetocurrent is 19 % which can be calculated by $MC=(I_C^P - I_C^{AP})/I_C^{AP}$ where I_C^P (I_C^{AP}) refers to the collector current for parallel (antiparallel) states of spin-valve base. A hot-hole collector current in a SVT is a portion of the emitter current which is able to reach to the collector diode with enough energy and right momentum at the collector Schottky diode after flowing in the metal base of the SVT. In fig 5.6 (b), the collector current of the same device as in fig 5.6 (a) with no applied magnetic field as a function of bias across the collector diode is plotted at 82 K for different emitter current injection. For 0 emitter current, the collector diode I-V characteristics is observed with a current less than 10^{-11} A in the reverse bias of the collector diode. For 5, 10, 15 and 20 mA of emitter current, a fraction of the emitter current is collected at the Si/Au diode. The absolute value of the collector current increases linearly with emitter current. The measurement in

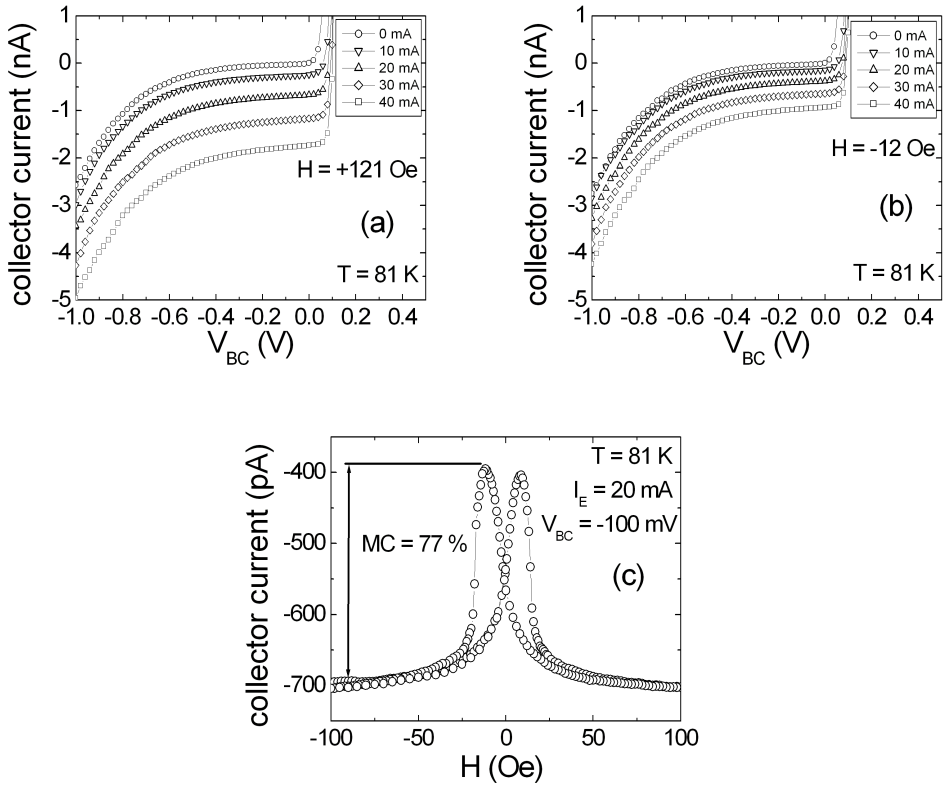

Figure 5.7: *The collector current as a function of applied bias across the collector diode at 81 K for different emitter currents for a device with p-Si/Au(3 nm)/NiFe(3 nm)/Au(10 nm)/Co(7.5 nm)/Cu(2 nm)//Cu(2 nm)/p-Si structure at (a) +121 Oe (b) -12 Oe. (c) The collector current as a function of the magnetic field for the same device as in (a) and (b). T= 81 K.* $I_E = 20mA$.

fig 5.6 (b) makes sure that the source of the collector current is the emitter current and if there is any leakage current, it can be measured at 0 mA emitter current. The leakage current is important since ,if present, it reduces the magnetocurrent. The leakage is the same for both I_C^P and I_C^{AP}. Therefore, leakage current does not effect I_C^P - I_C^{AP}. However, absolute value of I_C^{AP} increases which reduces the magnetocurrent. For the device in fig 5.6, the leakage current is around 10^{-11} A, meaning that the leakage current is small compared to the hot-hole current, thus it does not effect the magnetocurrent calculated in fig 5.6 (a).

In some of the devices especially those with thick Co films, the leakage current was not negligible compared to the hot-hole current. In that case, the transfer ratio and the magnetocurrent has to be corrected for the leakage current by

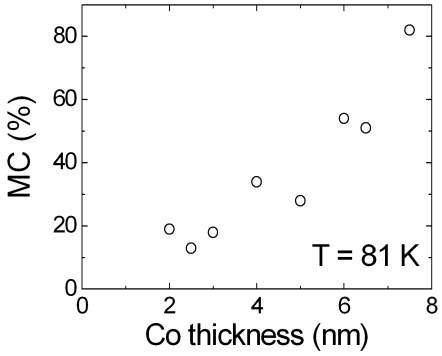

Figure 5.8: *The magnetocurrent as a function of Co thickness for devices with p-Si/Au(3 nm)/NiFe(3 nm)/Au(10 nm)/Co(x nm)/Cu(2 nm)//Cu(2 nm)/p-Si. T = 81 K.*

using the measurement of the collector current as a function of collector bias with different emitter currents. As an example in fig 5.7 (a) and (b), the collector current as a function of bias across the collector diode is plotted at +121 Oe (parallel alignment of magnetic moment of Co and NiFe) and -12 Oe (antiparallel alignment of magnetic moment of Co and NiFe) for a SVT with p-Si/Au(3 nm)/NiFe(3 nm)/Au(10 nm)/Co(7.5 nm)/Cu(2 nm)//Cu(2 nm)/p-Si structure. In both plots, a leakage current is observed for 0 mA emitter current especially for biases higher than 0.5 V. Even between 0.0 V and 0.5 V, there is a leakage current (40 pA) that adds up to the collector current. The leakage current is due the processed induced edge damage. In 5.7 (c), the collector current as a function of magnetic field is plotted for 20 mA emitter current at 81 K and -100 mV across the collector diode. The magnetocurrent is 77 % and the transfer ratio is 3.5×10^{-8}. The magnetocurrent and the transfer ratio that is calculated from fig 5.7 (c) has to be corrected due to the leakage contribution. The metal base characteristics in fig 5.7 (a) and (b) can be used to subtract the leakage current. The corrected magnetocurrent is 82 % and the transfer ratio is 3.3×10^{-8}.

Spin-dependent scattering of hot-holes in the *bulk* of the ferromagnetic film and at the non-magnetic (NM)/ferromagnetic (FM) *interfaces* can both result in magnetic field dependent effect. In order to investigate which mechanism is dominant, we have fabricated SVTs with p-Si/Au(3 nm)/NiFe(3 nm)/Au(10 nm)/Co(2.0-7.5 nm)/Cu(2 nm)//Cu(2 nm)/p-Si structure in which the thickness of Co is changed while keeping the NiFe layer thickness constant. If the spin-dependent scattering at the interfaces is dominant mechanism, a change in magnetocurrent should not be observed. The magnetocurrent as a function of Co thickness is plotted in fig 5.8. The magnetocurrent is increasing with increas-

ing Co thickness from 20% to 80%. Therefore, we conclude that there is a spin filtering effect in the *bulk* of the Co film. The magnetocurrent is small for the SVTs with hot-holes compared to the SVT with hot-electrons for the same thicknesses of ferromagnets.

5.5 Model and comparison with the experiment

It has been shown in previous two sections that the hot-hole transmission and spin-dependent hot-hole transport in Co depends on the thickness of Co. A spin-valve effect similar to that of hot-electron transport in SVT is observed for the hot-holes for a NiFe/Au/Co spin-valve base. However, the hot-hole transmission in Co differs from the hot-electron transmission in Co in a way that it cannot be fitted to a single exponential for which the slope is the attenuation length as shown in fig 5.5. There are two regions with a exponential fit with different slopes. In this section, a model will be introduced for explaining the hot-hole transmission in Co and spin-dependent transport in NiFe/Au/Co spin-valve base. The model is derived from the description of hot-electron spin-dependent transport in n-type SVT. First, the general case that is a single exponential dependence of hot-hole transmission in a ferromagnet will be introduced. Then, we discuss situation with two different scattering mechanism (elastic and inelastic) with different attenuation length.

The magnetocurrent for hot-holes can be written as;

$$MC = \frac{I^P - I^{AP}}{I^{AP}} \tag{5.1}$$

where the I^P and I^{AP} is the hot-hole current for parallel and antiparallel alignment of the base magnetic moments of the ferrogmagnets in the spin-valve base of the SVT. The magnetocurrent arises from the spin asymmetry of the hot-hole scattering resulting in spin-dependent transmission of majority T^M and minority T^m spin hot-holes. The transmission for majority and minority spin can be expressed as:

$$T^M_{FM} = \Gamma^M_{in} \exp(-\frac{t_{FM}}{\lambda^M_{FM}})\Gamma^M_{out}. \tag{5.2}$$

$$T^m_{FM} = \Gamma^m_{in} \exp(-\frac{t_{FM}}{\lambda^m_{FM}})\Gamma^m_{out}. \tag{5.3}$$

where t_{FM} is the film thickness, λ^M_{FM} and λ^m_{FM} the hot-hole attenuation lengths for majority and minority spin and FM denotes the ferromagnet. The Γ_{out} and Γ_{in} denote the transmission across the interface of the ferromagnet with the nonmagnetic metal at each side. The hot-hole current for parallel and antiparallel alignment is related to the hot-hole transmission of the majority and minority spin via:

$$I_C^P \propto T^M_{NiFe}T^M_{Co} + T^m_{NiFe}T^m_{Co}. \tag{5.4}$$

$$I_C^{AP} \propto T^M_{NiFe}T^m_{Co} + T^m_{NiFe}T^M_{Co}. \tag{5.5}$$

The hot-hole current is polarized after transmission of a ferromagnet which can be written as:

$$P_{FM} = \frac{T^M_{FM} - T^m_{FM}}{T^M_{FM} + T^m_{FM}}. \tag{5.6}$$

Finally, the magnetocurrent can be also expressed in terms of transmission polarizations by:

$$MC = \frac{2P_{NiFe}P_{Co}}{1 - P_{NiFe}P_{Co}}. \tag{5.7}$$

The experimental observation for hot-hole transmission in Co is that the equation 5.2 is not sufficient to explain the hot-hole collector current as a function of Co thickness. To understand the origin of two exponentials with each having a different attenuation length, the scattering mechanisms have to be considered. There are two types of scattering in the bulk of Co which are elastic scattering and inelastic scattering. The elastic scattering broadens the momentum distribution resulting some of the hot-holes cannot be collected since they do not have the right momentum. The inelastic scattering is a process that hot-holes lose energy so that they do not have sufficient energy to overcome the Schottky barrier at the collector. In a SVT the hot-holes are injected in a forward focused direction by the Schottky diode. As it passes each layer and interfaces, the distribution becomes isotropic after a certain distance in the metal base. Therefore, the elastic scattering removes more hot-holes from the collection in the first layers than the layers that are closer to collector diode. If we consider the same argument for the Co layer, it is important to stress on that the Co is the first ferromagnet after the emitter diode. Therefore, the momentum

distribution of the hot-holes are still forward focused when the holes enter the Co. The elastic scattering will be dominant in thin Co films. On the other hand, for thick Co films only inelastic scattering still results in hole attenuation since elastic scattering no longer leads to attenuation once the distribution has become isotropic. Therefore, we can write the hot-hole current transmission in parallel configuration where for thin (thick) film thicknesses the elastic (inelastic) scattering is dominant as:

$$T_{Co}^{M} = [(A-B)\exp(-\frac{t_{Co}}{\lambda_{M}^{el}}) + B]\exp(-\frac{t_{Co}}{\lambda_{M}^{in}}) \tag{5.8}$$

$$T_{Co}^{m} = [(A-B)\exp(-\frac{t_{Co}}{\lambda_{m}^{el}}) + B]\exp(-\frac{t_{Co}}{\lambda_{m}^{in}}) \tag{5.9}$$

where A and B are constants. t_{Co} is the Co thickness, λ^{el} is the elastic attenuation length and λ^{in} is the inelastic attenuation length in Co, and M and m denotes the majority and minority spin, respectively. In comparing the model to the experimental data, we consider two cases.

Case1

The first case is that there is no spin-dependent elastic scattering and no spin-dependent transmission at the Co/non-magnetic interfaces, i.e., λ_{M}^{el}=λ_{m}^{el} and Γ^{M}=Γ^{m}. The equation for hot-hole current from 5.4, 5.8 and 5.9 can be written as;

$$I_{C}^{P}(t_{Co}) = [(A-B)\exp(-\frac{t_{Co}}{\lambda_{M}^{el}}) + B][\exp(-\frac{t_{Co}}{\lambda_{M}^{in}}) + \exp(-\frac{t_{Co}}{\lambda_{m}^{in}})] \tag{5.10}$$

In fig 5.9 (left), the fit with equation 5.10 is shown along with the experimental data already given in fig 5.5. The hot-hole attenuation lengths for elastic scattering is 0.80±0.1 nm and inelastic scattering is 5.0±1.0 nm and is 2.7±0.5 nm for majority and minority spin, respectively. In fig 5.9 (right), the magnetocurrent already shown in fig 5.8 as a function of Co thickness is plotted with a fit that uses the equations 5.7, 5.10 and 5.6 with the attenuation lengths that are extracted from 5.9 (left). The parameters that are used for the fit is the same as in fig 5.9 (left) and the transmission polarization for NiFe is taken to be $P_{NiFe} = 0.45$. The collector current as a function of Co thickness fits quite well with the first case. The magnetocurrent data has some scatter and the fit reasonably describes the data.

Case2

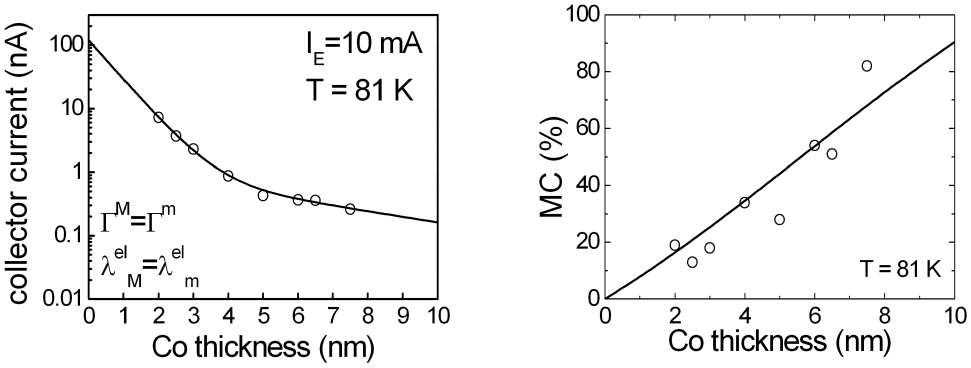

Figure 5.9: *Comparison of the data with model case 1: The collector current ($I_E = 10mA$) (left) and magnetocurrent (right) as a function of Co thickness for SVTs with p-Si/Au(3 nm)/NiFe(3 nm)/Au(10 nm)/Co(x nm)/Cu(2 nm)//Cu(2 nm)/p-Si structure. The circles are experimental data. The solid line is fit. T = 81 K. See text for the definitions of the parameters.*

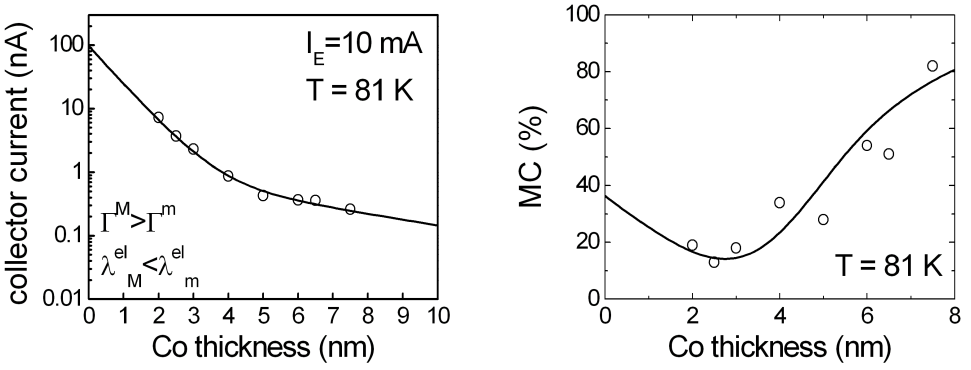

Figure 5.10: *Comparison of the data with model case 2: The collector current ($I_E = 10mA$) (left) and magnetocurrent (right) as a function of Co thickness for SVTs with p-Si/Au(3 nm)/NiFe(3 nm)/Au(10 nm)/Co(x nm)/Cu(2 nm)//Cu(2 nm)/p-Si structure. The circles are experimental data. The solid line is fit. T = 81 K. See text for the definitions of the parameters.*

We consider a second case, since a recent measurement in a p-type magnetic tunnel transistor with single metal base (Co) [69] has shown *negative* hole magnetocurrent for the devices with thin Co thicknesses indicating that there is spin-dependent elastic scattering and minority spin attenuation length is longer than the majority spin attenuation length for the elastic scattering. The transmission in Co for hot-hole current in this second case can then be described as:

$$T_{Co}^{M} = \Gamma^{M}[(A-B)\exp(-\frac{t_{Co}}{\lambda_{M}^{el}}) + B]\exp(-\frac{t_{Co}}{\lambda_{M}^{in}}) \tag{5.11}$$

$$T_{Co}^{m} = \Gamma^{m}[(A-B)\exp(-\frac{t_{Co}}{\lambda_{m}^{el}}) + B]\exp(-\frac{t_{Co}}{\lambda_{m}^{in}}) \tag{5.12}$$

where λ_{M}^{el}, λ_{m}^{el} are elastic attenuation lengths for majority spin and minority spin, respectively with $\lambda_{M}^{el} < \lambda_{m}^{el}$ and we have also included possible spin-dependent interface transmission $\Gamma^{M} \neq \Gamma^{m}$. In fig 5.10 (left), the calculated hot-hole current as a function of Co thickness is plotted for the second case for a ratio of transmission at Co/non-magnetic metal interface of $\frac{\Gamma^{M}}{\Gamma^{m}} = 1.5$ and a transmission polarization of NiFe $P_{FM} = 0.40$. The fit is as good as the first case. In fig 5.10 (right), the magnetocurrent as a function of Co thickness is plotted. The hot-electron attenuation lengths used for the fit are $\lambda_{M}^{el} = 0.80nm$, $\lambda_{m}^{el} = 1.15nm$, $\lambda_{M}^{in} = 5.0nm$ and $\lambda_{M}^{el} = 3.0nm$. It is important to note here that the spin asymmetry is opposite for elastic and inelastic attenuation lengths. The fit starts from a value above zero since there is a spin-dependent transmission at the Co/Cu interface. As it is clearly seen in both figures 5.9 and 5.10, the hot-hole transmission can be explained by two cases.

Let us compare the results for the p-SVT with those determined by BHMM [18, 19]. The attenuation length for structures with thinner Co in BHMM is extracted to be 0.65 nm (1.0 nm) for hot-holes that has an energy of 0.8 eV (2 eV). The SVT data for the hot-holes is at energies 0.5 eV. The hot-hole attenuation lengths that are reported in BHMM do not deviate much from the SVT data in this chapter for thinner Co thickness.

5.6 Discussion on spin-dependent hot-hole transport

The operation energy in the SVT is between 0.29 eV and 0.50 eV. The hot-holes are injected with energies around 0.50 eV. The hot-holes scatter elastically and inelastically in the base and the hot-holes that have enough energy and right momentum are collected by the semiconductor. There is a spin asymmetry for the energies between 0.29 eV and 0.40 eV in the Co density of states such that

the number of available states for minority spin is higher than the majority spin. This could yield a higher attenuation length for the majority spin than the minority spin for the inelastic attenuation lengths as observed. The magnetocurrent for hot-holes for a SVT with p-Si/Au(3 nm)/NiFe(3 nm)/Au(10 nm)/Co(3 nm)/Cu(2 nm)//Cu(2 nm)/p-Si structure is 18 % which is very small compared to the magnetocurrent (384 %) for hot-electrons for the same ferromagnet thicknesses (given in chapter 3 fig 3.5 (b)). The band structure does not provide sufficient explanation for the spin-dependent hot-hole transport. It also does not also explain the elastic behavior for the devices with thinner Co thicknesses.

Another mechanism that can cause an asymmetry in the attenuation lengths is spin waves. We first describe the spin asymmetry for hot electrons, and then for hot holes. The spontaneous spin wave emission flips the spin of the interacting electron due to the spin conservation. A majority spin electron with spin can absorb a spin wave with a spin $\sigma = -1\hbar$ and a minority spin $\sigma = +1/2\hbar$ is created with a spin $\sigma = -1/2\hbar$ because of the spin conservation requirement. At T=0 K, no thermal spin waves are possible. The only spin wave scattering is possible for minority spin because a minority spin can spontaneously emits a spin wave with a spin $\sigma = -1\hbar$. Due to the spontaneous spin wave emission, a majority spin hot-electron is created. Due to *spontaneous* spin wave emission, the lifetime of majority spin is not effected but the lifetime of the minority spin is reduced.

The process of spin wave scattering is reversed for the hot-holes. The spin wave emission is forbidden for hot holes in the minority spin band. However, a majority spin hot-hole can emit a spin wave causing an electron to flip its spin from minority to majority and leaving a hot-hole in the minority spin band. Spin wave interaction of majority spin hot-hole reduces its lifetime therefore predicting a shorter attenuation length for majority spin hot-hole.

5.7 Conclusion

In this chapter, hot-hole transport was presented in the spin-valve transistor. Motivation and background information is given for hot electrons and hot-holes in the first section of the chapter. The Schottky diodes are introduced for p-type Si and Au (Cu) contacts which are used as the emitter and the collector of the devices that are discussed in the chapter. In order to study the hot-hole transport in spin-valve structures, a series of devices are prepared with NiFe(3 nm)/Au(10 nm)/Co(x) spin-valve base.

The spin-valve transistor has Schottky diodes for current injection into the metal base and for current collection. In order to inject holes into the metal base p-type Si is used as the semiconductor. p-Si/Cu emitter diode is chosen to be emitter since it has a relatively high Schottky barrier height compared to other

p-Si/(nonmagnetic metal) diodes. p-Si/Au is chosen for collector since it has a Schottky barrier height of 0.29 eV which is lower than the Schottky barrier height (0.50 eV) of the p-Si/Cu diode. The diodes are characterized at around 80 K since at room temperature thermally activated leakage current is dominating the behavior of the diodes.

Hot-hole attenuation length in Co is investigated in devices with p-Si/Au(3 nm)/NiFe(3 nm)/Au(10 nm)/Co(2.0-7.5 nm)/Cu(2 nm)//Cu(2 nm)/p-Si structure. The collector current is measured when the magnetic moments of the Co and the NiFe are parallel as a function of Co thickness. There were two regions observed. When the Co thickness is lower than 4 nm, an exponential with a short attenuation length 0.80$\pm$0.1 nm can be fitted. The second region has an exponential with a longer attenuation length of 5.0$\pm$1.0 nm. Therefore, the hot-hole attenuation length in Co could not be fitted with a single attenuation length as in the case for hot-electron attenuation length in Co. We propose that for thinner films, the elastic scattering is the dominant mechanism since the momentum distribution of the hot-holes are forward focused due to the fact that the Co layer is the first ferromagnet that hot-holes are injected into. When the Co film becomes thick enough, the momentum distribution becomes isotropic. Then, the inelastic scattering dominates transport of the hot-holes in Co. Another observation is that the hot-hole transmission is three orders of magnitude smaller than the hot-electron transmission in the SVT. This is in agreement with the fact that there are more empty states for hot-holes to scatter into than the hot-electrons.

Spin-dependent hot-hole transport is observed for the SVTs with p-Si/Au/NiFe/Au/Co/Cu/p-Si structures. For 3 nm NiFe and 3 nm Co, 18 % of magnetocurrent is measured which is very low compared to the devices (384 % for the same ferromagnet thicknesses) that has electrons as the charge carriers. As the thickness of the Co layer increased, the magnetocurrent also increases. We introduce a model to describe I_C/I_E and magnetocurrent as a function of Co thickness. Two cases are considered and compared with the data. In case 1, we assume that there is no spin dependent transmission at the interfaces and no spin dependence in elastic scattering. It is found that the inelastic attenuation length for majority (minority) spin is 5.0 (2.7) nm and elastic attenuation length for majority (minority) spin is 0.8 (0.8) nm. However, a recent experimental result has shown that a *negative* magnetocurrent is observed in a p-type magnetic tunnel transistor indicating that the elastic minority attenuation length is shorter than the elastic majority attenuation length. Therefore, in the second case we assume that the elastic scattering is spin-dependent and there is spin-dependent transmission at Co/nonmagnetic film. In this case, the hot-hole current and the magnetocurrent experimental data can be fitted by a spin dependent transmission at the Co/Au interfaces which is 50 % higher for majority spin than the minority spin. The elastic minority (majority) spin attenuation length is found

to be 1.15 (0.80) nm. Thus, the elastic and inelastic attenuation lengths have opposite spin asymmetry.

The band structure of Co suggests that at energies above $E_F - 0.40$ eV, there is a spin asymmetry such that the inelastic minority attenuation length should be shorter than majority spin. However, below $E_F - 0.40$ eV the density of states for both spins are comparable. A decrease in magnetocurrent for hot-holes is observed compared to hot-electrons but the band structure is not enough to explain two different behavior in the attenuation lengths that are observed in Co. We argue that spontaneous spin wave emission predicts that the attenuation length for majority spin should be shorter than the minority spin. More experimental and theoretical work has to be carried out to explain the hot-hole transport in transition ferromagnetic metals.

Chapter 6

Spin-valve transistor with an n-type emitter and a p-type collector

In chapter 5, we have studied the spin-dependent transmission of hot-holes in a spin-valve transistor with a p-Si/Cu emitter and a p-Si/Au collector. In this chapter, the investigation focuses on a structure in which the holes are not directly injected. Rather an n-type Si/Au emitter is used to inject electrons which creates holes via inelastic scattering in the metal base. The excited hot-holes are collected by a p-Si/Cu Schottky diode. A NiFe/Au/Co spin-valve base is used in the metal base where the thickness of NiFe is changed to study the creation and transmission of excited hot-holes. A model is proposed to understand the spin-dependence of created hot-hole excitations along with a discussion.

6.1 Introduction

It is well known that an incident electron above the Fermi level can interact with an another electron below the Fermi level through Coulomb and exchange interaction and scatters it to above the Fermi level, thus creating an electron-hole pair [70]. In most experimental investigations of this, the transmitted (not scattered) hot-carriers are detected and analyzed which gives an indirect information about the scattering process. To probe directly the scattering process, it is desirable to detect the excited e-h pairs. In order to achieve this, the spin-valve transistor in chapter 3 and chapter 5 can be combined. The structure that would thus be used in this chapter is n-Si/Au/NiFe/Au/Co/Cu//Cu/p-Si. The n-Si/Au will provide hot-electron injection into the SVT base as shown i fig 6.1. The hot-electrons will scatter inelastically in the NiFe/Au/Co spin-valve to create excited hot-holes which can be collected by the p-Si/Cu Schottky diode. This

process was previously studied with reverse ballistic hole magnetic microscopy (RBHMM) [67, 19] which has an STM tip and a vacuum tunnel barrier as hot-electron emitter instead of a n-Si/Au Schottky diode. It has been shown that the excited hot-hole transmission is spin-dependent and the magnetocurrent is as high as 200% for a NiFe(1.8 nm)/Au(7 nm)/Co(1.8 nm) spin-valve base at hot-electron energies of 1.0 eV [19]. However, the study could not address all the questions about the scattering process.

In this chapter, our motivation is to study the excited hot-hole excitations in a different structure, namely the SVT, to understand the physical basis for the scattering mechanism for hot-carriers. The geometry of the SVT differs from the RBHMM in the sense that the energy distribution in SVT is in a smaller interval than RBHMM. The SVT could probe lower energies than the RBHMM. Another reason to use SVT is that thicker films could be grown to study which is not possible for RBHMM because the SVT can have higher emitter currents than the RBHMM thus having more collected current. In chapter 5, the study of devices with thick ferromagnetic films have provided additional information on the attenuation lengths in Co which could not be probed by BHMM [19, 67].

The chapter starts with a description of the structure of the SVT. The energy band diagram is presented along with the Schottky diodes that are required for hot-electron injection and hot-hole collection. In section 6.3, we investigate the excited hot-hole transmission in NiFe and determine the effective decay length in NiFe. Then, the spin-dependent transmission of excited hot-holes in a NiFe/Au/Co spin-valve base is presented. A model is introduced for explaining the spin-dependent transmission of the excited hot-holes. Discussion is done on the basis of model and experimental results.

6.2 Spin-valve transistor with hot-hole excitations

The structure of SVTs in this chapter is n-Si/Au/NiFe/Au/Co/Cu//Cu/p-Si where p-Si stands for p-type silicon (100) which is doped ($N_a \simeq 10^{16}$ cm^{-3}) with boron, n-Si stands for n-type silicon (100) which is doped ($N_d \simeq 10^{16}$ cm^{-3}) with phosphorus and "//"is the metal vacuum bonding that is realized in the deposition setup. The p-Si and n-Si substrates are cleaned to have hydrogen terminated surfaces before the deposition in the molecular beam epitaxy (MBE). Then, SVTs with 350μm^2 emitter (n-Si/Au) and 350x750μm^2 collector (p-Si/Cu) area are fabricated by photolithography, dry and wet etching techniques with a process that is similar to that described in chapter 2.1.

In order to study the excited holes, we have used a hot-electron emitter with a n-Si/Au Schottky diode, a hot-hole collector with a p-Si/Cu Schottky diode and a FM/NM/FM spin-valve base in between the two diodes as illustrated in fig 6.1 where FM and NM stands for ferromagnetic metal and nonmagnetic

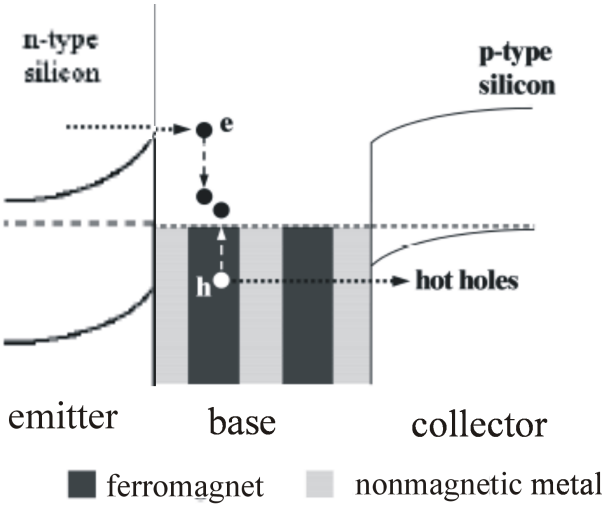

Figure 6.1: *Schematic energy band diagram of the spin-valve transistor used to study scattering processes in the ferromagnetic metals. A spin-valve base with ferromagnet/normal metal/ferromagnet is sandwiched in between n-Si/nonmagnetic metal (NM) and p-Si/NM diodes. Hot-electrons are injected from n-Si/NM Schottky diode. Inelastic scattering in the ferromagnetic layers creates electron-hole (e-h) pairs inducing a spin-dependent hot-hole current into the valence band of the collector semiconductor.*

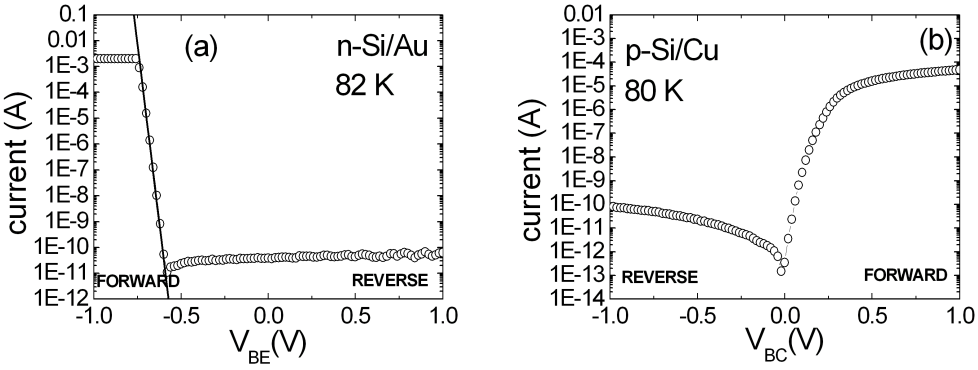

Figure 6.2: *The I-V characteristics of Schottky diodes for a n-type Si/Au(3 nm) at 80 K(left) and a p-type Si/Cu(4 nm) at 82 K structures. The n-Si/Au Schottky diode is used as hot-electron emitter and the p-Si/Cu Schottky diode used as hot-hole collector. The absolute value of the current is displayed.*

metal, respectively. In this configuration, hot-electrons injected from the emitter cannot be collected directly since the built-in Schottky-barrier potential of the collector opposes the hot-electron velocity and does not stop their leakage back into the base. However, hot-electrons can scatter inelastically and create e-h pairs. The hot-holes that are created can be transmitted through the spin-valve base and enter the valence band of the p-type silicon provided the holes have enough energy and the proper momentum to overcome the collector Schottky barrier. If the excited holes have spin-dependent attenuation lengths in the ferromagnetic layers (as shown in chapter 5 of this thesis), the collected hot-hole current will depend on the relative orientation of the magnetic moments of the ferromagnetic metals in the spin-valve base.

The Schottky diodes with n-type Si and p-type Si are already discussed in more detail in chapter 3.3 and 5.3, respectively. Here, we present the experimental data to show that the emitter (a) and the collector (b) diodes are reversed in polarity as expected from the structure that is depicted in fig 6.1. The Schottky barrier height for emitter diode n-Si/Au in fig 6.2 (a) for a SVT with n-Si/Au/NiFe/Au/Co/Cu/p-Si structure is determined to be 0.82 eV with an ideality factor 1.04. The collector diode p-Si/Cu in fig 6.2 (b) for the same device has a high contact resistance which makes the forward characteristics curved rather than a exponential dependence. So we cannot extract Schottky barrier height. However, we expect a Schottky barrier height of 0.5 eV for a p-Si/Cu diode since the silicon substrates, the preparation and the growth of the samples are similar to that presented in chapter 5. The operating bias for the emitter diode is in the forward direction (minus voltage) so that we have an emitter current of 10 mA. The collector diode is operated in the reverse bias (minus voltage between 0.0-0.5) direction. The current plotted in fig 6.2 are absolute values of the measured current.

6.3 Hot-hole excitations in NiFe

In order to study the hot-hole creation and subsequent transmission of hot-holes, we have measured the hole current as a function of NiFe in SVTs with n-Si/Au(3 nm)/NiFe(x)/Au(10 nm)/Co(3 nm)/Cu(2 nm)//Cu(2 nm)/p-Si structure. The investigation has two parts. In the first part, the effective decay lengths in NiFe which is related to the scattering of the injected hot-electrons and the collection of the excited hot-holes are presented. In the second part, spin-dependent transmission of the excited hot-holes are studied.

Effective decay lengths in NiFe

It is well known for hot-carriers that the transmitted current decays exponentially with thickness of the film. The attenuation lengths in a metal could

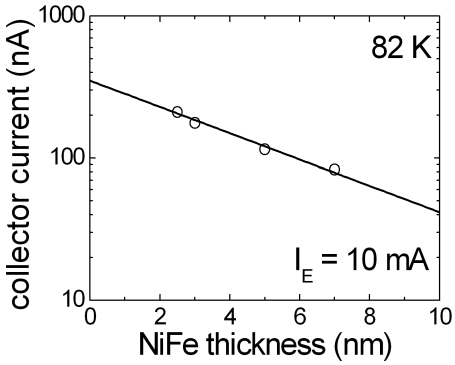

Figure 6.3: *The excited hot-hole current as a function of NiFe thickness for SVTs with n-Si/Au(3 nm)/NiFe(x)/Au(10 nm)/Co(3 nm)/Cu(2 nm)//Cu(2 nm)/p-Si structure. The circles are experimental data taken at emitter current of 10 mA and 82 K. Applied magnetic field is -100 Oe. The solid line is a fit for a single exponential.*

be measured by the plot of transmitted current as a function of the film thickness. The situation is different for the structures studied in this chapter since the excited hot-carriers (holes) are collected instead of the injected hot-carriers (electrons). Therefore, the decay length of the hole collector current is a combination of electron and hole scattering lengths.

In fig 6.3, the hot-hole current as a function of NiFe thickness is shown for SVTs with n-Si/Au(3 nm)/NiFe(x)/Au(10 nm)/Co(3 nm)/Cu(2 nm)//Cu(2 nm)/p-Si structure. The data is taken at 82 K and 10 mA of emitter current. The circles are experimental data points. The excited hot-hole current drops exponentially with increasing NiFe thickness. The data can be fitted with an exponential which can be expressed as:

$$I_C^P(t_{NiFe}) = I_C^P(0)\exp(-\frac{t_{NiFe}}{\lambda_{eff}}) \tag{6.1}$$

where $I_C^P(0)$ is the current when the solid line intersects the collector current axis at zero NiFe thickness, t_{NiFe} is the NiFe thickness and λ_{eff} is the effective decay length in NiFe. The data fits with the exponential line in fig 6.3 from which the effective hot-hole decay length in NiFe λ_{eff} is found to be 4.7 nm. The effective decay length in NiFe is slightly longer than the hot-electron attenuation length for majority spin $\lambda_e = 4.3nm$ in NiFe. The hot-hole attenuation length for majority spin λ_h in NiFe is reported measured by BHMM [19] is around 1.0 nm at 2.0 eV. However, the measurement is done for film thicknesses of lower than

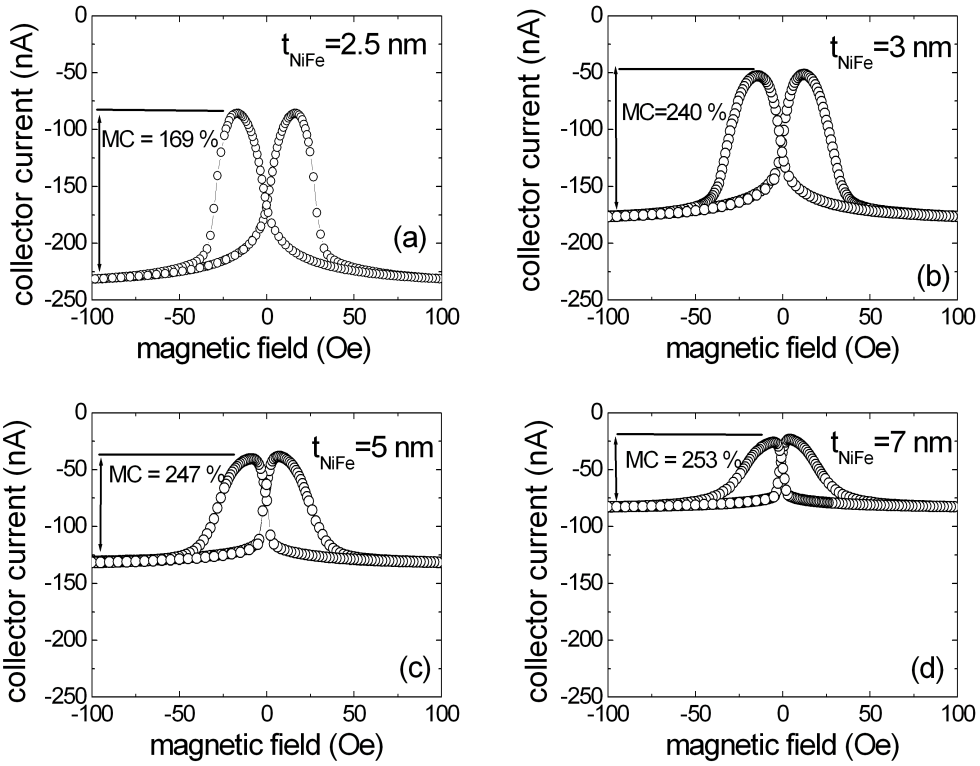

Figure 6.4: *The excited hot-hole current as a function of magnetic field for SVTs with n-Si/Au(3 nm)/NiFe(x)/Au(10 nm)/Co(3 nm)/Cu(2 nm)//Cu(2 nm)/p-Si where (a)x = 2.5 nm (b) 3 nm (c) 5 nm (d) 7 nm. The data is taken at emitter current of 10 mA and 82 K for all devices.*

3 nm. As it is observed in Co in chapter 5, there might be longer attenuation lengths for the hot-holes λ_h in NiFe. Since the effective decay length is the combination of both attenuation lengths, the 4.7 nm effective decay length suggests that the hot-hole attenuation length λ_h in NiFe might be as high as 5 nm as it is found in Co in chapter 5.

Spin-dependent transmission of excited hot-holes

In order to investigate the spin-dependent transmission of excited hot-holes, we have measured the excited hot-hole current as a function of magnetic fields. In fig 6.4 (a), the collector current as a function of magnetic field is shown for a SVT with n-Si/Au(3 nm)/NiFe(2.5 nm)/Au(10 nm)/Co(3 nm)/Cu(2 nm)//Cu(2 nm)/p-Si structure. The emitter current is 10 mA. The temperature is 82 K. The collector current is negative since holes are collected which means holes are flowing from metal base to the collector Si. The hole current is -231 nA (-86

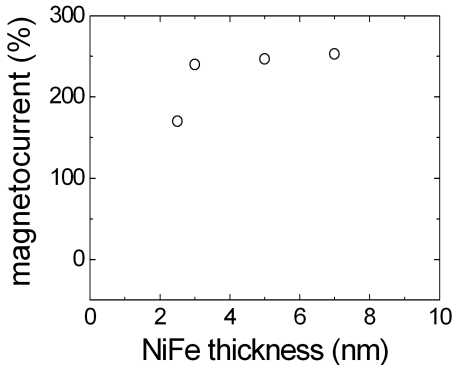

Figure 6.5: *The excited hot-hole magnetocurrent as a function of NiFe thickness for SVTs with n-Si/Au(3 nm)/NiFe(x)/Au(10 nm)/Co(3 nm)/Cu(2 nm)//Cu(2 nm)/p-Si structure. The data is taken at emitter current of 10 mA and 82 K.*

nA) when the magnetic moments of the NiFe and the Co film are parallel (antiparallel). As it is clearly seen, the excited hole current is spin-dependent. The magnetocurrent is 169 % and positive, i.e., $\mid I^P \mid > \mid I^{AP} \mid$. In fig 6.4 (b), (c) and (d), the collector current as a function of magnetic field for the devices with the same structure but with different NiFe thicknesses of 3, 5 and 7 nm are plotted. The magnetocurrent is 240%, 247% and 253%, respectively. The magnetocurrent of all four graphs in fig 6.4 are plotted as a function of NiFe thickness in fig 6.5. The magnetocurrent varies only little with thicker NiFe films and saturates at around 250%.

The magnetocurrent results are quite surprising due to the positive sign and the large magnitude of the MC. The excited hot-holes are created by the inelastic scattering of hot-electrons. It is known that the transmission of hot-electrons is higher in parallel state than the antiparallel state. To a first approximation, one might expect more hot-holes are created in the antiparallel state. Therefore, the excited hot-hole current was expected to be higher for antiparallel state than the parallel state, which would give a negative MC. However, this argument lacks two important aspects. Firstly, the excited hot-holes, once created, have spin-dependent transmission in the ferromagnetic films. Secondly, the creation of e-h pairs is spin-dependent since the hot-electron transmission in the ferromagnets is spin-dependent. Another point is that the magnetocurrent for devices with hole injection and collection is very small (10 times) compared to the magnetocurrent of the devices in fig 6.4 for the SVTs with similar ferromagnet thicknesses. In order to understand these experimental results, a model is introduced for a detailed analysis and discussion in the next section.

6.4 Model

In this section, a model for the calculation of the excited hot-hole current will be presented for the structures that has a NiFe/Au/Co spin-valve base. The model includes the spin-dependent decay of injected hot-electrons, the creation of electron hole (e-h) pairs and the spin-dependent transmission of the excited hot-holes into the collector.

The hole current is calculated for a spin-valve transistor that has a n-Si/Au/NiFe/Au/Co/Cu//Cu/p-Si structure where n-Si/Au is an unpolarized hot-electron emitter and Cu/p-Si is a hot-hole collector. The hot-electron and -hole scattering in Au and Cu are neglected since the inelastic lifetimes in these layers do not depend on spin and are generally large compared to the layer thickness. The scattering at the metal/metal and metal/silicon interfaces is also neglected. The spin-up $\uparrow$ electrons are aligned with the magnetization of the first ferromagnetic layer (NiFe) whose magnetization orientation is chosen to be fixed. The magnetization of the second layer (Co) is free to rotate. A spin-up $\uparrow$ electron is a majority (minority) electron in the second ferromagnet in the P (AP) state and it is similarly for spin-down $\downarrow$ electrons and for hot-holes.

The evolution of the number $f_e^{\uparrow}(x)$ and $f_e^{\downarrow}(x)$ of hot electrons in the first ferromagnetic layer with majority and minority spin can described respectively as:

$$\frac{\partial f_e^{\uparrow}(x)}{\partial x} = \frac{1}{\lambda_e^M} f_e^{\uparrow}(x) \tag{6.2}$$

$$\frac{\partial f_e^{\downarrow}(x)}{\partial x} = \frac{1}{\lambda_e^m} f_e^{\downarrow}(x) \tag{6.3}$$

where x is the spatial position within the first ferromagnet measured from the side of the electron injection, λ_e^M and λ_e^m are the spin-dependent hot-electron attenuation length for majority and minority spin hot-electron respectively. The solution to these equations gives exponential decay:

$$f_e^{\uparrow}(x) = f_0 \exp(-\frac{x}{\lambda_e^M}) \tag{6.4}$$

and

$$f_e^{\downarrow}(x) = f_0 \exp(-\frac{x}{\lambda_e^m}) \tag{6.5}$$

Since the current injected into the first ferromagnet is unpolarized, f_0 is equal for both spins.

The evolution of the number $g_e^{\uparrow}(x)$ and $g_e^{\downarrow}(x)$ of hot-holes with majority and minority spin that are excited in the first ferromagnet due to inelastic decay of hot-electrons can be described as:

$$\frac{\partial g_h^{\uparrow}(x)}{\partial x} = -\frac{1}{\lambda_h^M} g_h^{\uparrow}(x) + \frac{\alpha 1}{\lambda_e^M} f_e^{\uparrow}(x) + \frac{\beta 1}{\lambda_e^m} f_e^{\downarrow}(x) \tag{6.6}$$

$$\frac{\partial g_h^{\downarrow}(x)}{\partial x} = -\frac{1}{\lambda_h^m} g_h^{\uparrow}(x) + \frac{\alpha 2}{\lambda_e^M} f_e^{\uparrow}(x) + \frac{\beta 2}{\lambda_e^m} f_e^{\downarrow}(x) \tag{6.7}$$

The right hand side of the equations 6.6 and 6.7 contains three terms. The first term represents loss due to the inelastic scattering of holes. The other two terms represents the creation of holes by majority and minority electrons. The constants $\alpha 1$,$\alpha 2$,$\beta 1$ and $\beta 2$ are material dependent parameters. These parameters contain the information related to the efficiency of the hot-electrons to excite e-h pairs and the energy distribution of the excited hot-holes. The solutions of the equations 6.6 and 6.7 together with equations 6.2 and 6.3 gives 4 expressions for the hot-hole and hot-electron current which is transmitted to the second ferromagnet via Au spacer. The expressions are boundary conditions for the set of equations for the second ferromagnet. We can write equations to describe the evolution of the hot-electron and -hole current in the second ferromagnet for the parallel (P) state similarly:

$$\frac{\partial g_h^{\uparrow}(x)}{\partial x} = -\frac{1}{\lambda_h^M} g_h^{\uparrow}(x) + \frac{\alpha 3}{\lambda_e^M} f_e^{\uparrow}(x) + \frac{\beta 3}{\lambda_e^m} f_e^{\downarrow}(x) \tag{6.8}$$

$$\frac{\partial g_h^{\downarrow}(x)}{\partial x} = -\frac{1}{\lambda_h^m} g_h^{\uparrow}(x) + \frac{\alpha 4}{\lambda_e^M} f_e^{\uparrow}(x) + \frac{\beta 4}{\lambda_e^m} f_e^{\downarrow}(x) \tag{6.9}$$

The parameters $\alpha 3$ ($\beta 3$) and $\alpha 4$ ($\beta 4$) describe the efficiency of spin-up (spin-down) hot-electrons to create e-h pairs in majority and minority spin channel respectively. For the antiparallel alignment, the spin-up (spin-down) hot-carrier is now a minority (majority). Therefore, we interchange the attenuation lengths for majority and minority.

$$\frac{\partial g_h^{\uparrow}(x)}{\partial x} = -\frac{1}{\lambda_h^m} g_h^{\uparrow}(x) + \frac{\alpha 3}{\lambda_e^m} f_e^{\uparrow}(x) + \frac{\beta 3}{\lambda_e^M} f_e^{\downarrow}(x) \tag{6.10}$$

$$\frac{\partial g_h^{\downarrow}(x)}{\partial x} = -\frac{1}{\lambda_h^M} g_h^{\uparrow}(x) + \frac{\alpha 4}{\lambda_e^m} f_e^{\uparrow}(x) + \frac{\beta 4}{\lambda_e^M} f_e^{\downarrow}(x) \tag{6.11}$$

6.5 Discussion and comparison with the model

We make three assumptions for the calculations. First assumption is that the majority electrons generate e-h pairs in majority spin band while minority electrons generate e-h pairs in minority spin band. The second assumption is that the efficiency of generating e-h pairs for both majority and minority is same,i.e., $\alpha 1 = \alpha 3 = \beta 2 = \beta 4 = 1$ and $\alpha 2 = \alpha 4 = \beta 1 = \beta 3 = 0$. Third assumption is that the distribution of excited hot-holes are isotropic in momentum space.

The model calculations needs some parameters to make a fit with the data. The hot-electron attenuation lengths in Co have been previously measured by BEEM in energy range of 0.8-2.0 eV ($\lambda_e^M \approx 2.3nm$ and $\lambda_e^m \approx 0.7nm$) [20] and in NiFe are measured by SVT at energy $\approx$ 0.9 eV ($\lambda_e^M \approx 4.3nm$ and $\lambda_e^m \approx 1.0nm$) [22]. The attenuation lengths for hot-holes are quite important for the calculations. In chapter 5 of this thesis, we have presented spin-dependent hot-hole transmission in Co. The inelastic attenuation lengths in Co are found to be $\lambda_h^M = 5nm$ and $\lambda_h^m = 3nm$ for majority and minority spin, respectively. It is found for thin Co films a shorter attenuation length is observed which it is interpreted to be an elastic attenuation length. We assume here that the excited hot-hole distribution in momentum is isotropic. Therefore, any elastic scattering event will not effect the distribution of the excited hot-holes as a result, the excited hot-hole current is not attenuated by elastic scattering. Since the excited hot-hole current does not change with elastic scattering, the magnetocurrent will not be altered by elastic scattering events for the excited hot-hole current. However, short attenuation lengths in BHMM has shown to explain the data on spin-dependent excited hot-hole transport [19]. Therefore, we will consider two cases. The first case is that the inelastic hot-hole attenuation lengths are long as it is found in chapter 5. In this case, the excited hot-holes that are created everywhere in the metal base will contribute to the excited hot-hole current. The second case is that the hot-hole attenuation lengths are short. Due to short hot-hole attenuation lengths, the excited hot-holes that are created near to the collector Si can only contribute to the excited hot-hole current. The hot-holes created near to the emitter will be strongly attenuated. Since the hot-hole attenuation lengths in NiFe are not known, we will assume the same attenuation lengths for NiFe as in Co.

Case 1

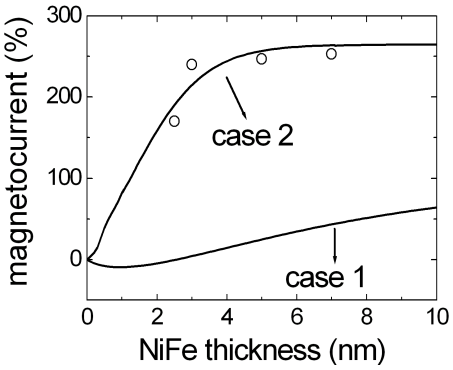

Figure 6.6: *The excited hot-hole magnetocurrent as a function of NiFe thickness for SVTs with n-Si/Au(3 nm)/NiFe(x)/Au(10 nm)/Co(3 nm)/Cu(2 nm)//Cu(2 nm)/p-Si structure. The circles are experimental data taken at emitter current of 10 mA and 82 K as shown previously shown in fig 6.5. The solid line is a fit. See text for the parameters.*

In fig 6.6, the calculated magnetocurrent (solid line) for case 1 as a function of NiFe thickness in SVTs with n-Si/Au(3 nm)/NiFe(x)/Au(10 nm)/Co(3 nm)/Cu(2 nm)//Cu(2 nm)/p-Si structure is plotted with the inelastic attenuation lengths $\lambda_h^M = 6.0nm$ and $\lambda_h^m = 2.5nm$ in Co and NiFe for majority and minority spin holes, respectively. The circles are the data points for SVTs that are discussed in section 6.3. The data does not fit with the calculation. The calculated MC is 10 times lower than the experimental result. Also for thinner NiFe thicknesses, the calculated MC is negative. There are two mechanisms that competes in this case. The number of minority excited hot-holes are more than the number of majority excited hot-holes since inelastic scattering of the minority spin electrons is more than inelastic scattering of the majority spin electrons. At the same time, the attenuation length of hot-holes for minority spin is shorter than the majority spin. Therefore, for NiFe thicknesses (thinner than 3 nm) comparable to the hot-hole minority attenuation length, the excited minority hot-holes contribute to the excited hot-hole current more than for the thicker NiFe films. As the film gets thicker, the contribution to the excited hot-hole current from the majority spin is higher thus making the magnetocurrent positive.

Case 2

In fig 6.6, the calculated (solid line) magnetocurrent as a function of NiFe thickness for case 2 is plotted. This time, the MC calculation (solid line) takes small values for the attenuation lengths for hot-holes with majority and minority spin: $\lambda_h^M = 1.0nm$ and $\lambda_h^m = 0.5nm$ in Co and NiFe. The calculated MC fits very

well with the experimental data. In this case, since the excited hot-holes have very short attenuation lengths compared to the ferromagnetic film thicknesses, the magnetocurrent is very high. First, we consider the excited hot-holes created in the first ferromagnetic layer (NiFe). The hot-hole attenuation lengths are taken very short compared to the film thickness. Therefore, the hot-holes that are created in NiFe will decay immediately which results in an energy lower than the Schottky barrier height of the collector. Even the hot-holes created at the collector side of the NiFe film, they still have to pass through 3 nm Co film. The attenuation lengths for both majority and minority spin is too short compared to the Co film thickness. The hot-hole current coming from NiFe will immediately decay and lose energy so that it cannot be collected due to the the Schottky barrier height at the collector. The hot-holes of the majority spin in the Co will be created mostly at the collector side of the Co film since the hot-electron attenuation length in Co for majority spin is around 2.3 nm. The hot-hole current for minority spin will mostly be created in the first half of the Co film on the emitter side since the hot-electron attenuation length for the minority spin is 0.7 nm. Therefore, the excited hot-holes for minority spin have to pass through 2 nm of Co which is much thicker than the hot-hole minority spin attenuation length (0.5 nm). Even though, the number of excited hot-hole current for minority spin is higher than the majority spin, it is filtered out by the Co film by inelastic process so that the hot-holes of minority spin do not have enough energy to overcome the Schottky barrier at the collector. Therefore, the collected hole current is dominated by holes excited in the second (Co) layer, due to inelastic decay of majority hot-electrons which makes the magnetocurrent positive and as high as 250%. The magnetocurrent stays constant at thick NiFe films since the magnetocurrent is determined by the excited hot-holes created in Co and the thickness of the Co is fixed at 3 nm.

In case 1, we use long hot-hole attenuation lengths (supposed to be inelastic attenuation lengths) that are measured in chapter 5 but the calculated MC does not explain the experimental data. In case 2, the short attenuation lengths (supposed to be elastic attenuation lengths) are used as in RBHMM which explains the data very well. The short inelastic attenuation length is not expected. However, elastic scattering, which has short attenuation length, is not expected to contribute if holes excited from electron decay have isotropic momentum distribution. Therefore, the model is inadequate to explain the experimental data. In chapter 5, we have found that there might be spin-dependent transmission at the Co/Au interface. The transmission of majority spin for hot-holes are higher than the transmission of minority spin for hot-holes. If we include this effect, the calculated magnetocurrent in case 1 would be higher. Another factor that should be checked is that the assumption of isotropic distribution in momentum of the excited hot-holes. If this is incorrect, the elastic attenuation lengths that are found in chapter 5 would be effecting magnetocurrent and it is seen

in case 2 that short hot-hole attenuation lengths are able to explain the experimental data very well. Therefore, a refined model is needed that includes the spin-dependent transmission of hot-holes at ferromagnet/nonmagnetic metal interface and the distribution in momentum of the excited hot-holes.

6.6 Conclusion

In this chapter, we have studied the creation of e-h pairs and the spin-dependent transmission of the excited hot-hole current in a NiFe/Au/Co spin-valve base which is sandwiched in between a n-Si/Au hot-electron emitter and a p-Si/Cu collector. An unpolarized hot-electron is injected by n-Si/Au at energies 0.82 eV. The hot-electrons scatter inelastically in the ferromagnets which creates electron-hole pairs. The injected hot-electrons could not be collected due to the built-in potential at the p-Si/Cu interface therefore allowing us only to collect excited hot-holes which has enough energy and right momentum to overcome the Schottky barrier.

The investigation started with effective decay lengths in NiFe for excited hot-holes with SVTs that has n-Si/Au(3 nm)/NiFe(x)/Au(10 nm)/Co(3 nm)/Cu(2 nm)//Cu(2 nm)/p-Si structure where x is varied from 2.5 nm to 7 nm. The effective decay length in NiFe is determined to be 4.7 nm. There is no data reported for hot-hole attenuation lengths in NiFe. However, the effective decay length is a combination of hot-electron and hot-hole attenuation lengths. The value we obtain is closer to the hot-electron attenuation lengths 4.3 nm in NiFe previously determined using SVT [22]. This suggests that the hot-hole attenuation lengths in NiFe could be higher than the hot-electron attenuation lengths in NiFe. However, the prediction of hot-hole attenuation length from the effective decay length in NiFe is shorthanded since it relies on some assumptions. One assumption is that the distribution of excited hot-holes are considered to be isotropic which is not conclusively observed.

It is shown for SVTs with n-Si/Au(3 nm)/NiFe(2.5-7.0 nm)/Au(10 nm)/Co(3 nm)/Cu(2 nm)//Cu(2 nm)/p-Si structure that the hot-electrons could create electron-hole pairs where the excited hot-holes transport through the spin-valve base spin-dependently. For the devices with 3, 5 and 7 nm NiFe, the magnetocurrent found to be around 250% and for the device with 2.5 nm NiFe the MC is 170%. This is much larger than the magnetocurrents (20%) for the device with p-Si/Au(3 nm)/NiFe(3 nm)/Au(10 nm)/Co(3 nm)/Cu(2 nm)//Cu(2 nm)/p-Si structure in chapter 5. The magnetocurrent results for the SVT with n-type emitter and p-type collector are quite surprising due the positive sign and the large magnitude of the MC. To a first approximation, more hot-holes are expected to be created in the antiparallel state than the parallel state which would result a

negative MC since the inelastic scattering of hot-electrons which is the source of e-h pair creation is more in the parallel state than the antiparallel state.

A model is introduced to understand the behavior of e-h creation and the spin-dependent transmission of the excited hot-holes in the SVTs. The model explains the data very well if we assume that the majority (minority) spin hot-electrons generate electron-hole pairs in majority (minority) spin band and the distribution of the excited hot-holes are isotropic in momentum. The attenuation lengths for hot-holes in Co and NiFe are taken to be 1.0 nm and 0.5 nm for majority and minority spin, respectively. In this case, the hot-holes that are created in the Co film contribute mostly to the excited hot-hole current rather than the hot-holes created in NiFe since the hot-holes that are created in NiFe have to travel through the whole ferromagnet stack and thereby lose energy before they reach to the collector. While the model describes well the data for the excited hot-holes for this case, it does not explain the long hot-hole attenuation lengths found in Co in chapter 5. If the data for hot-hole attenuation length in Co from chapter 5 is used in the model, the calculated magnetocurrent is 10 times less than the experimental results. In this case, the hot-holes that are created in NiFe and Co contribute to the excited hot-hole current thus resulting in a negative calculated MC for thin NiFe (less than 3 nm) film and small magnitude of MC for thick NiFe film. In both cases, the spin-dependent transmission at the ferromagnet/normal metal interfaces is not considered. There is an evidence in chapter 5 that there might be spin-dependent transmission at the Co/normal metal interfaces. Also, the assumption of the isotropic distribution of the excited hot-holes may not be correct. A refined model to explain the data for the spin-dependent excited hot-hole transmission in the NiFe/Au/Co spin-valve base should thus include the spin-dependent transmission of hot-holes at ferromagnet/nonmagnetic metal interfaces and the momentum distribution of the excited hot-holes.

Chapter 7

Conclusions

Hot-electron magnetotransport has been studied with various techniques, and the spin-valve transistor (SVT) has proven to be one of the spintronics devices that could be used for this purpose. In this thesis, the SVT is used to address some of issues on the hot-carrier transport in hybrid structures that consists of semiconductors and metals (ferromagnetic and nonmagnetic metal). In effect, the study could answer some of the topics that could be used to develop new devices which uses the spin-filtering property of the ferromagnets and the compatibility of the semiconductor into the conventional electronics. One of the topics is that the role of interfaces in the hot-electron transport which has been a major source of elastic scattering thus reducing the output of the device. Spin-relaxation in nonmagnetic materials such as Ta is addressed in order to study the mechanisms of spin loss information that devoid the spin functionality in spintronics devices. Therefore, it is important to know how long a spin can travel in the nonmagnetic metals that are often used as spacer between the various ferromagnetic layers. In order to have spintronics to be able to improve technological stage at this moment, it should use both electrons and holes which gives an advantage of low power consumption and improve the device characteristic. Thus, we have used the SVT to study the spin-dependent hot-hole transport. Finally, the inelastic scattering of hot-electrons is investigated by studying the created hot-holes during the process of electron hole pair generation. This gives information on both the hot-electron and hole scattering in the ferromagnets.

In chapter 3, the hot-electron transport in the SVT is studied focusing on the role of interfaces. The Schottky diodes are discussed first since these determine the energy and the distribution of the hot-electrons are determined. The n-Si/Au diode injects hot-electrons with an energy of 0.80 eV. The n-Si/Cu diode is used to collect the transmitted electrons provided that they have enough energy and the right momentum. The collector diode n-Si/Cu has a 0.65 eV barrier height. Then, we have shown that a SVT with a NiFe/Cu/Co spin-valve

base has a higher transmission than a SVT with a NiFe/Au/Co spin-valve base. The former device has 2 times higher than the latter unlike the MTTs reported in literature that has 10 times difference for the similar spin-valve bases with Au and Cu spacers. The improvement is attributed to better transmission at Cu/ferromagnet interfaces than Au/ferromagnet interfaces. The magnetic sensitivity of both devices is more than 250%. If a third device with a Cu/Au/Cu nonmagnetic spacer is considered, it has a transfer ratio between the transfer ratios of the devices with Au and Cu spacers. However, the transfer ratio for this device is still higher than the device with Au spacer. It has a comparable magnetocurrent with the first two SVTs. Additional interfaces are inserted in between the Si/Au diode and the NiFe/Cu/Au/Cu/Co spin-valve base for having all interfaces with ferromagnets by Cu. However, the Cu and Au in n-Si/Au/Cu diode intermixes reducing the barrier height resulting lower hot-electron energies, which results in lowered transmission instead of improved transmission.

The collector current, the transfer ratio and the magnetocurrent has also been studied by varying the emitter current. The collector current increases almost linearly with emitter current without changing the magnetocurrent. The highest I_C of 64 μA of collector current is achieved. There is a slight increase in the transfer ratio at high emitter currents due to the Schottky barrier enhancement because of the changes of the image forces.

In chapter 4, the spin-dependent transport in Ta and at Ta/ferromagnet interfaces are studied. Hot-electron transport in SVT is based on the assumption that the spin-relaxation in nonmagnetic metals are much longer compared to the thicknesses of those materials which is the case for Au and Cu. However, the spin-relaxation has to be considered for Ta. The SVT model that describes the hot-electron transport is extended to include the spin-relaxation in the nonmagnetic spacer. It is found that the hot-electron current in Ta attenuates with a very short length which is determined to be 1.3 nm unlike Au and Cu that has hundreds of nm spin relaxation length. In addition to this, the transmission at the interfaces of Ta/ferromagnet is 19.6 times lower than the Cu/ferromagnet interfaces. This is attributed to large available density of states in a partially empty d band. The scattering probability of a hot-electron is higher for materials that have many available states just it is observed in ferromagnets. The short hot-electron attenuation lengths are consistent with the reported short inelastic lifetime for Ta measured by time-resolved two photon photoemission.

It has been shown for the magnetocurrent of the SVT that it depends on the thickness of the Ta layer when the Ta is in the spacer of the spin-valve base. The magnetocurrent for a device with 3 nm Ta spacer is 26% while the magnetocurrent for a device with Au or Cu is around 300%. The drop in MC compared to devices with Au or Cu and the thickness dependence of the MC is due to the spin-relaxation in Ta. The spin relaxes in Ta so that the spins that are polarized in the first ferromagnet (NiFe) layer have lost almost most of the spin informa-

tion before reaching the second (Co) ferromagnet layer that acts as analyzer. The spin-relaxation length in Ta is found to be 2.1 nm which is very short compared to hundreds of nanometers for Au or Cu. This is attributed to the strong spin-orbit coupling and momentum scattering which is related to the high number unoccupied available states in partially empty d states in Ta. The transmission at the Ta/ferromagnet interfaces are found to be almost spin-independent.

After discussing the hot-electron transmission in the SVT in chapter 3 and 4, we have investigated the spin-dependent hot-hole transport in the SVT particularly in the Co layer. In chapter 5, it is important for complementariness in spintronics devices that we study the hot-holes along with the hot-electron transport. In order to inject and collect hot-holes, p-type Si is used. p-Si/Cu Schottky diode which has a barrier height of 0.5 eV injects hot-holes into the metal base of the SVT. A p-Si/Au Schottky diode (that has 0.29 eV barrier height) is used to collect hot-holes. The measurements are done at low temperatures since thermally activated current dominates the output current at room temperature.

It has been shown for a p-type SVT with NiFe/Au/Co spin-valve base that the hot-hole current is spin-dependent. The magnetocurrent for 3 nm NiFe and 3 nm Co is 18%. As the Co thickness increased, the magnetocurrent increases to 80% for 7.5 nm Co. There is a spin-filtering of hot-hole in Co however it is not as strong as with hot-electrons where we observe 300% of MC. A second observation is that the hot-hole transmission depends on the thickness of the Co layer. We have found that the SVTs with Co films thinner than 4 nm, the dominant scattering is elastic scattering and the elastic attenuation length of hot-holes for majority and minority spin is found to be 0.8 nm. For the devices with thicker Co films, the inelastic scattering dominates the hot-hole transport. The inelastic attenuation length of hot-holes for majority and minority spin is found to be 5.0 nm and 3.0 nm, respectively. No spin-dependent transmission at the ferromagnet/nonmagnetic metal interfaces are considered. However, a recent experimental work by a p-type MTT have shown that for thin Co film thicknesses, the magnetocurrent is reported to be negative, indicating that the minority spin attenuation length of hot-hole is shorter than the majority spin of hot-holes. The experiments done by SVT in this chapter can be explained with this explanation as well if we take the elastic minority and majority attenuation length of hot-holes to be 1.15 nm and 0.80 nm, respectively. For this case, the transmission at Co/ferromagnet interface is spin-dependent and the majority spin of hot-holes transmission is 1.5 times higher than the minority spin of hot-holes.

So far we have injected and collected the transmitted hot-carriers to study the scattering of hot-electrons and hot-holes in the feromagnets. In chapter 6, we have studied the created hot-holes by inelastic scattering of hot-electrons in the ferromagnets, which gives more direct information about the scattering mechanisms for the hot-electrons in the ferromagnets. n-Si/Au Schottky diode

is used to inject hot-electrons which decay inealstically through e-h pair excitation. The hot-holes that are thus created in the ferromagnets are transported spin-dependently in the metal base since it is shown that hot-hole transmission in the ferromagnets is spin-dependent. The magnetocurrent for a SVT with n-Si emitter, p-Si collector and a base of NiFe(3 nm)/Au(10 nm)/Co(3 nm) is 240%. The magnetocurrent is surprisingly high and moreover has a positive sign. Since the hot-holes are created by the inelastic scattering of hot-electrons and the inelastic scattering is higher for the anti-parallel magnetization alignment of the NiFe and Co film, we expected to have high current in the antiparallel alignment,i. e., negative magnetocurrent. As we change the thickness of the NiFe layer in the spin-valve base, the magnetocurrent remains around 250% even for 7 nm NiFe. A model is introduced to explain the creation of the hot-holes and the subsequent transport of the created hot-holes. It is based on the assumptions that the majority (minority) spin of hot-electrons generate hot-holes in the majority (minority) spin band. Secondly, the created hot-holes have an isotropic momentum distribution. The experimental data can then be explained with short hot-hole attenuation lengths (1.0 nm and 0.5 nm for majority and minority spin, respectively). However, this is in contradiction with the results of chapter 5 if the second assumption above is correct. If the created hot-holes have isotropic momentum distribution, the elastic scattering attenuation length (reported in chapter 5) for hot-holes should not have any effect on the magnetocurrent. If long attenuation lengths (5.0 nm and 3.0 nm for majority and minority spin) are used, the data and calculation have one order difference. Therefore, a refined model is needed for explaining the spin-dependent transport of created hot-holes. It should include the spin-dependent transmission at the interfaces and possibly anisotropic momentum distribution of the created hot-holes. Nevertheless, the work in this thesis has shown that besides the hot-electron based SVT, other configurations using holes may also yield large magnetic sensitivity of hot electrons as well as holes.

Bibliography

[1] G. A. Prinz. "Magnetoelectronics". *Science* **282**, 1660–1663 (1998).

[2] D. J. Monsma, J. C. Lodder, Th. J. A. Popma and B. Dieny. "Perpendicular hot electron spin-valve effect in a new magnetic field sensor:The Spinv-valve Transistor". *Phys. Rev. Lett.* **74**, 5260–5263 (1995).

[3] M. N. Baibich, J. M. Broto, A. Fert, F. Nguyen Van Dau and F. Petroff. "Giant magnetoresistance of (001)Fe/(001)Cr magnetic superlattices". *Phys. Rev. Lett.* **61**, 2472–2475 (1988).

[4] S. A. Wolf, D. D. Awschalom, R. A. Buhrman, J. M. Daughton, S. von Molnár, M. L. Roukes, A. Y. Chtchelkanova and D. M. Treger. "Spintronics:A spin-based electronics vision for the future". *Science* **294**, 1488 (2001).

[5] S. S. P. Parkin adn X. Jiang, C. Kaiser, A. Panchula, K. Roche and M. Samant. "Magnetically engineered spintronic sensors and memory". *Proc IEEE* **91**, 661–680 (2003).

[6] J. S. Moodera, L. R. Kinder, T. M. Wong and R. Meservey. "Large magnetoresistance at room temperature in ferromagnetic thin film tunnel junctions". *Phys. Rev. Lett.* **74**, 3273–3276 (1995).

[7] S. S. P. Parkin, K. P. Roche, M. G. Samant, P. M. Rice, R. B. Beyers, R. E. Scheuerlein, E. J. O'Sullivan, S. L. Brown, J. Bucchigano, D. W. Abraham, Y. Lu, M. Rooks, P. L. Trouilloud, R. A. Wanner and W. J. Gallagher. "Exchanged-biased magnetic tunnel junctions and application to nonvolatile magnetic random access memory (invited)". *J. Appl. Phys.* **85**, 5828–5833 (1999).

[8] J. de Boeck and G. Borghs. "Magnetoelectronics". *Physics World* **12**, 27–32 (1999).

[9] S. Tehrani, J. M. Slaughter, M. Deherrera, B. N. Engel, N. D. Rizzo, J. Salter, M. Durlam, R. W. Dave, J. Janesky, B. Butcher, K. Smith and G. Grynkeciwch. "Magnetoresistance random access memory using magnetic tunnel junctions". *Proc IEEE* **91**, 703–714 (2003).

[10] J. M. Kikkawa and D. D. Awschalom. "Resonant spin amplification in n-type GaAs". *Phys. Rev. Lett.* **80**, 4313–4316 (1998).

[11] J. M. Kikkawa and D. D. Awschalom. "Lateral drag of spin coherence in gallium arsenide". *Nature* **397**, 139–141 (1999).

[12] H. Ohno. "Making nonmagnetic semiconductors ferromagnetic". *Science* **281**, 951–956 (1998).

[13] R. Jansen. "The spin-valve transistor: a review and outlook". *J. Phys. D:Appl. Phys.* **36**, R289–R308 (2003).

[14] D. T. Pierce and H. C. Siegmann. "Hot-electron scattering length by measurement of spin polarization". *Phys. Rev. B* **9**, 4035–4037 (1974).

[15] J. C. Gröbli, D. Guarisco, S. Frank and F. Meier. "Spin-dependent transmission of polarized electrons through a ferromagnetic iron film". *Phys. Rev. B* **51**, 2945–2949 (1995).

[16] D. P. Pappas, K.-P. Kamper, B. P. Miller, H. Hopster, D.E. Fowler, C. R. Brundle, A. C. Luntz and Z.-X. Shen. "Spin-dependent electron attenuation by transmission through thin ferromagnetic films". *Phys. Rev. Lett.* **66**, 504–507 (1991).

[17] J. C. Gröbli, D. Oberli and F. Meier. "Crucial test of spin filtering". *Phys. Rev. B* **52**, R13095–R13097 (1995).

[18] T. Banerjee, E. Haq, M. H. Siekman, J. C. Lodder and R. Jansen. "Spin filtering of hot-holes in a metallic ferromagnet". *Phys. Rev. Lett.* **94**, 027204 (2005).

[19] E. Haq. "Nanoscale spin-dependent transport of electrons and holes in Si-ferromagnet structures". Ph.D. thesis University of Twente, The Netherlands (2005).

[20] W. H. Rippard and R. A. Buhrman. "Spin-dependent hot electron transport in Co/Cu thin films". *Phys. Rev. Lett.* **84**, 971–974 (2000).

[21] W. H. Rippard and R. A. Buhrman. "Ballistic electron magnetic microscopy: Imaging magnetic domains with nanometer resolution". *Appl. Phys. Lett.* **175**, 1001–1003 (1999).

[22] R. Vlutters, O. M. J. van't Erve, S. D. Kim, R. Jansen and J. C. Lodder. "Interface, volume, and thermal attenuation of hot-electron spins in $Ni_{80}Fe_{20}$ and Co". *Phys. Rev. Lett.* **88**, 027202 (2002).

[23] R. Vlutters, R. Jansen, O. M. J. van't Erve, S. D. Kim and J. C. Lodder. "Hot-electron transport through $Ni_{80}Fe_{20}$ in a spin-valve transistor". *J. Appl. Phys.* **89**, 7305–7307 (2001).

[24] O. M. J. van't Erve, R. Vlutters, P. S. Anil Kumar, S.D. Kim, F. M. Postma, R. Jansen and J. C. Lodder. "Transfer ratio of the spin-valve transistor". *Appl. Phys. Lett.* **80**, 3787–3789 (2002).

[25] S. van Dijken, X. Jiang and S. S. P. Parkin. "Spin-dependent hot electron transport in $Ni_{81}Fe_{19}$ and $Co_{84}Fe_{16}$ films on GaAs(001)". *Phys. Rev. B* **66**, 094417 (2002).

[26] M. Plihal, D. L. Mills and Kirschner. "Spin wave signature in the spin-polarized electron energy loss spectrum of ultrathin Fe films: Theory and experiments". *Phys. Rev. Lett.* **82**, 2579–2582 (1999).

[27] R. Jansen, P. S. Anil Kumar, O. M. J. van't Erve, R. Vlutters, P. de Haan and J. C. Lodder. "Thermal spin-wave scattering in hot-electron magnetotransport across a spin valve". *Phys. Rev. Lett.* **85**, 3277–3280 (2000).

[28] V. P. Zhukov, E. V. Chulkov and P. M. Echenique. "Lifetimes of excited electrons in Fe and Ni: First-principles GW and the T-matrix theory". *Phys. Rev. Lett.* **93**, 096401 (2004).

[29] J. Hong and D. L. Mills. "Theory of the spin dependence of the inelastic mean free path of electrons in ferromagnetic metals: A model study". *Phys. Rev. B* **59**, 13840–13848 (1999).

[30] J. Hong and D. L. Mills. "Spin dependence of the inelastic electron mean free path in Fe and Ni: Explicit calculations and implications". *Phys. Rev. B* **62**, 5589–5599 (2000).

[31] O. M. J. van't Erve. "Device properties of the spin-valve transistor and the magnetic tunnel transistor". Ph.D. thesis University of Twente, The Netherlands (2002).

[32] R. Vlutters. "Hot-electron transport in the spin-valve transistor". Ph.D. thesis University of Twente, The Netherlands (2001).

[33] T. Shimatsu, R. H. Mollema, D. Monsma, E. G. Keim and J. C. Lodder. "Metal bonding during sputter film deposition". *J. Vac. Sci. Technol. A* **16**, 2125–2131 (1998).

[34] D. J. Monsma. "The spin-valve transistor". Ph.D. thesis University of Twente, The Netherlands (1998).

[35] K. Mizushima, T. Kinno, T. Yamauchi and K. Tanaka. "Energy-dependent hot electron transport across a spin-valve". *IEEE Trans. Magn.* **3**, 3500–3504 (1995).

[36] S. D. Kim, O. M. J. van't Erve, R. Vlutters, R. Jansen and J. C. Lodder. "Size dependence of the magnetic and electrical properties of the spin-valve transistor". *IEEE Trans. Electron Devices* **49**, 847–851 (2002).

[37] R. Vlutters, O. M. J. van't Erve, R. Jansen, S. D. Kim, J. C. Lodder, A. Vedyayev, and B. Dieny. "Modeling of spin-dependent hot-electron transport in the spin-valve transistor". *Phys. Rev. B* **65**, 024416 (2002).

[38] S. van Dijken, X. Jiang and S. S. P. Parkin. "Comparison of magnetocurrent and transfer ratio in magnetic tunnel transistors with spin-valve bases containing Cu and Au spacer layers". *Appl. Phys. Lett.* **82**, 775–777 (2003).

[39] S. M. Sze. "Physics of semiconductor devices 2nd edition". John Wiley & Sons Inc (1981).

[40] M. K. Weilmeier, W. H. Rippard and R. A. Buhrman. "Ballistic electron transport through Au(111)/Si(111) and Au(111)/Si(100) interfaces". *Phys. Rev. B* **59**, R2521–R2524 (1999).

[41] L. D. Bell. "Evidence of momentum conservation at a nonepitaxial metal/semiconductor interface using ballistic electron emission microscopy". *Phys. Rev. Lett.* **77**, 3893–3896 (1996).

[42] R. P. Lu, B. A. Morgan, K. L. Kavanagh, C. J. Powell, P. J. Chen, F. G. Serpa and Jr. W. F. Egelhoff. "Hot-electron attenuation lengths in ultrathin magnetic films". *J. Appl. Phys.* **87**, 5164–5166 (2000).

[43] R. Jansen, H. Gokcan, O. M. J. van't Erve, F. M. Postma and J. C. Lodder. "Spin-valve transistors with high magnetocurrent and 40μA output current". *J. Appl. Phys.* **95**, 6927–6929 (2004).

[44] I. *Žutić*, J. Fabian and S. Das Sarma. "Spintronics: Fundeamentals and applications". *Rev. Mod. Phys.* **76**, 323–410 (2004).

[45] F. J. Jedema, A. T. Filip and B. J. van Wees. "Electrical spin injection and accumulation at room temperature in an all mesoscopic spin-valve". *Nature* **410**, 345–348 (2001).

[46] F. J. Jedema, M. S. Nifboer, A. T. Filip and B. J. van Wees. "Spin injection and spin accumulation in all-mesoscopic spin-valves". *Phys. Rev. B* **67**, 85319 (2003).

[47] R. J. Elliot. "Theory of the effect of spin-orbit coupling on magnetic resonance in some semiconductors". *Phys. Rev.* **96**, 266–279 (1954).

[48] Y. Yafet. "Solid State Physics". Academic (1963).

[49] J. Bass. "Metals: Electronic Transport Phenomena, vol 15, Part a of Landolt-Börnstein". Springer-Verlag (1982).

[50] F. Beuneu and P. Monod. "The Elliot relation in pure metals". *Phys. Rev. B* **18**, 2422–2425 (1978).

[51] P. Monod and F. Beuneu. "Conduction-electron spin flip by phonons in metals: Analysis of experimental data". *Phys. Rev. B* **19**, 911–916 (1979).

[52] J. Fabian and S. Das Sarma. "Spin relaxation of conduction electrons in polyvalent metals: Theory and a realistic calculation". *Phys. Rev. Lett.* **81**, 5624–5627 (1998).

[53] J. Fabian and S. Das Sarma. "Band-structure effects in the spin relaxation of conduction electrons (invited)". *J. App. Phys.* **85**, 5075–5079 (1999).

[54] *http://cst-www.nrl.navy.mil/ElectronicStructureDatabase/.*

[55] J. Cao, Y. Gao, H. E. Elsayed-Ali, R. J. D. Miller and D. A. Mantell. "Femtosecond photoemission study of ultrafast electron dynamics in single-crystal Au(111) films". *Phys. Rev. B* **58**, 10948–10952 (1998).

[56] R. Keyling, W. D. Schöne and W. Ekardt. "Comparison of the lifetime of excited electrons in noble metals". *Phys. Rev. B* **61**, 1670–1673 (1998).

[57] V. P. Zhukov, O. Andreyev, D. Hoffmann, M. Bauer, M. Aeschlimann, E. V. Chulkov and P. M. Echenique. "Lifetimes of excited electrons in Ta: Experimetal time-resolved photoemission data and first-principles GW+T theory". *Phys. Rev. B* **70**, 233106 (2004).

[58] E. Knoesel, A. Hotzel and M Wolf. "Ulytafast dynamics of hot-electrons and holes in copper: Excitation, energy relaxation, and transport effects". *Phys. Rev. B* **57**, 12812–12824 (1998).

[59] L. Gan, R. D. Gomez, C. J. Powell, R. D. McMichael, P. J. Chen and Jr. W. F. Egelhoff. "Thin Al, Au, Cu, Ni, Fe, and Ta films as oxidation barriers for Co in air". *J. App. Phys.* **93**, 8731–8733 (2003).

[60] M. Kowalewski, W. H. Butler, N. Moghadam, G. M. Stocks, T. C. Schulthess, K. J. Song, J. R. Thompson, A. S. Arrott, T. Zhu, J. Drewes, R. R. Katti, M. T. McClure and O. Escorcia. "The effect of Ta on the magnetic thickness of permalloy (Ni_81Fe_19) films". *J. App. Phys* **87**, 5732–5734 (2000).

[61] S. Das Sarma, J. Fabian, X. Hu and I. Žutić. "Spintronics:electron spin coherence, entanglement, and transport". *Superlattices and Microstructures* **27**, 289–295 (2000).

[62] D. Oberli, R. Burgermeister, S. Riesen, W. Weber and H. C. Siegman. "Total scattering cross section and a spin motion of low energy electrons passing through a ferromagnet". *Phys. Rev. Lett.* **81**, 4228–4231 (1998).

[63] M. Aeschilmann, M. Bauer, S. Pawlik, W. Weber, R. Burgermeister, D. Oberli and H. C. Siegman. "Ultra spin-dependent electron dynamics in fcc Co". *Phys. Rev. Lett.* **79**, 5158–5161 (1997).

[64] W. Weber, S. Riesen and H. C. Siegman. "Magnetization precession by hot spin injection". *Science* **291**, 1015 (2001).

[65] R. Knorren, K. H. Bennemann, R. Burgermeister and M. Aeschilmann. "Dynamics of excited electrons in copper and ferromagnetic transition metals: Theory and experiment". *Phys. Rev. B* **61**, 9427–9440 (2000).

[66] H. Gokcan, J. C. Lodder and R. Jansen. "Effect of nonmagnetic spacer on hot-electron transport in the spin-valve transistor". *Materials Science and Engineering B* **126**, 129–132 (2006).

[67] E. Haq, T. Banerjee, M. H. Siekman, J. C. Lodder and R. Jansen. "Ballistic hole magnetic microscopy". *App. Phys. Lett.* **86**, 082502 (2005).

[68] I. Campillo, A. Rubio, J. M. Pitarke, A. Goldmann and P. M. Echenique. "Hole dynamics in noble metals". *Phys. Rev. Lett.* **85**, 3241–3244 (2000).

[69] B. G. Park, T. Banerjee, J. C. Lodder and R. Jansen. "Opposite spin asymmetry of elastic and inelastic scattering of holes in Co". in preparation (2006).

[70] E. Zarate, P. Apell and P. M. Echenique. "Calculation of low-energy-electron lifetimes". *Phys. Rev. B* **60**, 2326–2332 (1999).

Summary

The conventional electronics uses the charge property of the electrons and holes. The building blocks are semiconductors which can be tuned to change the properties of the devices. In the field of spintronics, the spin property of the charge carriers is added to the functionality of the devices. The spin-valve transistor (SVT) is one of the spintronics devices which allows us to study the spin-dependent transport characteristic of non-equilibrium electrons and holes in semiconductor/ferromagnetic hybrid structures. The SVT uses Schottky barriers to inject and collect hot-carriers. In the metal base of the device, two ferromagnetic metals separated by a nonmagnetic metal are utilized to analyze the spin-dependent transport of the electrons and holes. In this thesis, one of the motivations is to understand the role of interfaces in the hot-electron transport. Another motivation is to study the spin relaxation in metals which is crucial for adding the functionality of spin property. Finally, it is important to understand the hot-hole transport since the devices working with holes and electrons offer better performances.

In chapter 2, the experimental procedures to fabricate and electrically characterize a spin-valve transistor are described briefly. Then, hot-electron transport in the SVT is studied by using different nonmagnetic spacers that results in different interfaces in the metal base of the device (chapter 3). The hot-electrons are injected by a Si/Au Schottky diode and collected by a Si/Cu diode. We have found that a SVT with a NiFe/Cu/Co spin-valve base has a higher transmission than a SVT with a NiFe/Au/Co spin-valve base. The transfer ratio is 2 times higher for the former device. The magnetic sensitivity is not affected by the choice of spacers or interfaces. It is also found that additional interfaces reduces the transfer ratio but do not affect the magnetic sensitivity. The properties of the device such as the collector current, the transfer ratio and the magnetocurrent are investigated as a function of the emitter current. An almost linear dependence of the collector current is observed. 64 μA of collector current is achieved without losing the magnetic sensitivity which is around 300 %. In chapter 3, it has thus been shown that the interfaces are a major source of scattering which affects the output of the device.

An important question for devices is whether spin-relaxation occurs in the

non-magnetic layers. We have studied this for tantalum (chapter 4). For Au and Cu, the spin-relaxation lengths are hundreds of nanometers long. However, it is observed for Ta that the spin relaxes faster than Au and Cu. Two cases were studied. In the first case, we have SVTs with a NiFe/Ta/Co spin-valve base where the spin of the current polarized in NiFe, relaxes in Ta before it reaches the analyzer Co layer. The magnetocurrent is around 10 % for the devices with Ta spacer which is 2 orders of magnitude smaller than the devices with Au or Cu spacer. The transfer ratio for devices with Ta spacer dropped three orders of magnitude compared to SVTs with Au and Cu and the attenuation length in Ta is found to be 1.3 nm. In the second case, SVTs with NiFe/Au/Co/Ta spin-valve base is considered. The magnetocurrent for these devices are as high as 280 % since the spin information of the electron is already analyzed before it is transported in Ta. A model is developed to explain both cases. The spin-relaxation length in Ta was found to be around 2.1 nm. It is argued that the localized partially empty d states are the cause of short attenuation length and together with the spin-orbit interaction also causes short spin-relaxation length. Ta as a nonmagnetic transition metal with partially empty d states causes the spin information to be lost via spin relaxation for distances above approximately 1 nm. Thus, Ta should not be used as the spacer in hot-electron devices.

Although the hot-electron transport above the Fermi level has been studied widely, this is not so for hot-holes below the Fermi level. A complete picture of the non-equilibrium carrier transport requires the investigation of hot-holes. To explore hot-hole transport, a SVT with p-type Si is used to inject and collect hot-holes in chapter 5. We have observed that the hot-hole attenuation length in Co is not a single exponential dependence as in the case for the hot-electron attenuation length in Co. Instead there are two regimes that have 0.8 nm and 5.0 nm attenuation lengths in Co for SVTs with Co thicknesses below and above approximately 4 nm, respectively. The short attenuation length is attributed to the elastic scattering processes whereas the long attenuation length is attributed to the inelastic scattering processes. We also have observed that the hot-hole current is spin-dependent for the SVTs with p-Si/Au/NiFe/Au/Co/Cu/p-Si structure. For 3 nm NiFe and 3 nm Co, 18 % of magnetocurrent is measured. This is rather low compared to the devices (384 %) that has electrons as the charge carriers. This can be explained by the opposite spin asymmetry for elastic and inelastic scattering. Although there is no significant spin asymmetry in the density of states of Co below the Fermi level, we observe spin filtering of hot-holes below the Fermi level in Co and NiFe.

In chapter 6, rather than transmitted carriers, the hot-holes excited due to inelastic decay of hot electrons are studied in order to investigate the hot carrier scattering in ferromagnets. n-Si is used to inject hot-electrons and p-Si is used to collect excited hot-holes in the metal base of the SVT. We observed high magnetocurrent around 250 % for the devices that have 3 nm NiFe and 3 nm Co which

stays almost constant as NiFe thickness is increased to 7 nm. This is one order higher than the devices (20 %) that have hole injection and collection studied in chapter 5. Apart from high magnetocurrent, the positive sign of the magnetocurrent is surprising since the excited hot-hole is expected to be originating from inelastic scattering which should produce more current for the antiparallel alignment of the base magnetic moments compared to the parallel alignment and thus negative magnetocurrent was expected. A model is developed to understand the scattering mechanism for both hot-electrons and holes. It is shown that the contribution of interfaces to the spin-dependent transport has to be included to understand the excited hot-hole transport. Also the distribution of the excited hot-holes has to be taken into account to understand the scattering mechanism of hot-carriers. In this dissertation, it has been shown that hot holes as the charge and spin carriers in the SVT with different configurations may also yield large magnetic sensitivity as hot electrons in the SVT.

Samenvatting

In de conventionele elektronica wordt gebruik gemaakt van lading en gaten transport terwijl in het domein van de spin-electronica ook de spin eigenschap van de ladingsdragers wordt gebruikt. De Spin Valve Transistor (SVT) is een device waarmee het spinafhankelijk elektronische transport van niet-evenwichts (hete) elektronen en gaten in halfgeleider/ferromagnetisch hybride structuren kan worden onderzocht. De SVT gebruikt Schottky barrires om hete ladingdragers te injecteren en te detecteren. De metalen basis van de SVT bestaat uit twee ferromagnetische metalen, die gescheiden zijn door een niet-magnetische metaal. Deze zorgen ervoor dat de SVT kan worden gebruikt om het spinafhankelijke transport van de elektronen en gaten te analyseren. Een van de belangrijkste motivaties voor dit proefschrift is het begrijpen van de rol van de interfaces gedurende het transport van hete elektronen. Een andere motivatie is het bestuderen van de spin relaxatie in metalen die cruciaal is voor de functionaliteit van de spin eigenschappen. Tot slot is het van belang om het transport van hete gaten te begrijpen voor de realisatie van nieuwe spin elektronische devices die zowel gaten als elektronen gebruiken als ladingsdragers.

In hoofdstuk 2 zijn de experimentele procedures om een SVT te fabriceren en elektrische eigenschappen te karakteriseren kort beschreven, terwijl in hoofdstuk 3 het transport van hete elektronen nader wordt bestudeerd door verschillende niet-magnetische tussenlagen te gebruiken. Dit resulteert in verschillende interface structuren van de metalen basis. In de bestudeerde SVT's worden de hete elektronen door een Si/Au Schottky diode genjecteerd en door een Si/Cu diode gedetecteerd. In dit hoofdstuk wordt geconcludeerd dat een SVT met een NiFe/Cu/Co spin-valve basis een hogere transmissie heeft dan een device met een NiFe/Au/Co basis. De overdrachtsverhouding is tweemaal hoger dan devices die in het verleden gemaakt zijn. De magnetische gevoeligheid wordt niet benvloed door de keuze van de tussenlaag en de verschillende interfaces. Ook is gevonden dat de extra interfaces (door toevoeging van extra lagen) de overdrachtverhouding reduceren maar geen invloed hebben op de magnetische gevoeligheid. In dit hoofdstuk zijn ook andere eigenschappen van het device, zoals collectorstroom, overdrachtsverhouding en de magnetostroom onderzocht als functie van de emitterstroom. Een bijna lineaire afhankelijkheid van

de collectorstroom is gemeten. Zonder verlies van magnetische gevoeligheid (MC = 300%) is een collectorstroom van 64 uA gemeten. In hoofdstuk 3 is dus bewezen dat de interfaces de meest belangrijke bron zijn voor de verstrooiing en daarmee een grote invloed hebben op de uiteindelijke output van het device.

Een zeer belangrijke vraag voor componenten is of er ook spin relaxatie optreedt in de niet-magnetische lagen. Daarom is in hoofdstuk 4 het niet-magnetische tantaal (Ta) bestudeerd. We weten dat voor Au en Cu de spin relaxatie lengtes honderden nanometers lang zijn. Echter voor Ta is waargenomen dat de spin sneller relaxeert dan in Au en Cu. Om dit nader te bestuderen zijn twee deviceontwerpen onderzocht. In het eerste geval hebben we SVTs met een NiFe/Ta/Co spin-valve basis gemaakt waarbij de spin wordt gepolariseerd in de NiFe laag, daarna in het Ta relaxeert voordat het de analysator laag (Co) bereikt. De magnetostroom is ongeveer 10% voor het device met Ta en dat is 30 keer kleiner dan in de devices met alleen Au of Cu laag. De overdrachtsverhouding voor de devices met Ta tussenlaag is 3 grootteordes kleiner in vergelijking met SVTs bestaande uit Au en Cu. Ook is vastgesteld dat de karakteristieke lengte voor devices met Ta 1.3 nm bedraagt. In het tweede geval is de SVTs gerealiseerd met een basis bestaande uit NiFe/Au/Co/Ta. De magnetostroom voor dit type device is zeer hoog namelijk 280%. Dit komt omdat de spin reeds is geanalyseerd voordat het de Ta laag bereikt. Ook in dit hoofdstuk is een model ontwikkeld om de beide gevallen te verklaren. Een resultaat is dat de spin relaxatie lengte in Ta 2.1 nm bedraagt. De kleine karakteristieke lengte kan worden verklaard door de gelokaliseerde, gedeeltelijk lege d toestanden en samen met de spin-baan interactie resulteert dit in de kleine spin relaxatie lengte. De conclusie van dit hoofdstuk is dan ook dat het niet-magnetische overgangsmetaal Ta, met gedeeltelijk lege d toestanden ervoor zorgt dat de spin informatie verloren gaat via spin relaxatie voor grotere afstanden dan ongeveer 1 nm. Met andere woorden: Ta is dus een ongeschikt materiaal als tussenlaag in devices gebaseerd op hete elektronen transport.

Hoewel het transport van hete elektronen boven Fermi niveau veel is bestudeerd, is er nog weinig onderzoek verricht voor hete gaten transport beneden het Fermi niveau. In hoofdstuk 5 wordt een aanzet gegeven om een compleet beeld van het niet-evenwicht transport te verkrijgen en daar worden dus onderzoeksresultaten gepresenteerd van hete gaten transport. Om dit te realiseren is er een SVT met p-type Si gebruikt om de hete gaten te injecteren en te analyseren. We hebben waargenomen dat de karakteristieke lengte van hete gaten in Co niet kan worden weergegeven met een exponentiele afhankelijkheid zoals is vastgesteld voor hete elektronen. De afhankelijkheid is gesplitst in twee gebieden die respectievelijk een karakteristieke lengte hebben van 0.8 nm en 5.0 nm voor SVTs met Co laagdikte van beneden en boven ongeveer 4.0 nm. De korte karakteristiekenlengte wordt toegeschreven aan het elastische verstrooiingsproces terwijl de lange karakteristiekenlengte wordt verklaard met de niet-elastische ver-

strooiing. Ook is waargenomen dat hete gaten stroom spin afhankelijk is voor de SVTs met p-Si/Au/NiFe/Au/Co/Cu/p-Si structuur. Voor 3 nm NiFe en 3 nm Co, is een magnetostroom van 18% gemeten. Dit is zeer laag in vergelijking met de devices die elektronen als ladingdragers gebruiken (384%). Dit kan worden verklaard door de tegengestelde spin asymmetrie voor elastische en niet-elastische verstrooiing. Hoewel er geen significante spin asymmetrie is in de dichtheid van de toestanden van Co beneden het Fermi niveau, nemen we wel spin filtering waar van hete gaten beneden het Fermi niveau in Co en NiFe lagen.

De verstrooiing van hete ladingdragers in ferromagneten is beschreven in hoofdstuk 6. Met name de gexciteerde hete gaten, die ontstaan door inelastische verstrooiing van hete elektronen wordt beschreven. Voor de injectie en detectie van hete elektronen en gaten, gebruiken we respectievelijk n-Si en p-Si. Een hoge magnetostroom is waargenomen (250%) voor de devices met 3 nm NiFe en 3 nm Co en blijft nagenoeg constant tot een NiFe dikte van 7 nm. Dit is meer dan een factor 10 groter dan de devices (20%) met injectie en detectie van gaten zoals bestudeerd zijn in hoofdstuk 5. Behalve de hogere magneetstroom is het positieve teken van de magneetstroom verrassend omdat dit niet werd verwacht van de gexciteerde hete gaten die afkomstig zijn van niet-elastische verstrooiingsprocessen. Dit zou meer stroom leveren voor de antiparallelle stand van de magnetisatie in vergelijking tot parallelle stand van de magnetisatie en dus werd een negatieve magneetstroom verwacht. Een model is ontwikkeld om het verstrooiingsmechanisme voor hete elektronen en gaten te begrijpen. Hiermee is aangetoond dat de interface bijdrage aan spin afhankelijk transport essentieel is voor een beter begrip van het gexciteerde hete gaten transport. Om het verstrooiingmechanisme van hete dragers te begrijpen is het tevens van belang rekening te houden met de distributie van de gexciteerde hete gaten. Voor verschillende configuratie SVT's is aangetoond dat ook ingeval van hete gaten een hogere magnetische gevoeligheid kan worden gerealiseerd zoals ook in het verleden is bewezen voor de SVT die alleen gebruik maakte van hete elektronen.

Acknowledgements

I have enjoyed working in SMI group at the University of Twente during my four years of my Ph.D. thesis. I would like to express my gratitude and special thanks to people who contributed to realize my Ph.D. thesis in any way.

I would like to thank my promotor Prof Cock Lodder who has been always supportive in my research and settling down in the Netherlands. He was there whenever I needed him.

This thesis could not have been the same without my daily supervisor Dr. Ronnie Jansen. His critical analysis of my results set the quality of the research high. His guidance were helpful in planning, conducting of my experiments and presenting the results with presentations, papers. He helped me to improve my skills by demanding the best.

I am very thankful to Johnny Sanderink for his technical support. Whenever we needed something in the cleanroom, Johnny was there to deliver it as quickly as possible. I enjoyed a lot talking with him about our social life and his trips to Turkey.

I'd like to thank Olaf van't Erve for introducing me the MBE system and the bond robot. Very special thanks to Tamalika Banerjee, Ehtsham-ul Haq, Ferry Postma, Rajesh Ramaneti, Byong-Guk Park, Byoung-Chul Min, Mercy Mathews and Ivan Vera Marún for the useful discussions in the SVT meetings.

Thanks to Rogelio Murillo and Takahiro Onoue for making the office life enjoyable. We had long chats comparing the Dutch culture with our own. It was an international office with representatives from Asia, Europe and America.

I'd like to thank SMI secretaries Thelma and Karen for their support especially for the help in translating the official Dutch papers. Thanks to Thijs for making sure that the computers are working.

Very special thanks to Salih Kilic who helped a lot in my life in Enchede. He was a good friend and very supportive. His car was available whenever we needed to go to airport or supermarkets in Germany. I'd like to thank Hatice for making life enjoyable for my wife. Thanks to Nuri, Sema, Oguzhan, Fulya, Bulent Deniz, Huseyin Amca, Musaade Teyze, Bedir Abi, Leyla, Mustafa, Gurhan, Zafer for making our social life colorful and enjoyable otherwise uneventful life in Enschede.

The words are not enough to describe my wife Elif's support. The sacrifices she made for me is uncountable. She is the warmness and joy in my heart and my life. The most difficult times in these four years were not the days when I was writing the thesis or making the experiments but the days she was not with me. My sincere gratitude and very special thanks to my beloved wife Elif for being with me in the Netherlands. My daughter Asude joined our family in my last year in the Ph.D. Her presence were enough to give Elif and me a smile on the face in every day. Finally, I'd like to thank my parents Mustafa and Necmiye for their support.